STRUCTURAL PLASTICITY AND ASSOCIATIVE MEMORY IN BALANCED NEURAL NETWORKS WITH SPIKE-TIME DEPENDENT INHIBITORY PLASTICITY

SUBMITTED TO THE UNIVERSITY OF HERTFORDSHIRE IN PARTIAL FULFILMENT OF THE REQUIREMENTS OF THE DEGREE OF

DOCTOR OF PHILOSOPHY

ANKUR SINHA
UH BIOCOMPUTATION GROUP
CENTRE FOR COMPUTER SCIENCE AND INFORMATICS RESEARCH
UNIVERSITY OF HERTFORDSHIRE
HATFIELD

SUPERVISORS:

PROFESSOR VOLKER STEUBER
DR CHRISTOPH METZNER
PROFESSOR ROD ADAMS
PROFESSOR MICHAEL SCHMUKER
DR NEIL DAVEY

MAY, 2020

ACKNOWLEDGEMENTS

> No man is an island,
> Entire of itself,
> Every man is a piece of the continent,
> A part of the main.
>
> John Donne

What Donne says so elegantly in four short lines takes years to realise. As a youngster, I too had thought that I could do everything alone, by myself, without ever having to ask another soul for assistance. The more I live and see, the more I am convinced that this is not true. One simply cannot disassociate themself from 'the main'.

I have come to understand that a great many people have taken on the role of potters at different times in my life to shape it to what it is today. It is therefore, with great affection that I take this opportunity to thank them for I shall forever be indebted to them.

I must begin with my immediate family. I could not have wished for better parents, Dr Kalpana Sinha and Dr Sanjay Kumar Sinha. They have always been there to guide me towards the right and away from wrong. They, both being doctors, have showed me the beauty of nature and the human body from a young age. They, knowing the importance of education and exposure to the world, have made many sacrifices to ensure that I got the best education possible. They, being people of science, have taught me the importance of the truth. It is through their lives that I have learned the importance of knowledge and hard work. They continue to guide me today and I do not know what I would do without them.

My sibling, Dr Rati Sinha, has always lead the way for me. Despite the expected tiffs and quarrels that all siblings must endure, I know that I can always count on her unconditional love. I would perhaps not have gone into research at all had she not lead by doing her doctorate first. Her advice, whether professional or personal, has been invaluable to me and will continue to be so in the future. In her husband, Kunal, I have found the brother that I did not have. His counsel continues to help me improve every day. In my nieces, Tia, and Tisha, who have very recently made our lives so much more fulfilling and enjoyable, I have found even more reason to strive towards being

a better person. I pine to see them all again, for they have now become my second home.

Listing all my teachers is a mammoth task, for there are so many of them that have taught me such a variety of lessons, both academic and not, over the years. Here, I endeavour to mention ones that I remember, but this does not imply that the others did not shape me. It is merely that my memories from the earlier years of my life are not as vivid as they once were.

My years at Sherwood College, Naini Tal, have probably contributed most to my character today. The school's motto—*Mereat Quisque Palman (let each one merit his prize)*—set a strong principle for us to follow from the onset. At Sherwood, I had the fortune of being tutored by, among others, Ms May Parker, Mr Sharma, and Mr Das in junior school, and Ms Sharma, Mr Virk, Mr Sah, Mr Pant, Mr Kerr, Mr Dopaishi, Mr Chatterjee, Mr Pandey, Mr Tripathi, and Mr Choudhuri in senior school. In their own way, they trained me in subjects as varied as ethics, academics, sports, co-curricular activities such as elocution, art, and debating, and life in general. While our principal, Mr D. R. A. Mountford, did not teach me a subject off the syllabus, his weekly speeches at assembly gave us all much to think about. Various seniors, classmates, and juniors at school also contributed to my character via our constant interactions, and the lessons I learned at school will always remain with me.

My three years of coaching at Kota were an eye opener. It was the first time I had stepped out of the rather protected environment of school to compete with students from the whole of India. Studying with the best brains in the country made me realise how being one of the better ones in class at ones school was simply not good enough. Standards outside were higher, as they are in the global research community too. This exposure to higher standards of study and a more complex curriculum of science and maths helped me build solid foundations crucial to my research work.

It was at university that I finally started to learn computer science. I cannot thank my lecturers, Ms Shenoy, Ms Archana Kumar, Ms Shanti, Dr Dinesh Acharya, Dr Harish S. V., Dr Sudhakara, Mr Kumar Abhishek, and others enough. It was all the effort that they put in everyday that has ensured that I learned the skills necessary for a career that requires computer science.

During my undergraduate education, it was my two internships at the Indian Institute of Science under the supervision of Dr K. V. Raghavan where I was first introduced to the world of research. I am most grateful to him for taking on an undergraduate student that knew

nothing about research in programming languages. My interactions with various research students at the institute, and the workshops they held for us convinced me of my interest in research. The first paper I ever read, 'You and your research' (Hamming and Kaiser 1986), was suggested to us at one of these sessions, and I encourage early researchers to read it too.

It was also during my undergraduate education that I became a part of the Free software community (Stallman 2002) by joining the Linux Users' Group at university. Over the better part of a decade, apart from a plethora of technical skills, I have learned how to work in a collaborative environment that consists of people from different parts of the world, different walks of life, and with different interests. I continue to work with and learn from my colleagues at the Fedora project (RedHat 2008). I will continue to work towards furthering the Free software movement, for it goes hand in hand with the Open Science movement.

My first formal foray into the world of research began under the tutelage of Dr Jiangou Wang at the University of Technology, Sydney. The two years I spent pursuing my Masters (by research) degree taught me much about research. I am most grateful that as my supervisor Dr Wang permitted me to explore my research interests. This enabled me to work on a combination of neuroscience and robotics, and this paved the way to my switch to computational neuroscience. The high standards set by the Centre of Autonomous Systems, even on the football pitch with Dr Shoudong Huang's group, have given me an understanding of how a research group works together as a team, building on each member's strengths.

Whatever gratitude I show to everyone here at the University of Hertfordshire is perhaps insufficient. The research degree administrators, Ms Lorainne Nicholls, Ms Emma Thorougood, Ms Lynette Spelman, and Ms Michaella Guarnieri have efficiently managed all the paperwork that we must necessarily navigate. At the Doctoral College, Ms Kathy Lee, Ms Nicola Carter, Ms Emma King, and Dr Susan Grey have constantly kept an eye on us to ensure that nothing distracted us from our research. I am most grateful for the various efforts they have made to ensure that we make good independent researchers—grants, conferences, the Three Minute Thesis (3MT) competition. The teaching staff at the School of Computer Science accepted me as a Visiting Lecturer and permitted me to learn to be an educator as I worked with them. The administrators at the school, especially Ms Jo Horridge and Ms Suzanne Wild, have always been most helpful whether it be teaching related tasks or research conference bookings.

Before I thank my supervisors, I must thank the other members of staff here that have made time to improve me: Dr Yi Sun, Dr Rene te Boekhoerst, and Dr Bernadette Byrne. I am especially grateful to Professor Chrystopher Nehaniv who was my internal assessor throughout my Ph.D. and provided detailed feedback at my assessments to enable me to improve all aspects of my research work. The simulations that I run would not be possible without the UH High Performance Cluster (UHHPC), and I am most grateful to Professor Martin Hardcastle who, in spite of his extremely busy schedule, looks after it for us.

I cannot thank my supervision team enough—Professor Volker Steuber, Dr Christopher Metzner, Professor Rod Adams, Professor Michael Schmuker, and Dr Neil Davey. At every weekly meeting over these last few years, they have guided me. They have kept me focussed on my research question. In moments where I lacked enthusiasm, they have kept me trudging on. They have curtailed my tendency to get ahead of myself. They have managed my weaknesses and helped me develop my strengths. They have been stern when it was needed, and forgiven my many faults and mistakes. They have taught me the scientific method. They have taught me how to be a researcher. I hope that I will make good use of the lessons they have imparted to me in my future research endeavours.

I have been fortunate enough to have the opportunity to interact with the research community during my Ph.D. I have learned much from the members of the NEST initiative, where senior researchers such as Professor Hans Ekkehard Plesser and Dr Alexander Peyser have reviewed my work. I would not have been successful in my modelling of structural plasticity without the work of Sandra Diaz-Pier, a fellow doctoral candidate who did much of the work on adding it to the NEST simulator. I hope to continue collaborating with them all in the future. Other senior researchers such as Dr Benjamin Torben-Nielsen, who has shown me the beauty of dendrites among other things, and Dr Borys Wróbel, who taught me bifurcation analysis over a visit, have helped me immensely. The academic community on Twitter helps me stay aware of all that is going on in the community all over the world and I am thankful for their posts.

Finally, the people that keep me in line and help me maintain a good balance between work and life. Rachel, who reminds me of what is important in life and helps me be better everyday, I cannot thank enough. My friends, Ankita and Amitabh, Barbara and Saahil, Nancy and Alex, Maria and Dimitris, Jean, Marco, Sonia, and the many lab mates I have shared the office space with—Sam, Ed, Emil, Nathan, Julia, Ritesh, Yaqoob, Deepak, Ronak, Weam, Rebecca, and others—are my extended family. Also a part of my extended family are Ketki and Sheryll, who draw me to Sydney each day.

I apologise sincerely to those I may have missed. You forever have my thanks. I am the sum-total of all my experiences, and whether I consciously remember them them or not, your influence on me shall forever be a part of me.

Through my involvement in the Free/Open Source software (FOSS) (Stallman 2002) community over the years, I have learned to 'default to open'. Openness in the Free/Open source community is ensured by the Free Software Philosophy that protects, and ensures freedom of the user. It ensures that the user is able to 'run, copy, distribute, study, change, and improve software' and related resources.

In the short period that I have been a part of the scientific community, I have seen the community request similar rights over scientific resources too. Open Science is necessary for better science. For example, the reproduction, replication, and validation of scientific results is a critical part of the scientific process, and is stifled by the use of restricted methodologies (Crook, Davison and Plesser 2013). The complete set of resources related to a scientific study must be openly available to all—academics and society in general. This includes the tools used to gather the data, the data itself, the tools used to analyse the data and present the results, the results, and the accompanying manuscript that disseminates the contributions of the work to the body of knowledge. It must all be accessible to everyone, without exceptions.

It is easy to see that these requirements are very similar to the requirements laid out by the Free software philosophy. Recently, researchers from the computational neuroscience community signed an open letter committing to the use of Open Source software for all research work (Gleeson et al. 2017). I too have signed this letter, and here in my dissertation, I reiterate that I have made every effort to use Free/Open Source software that is available to all, and that all the tools, data, and results related to my work shall be openly available for all to run, copy, distribute, study, change, and improve. I hope that this will enable other researchers to validate, reproduce and replicate, and improve my work—furthering scientific knowledge as they do so.

This study relied heavily on FOSS tools. An incomplete list is below:

- NEST, Auryn simulators with MPICH/OpenMPI support,

- Vim with a plethora of plug-ins as the general purpose text editor,

- various command line utilities such as sed, awk, grep, Ag, rsync, Git, and OpenSSH for daily and remote work,

- the Python Science Stack and other modules usually with the Pew virtual environment manager, C++ libraries such as Boost, the GNU Debugger for investigating bugs in the NEST source code, bash shell scripts for processing and analysis, with GnuPlot for plotting,

- LaTeX for journaling, along with Overleaf for academic writing; JabRef for reference management; LibreOffice applications for non-plain-text writing,

- Inkscape, GIMP, Dia, ImageMagick, and the PGF/TikZ LaTeX packages for image creation and processing; Vimiv for image viewing,

- Byobu on Tmux for terminal multiplexing,

- Evolution or Neomutt with offlineimap and msmtp for e-mailing, Weechat/Irssi for communication over IRC and Slack,

- Taskwarrior, Vit, Timewarrior, Gnome-Pomodoro for time and task management,

- Qutebrowser/Firefox for web-browsing, Newsboat for RSS feed tracking, Zathura for document viewing,

- Syncthing for data backups and synchronization,

- Virt-manager and Gnome-Boxes for virtualisation,

- all on the GNOME integrated desktop environment,

- on Fedora Linux Operating System.

I am most grateful to the developers of these tools, and the generally volunteer driven communities that support them.

ABSTRACT

Several homeostatic mechanisms enable the brain to maintain desired levels of neuronal activity. One of these, homeostatic structural plasticity, has been reported to restore activity in networks disrupted by peripheral lesions by altering their neuronal connectivity. While multiple lesion experiments have studied the changes in neurite morphology that underlie modifications of synapses in these networks, the underlying mechanisms that drive these changes and the effects of the altered connectivity on network function are yet to be explained.

Experimental evidence suggests that neuronal activity modulates neurite morphology and that it may stimulate neurites to selectively sprout or retract to restore network activity levels. In this study, a new spiking network model was developed to investigate these activity dependent growth regimes of neurites. Simulations of the model accurately reproduce network rewiring after peripheral lesions as reported in experiments. To ensure that these simulations closely resembled the behaviour of networks in the brain, a biologically realistic network model that exhibits low frequency Asynchronous Irregular (AI) activity as observed in cerebral cortex was deafferented. Furthermore, to study the functional effects of peripheral lesioning and subsequent network repair by homeostatic structural plasticity, associative memories were stored in the network and their recall performances before deafferentation and after, during the repair process, were compared.

The simulation results indicate that the re-establishment of activity in neurons both within and outside the deprived region, the Lesion Projection Zone (LPZ), requires opposite activity dependent growth rules for excitatory and inhibitory post-synaptic elements. Analysis of these growth regimes indicates that they also contribute to the maintenance of activity levels in individual neurons. In this model, the directional formation of synapses that is observed in experiments requires that pre-synaptic excitatory and inhibitory elements also follow opposite growth rules. Furthermore, it was observed that the proposed model of homeostatic structural plasticity and the inhibitory synaptic plasticity mechanism that also balances the AI network are both necessary for successful rewiring. Next, even though average activity was restored to deprived neurons, these neurons did not retain their AI firing characteristics after repair. Finally, the recall performance of associative memories, which deteriorated after deafferentation, was not restored after network reorganisation.

9

CONTENTS

LIST OF TABLES

INTRODUCTION

> I keep six honest serving men (they taught me all I knew); their names are What and Why and When and How and Where and Who.
>
> Rudyard Kipling

1.1 MOTIVATION

Multiple plasticity mechanisms act simultaneously and at differing time scales on neuronal networks in the brain. Whilst synaptic plasticity is limited to the changes in efficacy of pre-existing synapses, *structural* plasticity includes the formation and removal of whole neurites and synapses. Thus, structural plasticity can cause major changes in network function through alterations in connectivity. Along with confirmation of structural plasticity in the adult brain (May 2011; A. K. Majewska, Newton and Sur 2006; Knott, Quairiaux et al. 2002; Lee et al. 2005), recent work has also shown that axonal boutons and branches (Stettler et al. 2006; Marik, Yamahachi, McManus et al. 2010; De Paola et al. 2006; Gogolla, Galimberti and Caroni 2007; Marik, Yamahachi, Alten Borgloh et al. 2014; J. L. Chen, Lin et al. 2011), and both inhibitory (J. L. Chen, Villa et al. 2012; Villa et al. 2016) and excitatory dendritic structures (Trachtenberg et al. 2002; A. J. G. D. Holtmaat et al. 2005) are highly dynamic even in physiological networks.

Stability in spite of such continuous plasticity suggests homeostatic forms of structural plasticity. A multitude of peripheral lesion experiments support the existence of such homeostatic structural plasticity mechanisms (Rosier et al. 1995; Heinen and Skavenski 1991; Rasmusson 1982; Wall and Cusick 1984; Pons et al. 1991; Darian-Smith and Gilbert 1994; Darian-Smith and Gilbert 1995; Salin et al. 1995; Florence, Taub and Jon H. Kaas 1998; Rajan et al. 1993; Allard et al. 1991; Sammons and Keck 2015). A common feature observed in these studies is the substantial network reorganisation that follows deafferentation. Recent time-lapse imaging studies of neurites in the cortex during the rewiring process show that both axonal (Yamahachi et al. 2009; Marik,

Yamahachi, McManus et al. 2010; J. L. Chen, Lin et al. 2011) and dendritic structures display increased turnover rates (Keck, Mrsic-Flogel et al. 2008; Trachtenberg et al. 2002; J. L. Chen, Lin et al. 2011; Hickmott and Steen 2005) in and around the area deafferented by the peripheral lesion, the Lesion Projection Zone (LPZ). Specifically, while excitatory neurons outside the LPZ sprout new axonal collaterals into the LPZ, inhibitory neurons inside the LPZ extend new axons outwards (Marik, Yamahachi, McManus et al. 2010). Along with an increased excitatory dendritic spine gain (Keck, Mrsic-Flogel et al. 2008) and a marked loss of inhibitory shaft synapses (J. L. Chen, Villa et al. 2012; Keck, Scheuss et al. 2011) in the LPZ, the rewiring of synapses in the network successfully restores activity to deprived LPZ neurons in many cases.

Access to such data and recent advances in simulation technology have enabled computational modelling of activity dependent structural plasticity (Butz, Van Ooyen and Wörgötter 2009; Deger et al. 2012; Butz and van Ooyen 2013; Butz and van Ooyen 2014; Butz, Steenbuck and van Ooyen 2014a; Butz, Steenbuck and van Ooyen 2014b; van Ooyen and Butz 2017). In their seminal work, Butz and van Ooyen introduced the Model of Structural Plasticity (MSP) framework (Butz, Van Ooyen and Wörgötter 2009). It has since been partially implemented in the NEST simulator (Diaz-Pier et al. 2016) and is an important tool for the computational modelling of structural plasticity (Gallinaro and Rotter 2018; Lu, Gallinaro and Rotter 2018). Butz and van Ooyen further demonstrated the utility of the MSP framework by simulating a peripheral lesioning study to explore the activity dependent growth rules of neurites (Butz and van Ooyen 2013; Butz and van Ooyen 2014).

Although these experimental and modelling works have added to our knowledge of structural plasticity, even though it is accepted that structural plasticity can cause significant changes in the functioning of brain networks, these changes have not yet been studied.

1.2 AIMS

The aim of this thesis is to contribute to the understanding of activity-dependent structural plasticity and its functional effects on injured networks using computational modelling techniques. Specifically, it reports the change in the ability of a simplified cortical balanced spiking network model to recall associative memories stored in it after the network has undergone deafferentation and subsequent repair by structural plasticity.

Thus, this thesis addresses the following question:

> How does repair by activity-dependent structural plasticity affect the function of a neuronal network as an associative memory store?

However, since this query requires the computational modelling of peripheral lesioning and activity-dependent structural plasticity, it must first address:

> How can neurites in a cortical network react to changes in the host neuron's activity to allow the restoration of stable activity in a deafferented network?

To address these questions, a balanced cortical spiking network model, which has been shown to serve as an associative memory store (Vogels et al. 2011), is deafferented and allowed to reorganise under the action of activity-dependent structural plasticity. Associative memories stored in this network in the form of Hebbian assemblies are recalled with and without network deafferentation and the difference in the Signal to Noise Ratio (SNR) compared to assess the effect of network re-organisation on the stored memories.

1.3 RESULTS

This dissertation makes the following contributions to the current state of the art:

- it reports on the capacity of cortical balanced spiking neural networks as stores of associative memory;

- it describes a novel biologically plausible spiking neural network model of peripheral lesioning and subsequent repair by activity-dependent structural plasticity;

- it proposes new activity dependent growth rules for various neurites;

- it indicates that activity-dependent structural plasticity may act as a homeostatic mechanism to stabilise individual neurons;

- it suggests that both structural and synaptic homeostatic mechanisms may be necessary for successful repair of an injured network;

- it shows that the recall performance of associative memories may not necessarily improve after an injured network has been repaired by homeostatic structural plasticity.

1.4 OVERVIEW OF THE THESIS

The thesis is organised into two parts. In Part i, I summarise the current state of our knowledge on the subject, and the contributions to the field are reported in Part ii.

In Part i, Chapter 1 documents currently available information on structural plasticity, with special focus on activity-dependent structural plasticity. Chapter 2 reviews our knowledge of associative memory from the perspective of its use as a proxy to study network function.

In Part ii, I report on the memory capacity of a balanced cortical spiking neural network model in its physiological state in Chapter 1. Next, in Chapter 2, I present the new model of peripheral lesioning and repair by activity-dependent structural plasticity. In Chapter 3, the new activity dependent growth rules for neurites distilled from the new model are documented. Chapter 4 records findings on the functioning of the cortical spiking neural model after peripheral lesioning in repair. Finally, in Chapter 5, I sum up my findings, detail their scope and limitations, and state the various avenues for future research that can be conducted based on my work.

Part I

CURRENT STATE OF THE ART

1

STRUCTURAL PLASTICITY

Structural plasticity, in general, refers to any changes in the structure or morphology of neurons in the brain. Given that neurons and the synapses between them underlie brain function, changes to either may alter it. This makes structural plasticity an important process that has received, and continues to merit, much attention.

Structural plasticity is most easily observed during development, where an initial aggressive period of synaptogenesis is followed by an equally active period of synaptic pruning in a 'critical period' (Wolff and Missler 1992). However, advances in experimental techniques have allowed a multitude of investigations to confirm that neurites constantly form and retract even in the adult brain (May 2011; A. K. Majewska, Newton and Sur 2006; Knott, Quairiaux et al. 2002; Lee et al. 2005; Stettler et al. 2006; Marik, Yamahachi, McManus et al. 2010; De Paola et al. 2006; Gogolla, Galimberti and Caroni 2007; Marik, Yamahachi, Alten Borgloh et al. 2014; J. L. Chen, Lin et al. 2011; J. L. Chen, Villa et al. 2012; Villa et al. 2016; Trachtenberg et al. 2002; A. J. G. D. Holtmaat et al. 2005).

Given the large set of entities that fall under the umbrella of structural plasticity, it is imperative to define the particular aspect of structural plasticity that this thesis discusses. First, since the research documented in this dissertation uses data gathered from peripheral lesion experiments in adult brains, the study of structural plasticity here was also limited to changes caused by peripheral lesions to the mature brain only. Second, the study focussed on changes in the growth of neurites due to changes in the activity of the neuron only: activity-dependent structural plasticity. It does not delve into the plethora of chemical agents or processes that are involved in the growth of dendritic (M. Fischer, Kaech, Knutti et al. 1998; Matus 2000; Matus, Brinkhaus and U. Wagner 2000; Rao and Craig 2000; Krucker, Siggins and Halpain 2000; M. Fischer, Kaech, U. Wagner et al. 2000; Halpain 2000; Star, Kwiatkowski and Murthy 2002; Brünig et al. 2004; Basu and Lamprecht 2018) or axonal structures (Gomez and Letourneau 2014; Dickson 2002; Tessier-Lavigne and Goodman 1996; Conti, S. J. Fischer and Windebank 2004; Rich and Terman 2018; S.-Y. Chen et al. 2018; Blanquie and Bradke 2018; Y. Liu et al. 2018; Gasperini et al. 2017). Finally, as this study investigated the functional consequences

of the reconfiguration of network connectivity by structural plasticity in terms of associative memory using a spiking neural network model, structural plasticity here is further limited to the formation and removal of neurites and the accompanying alterations in network structure only.

This chapter summarises information on activity-dependent structural plasticity currently available in the literature and computational modelling that has been used to investigate it.

1.1 EXPERIMENTAL EVIDENCE

Improvements in imaging technology now allow researchers to image microscopic neuronal structures in the brain. Structural plasticity, however, was detected indirectly in peripheral lesioning experiments long before these new tools came into being. Since peripheral lesions do not injure the brain itself, they provide a suitable paradigm for studying changes in the brain as a result of modulations in projecting inputs that affect network activity. This peripheral lesion protocol is still commonly used today.

To choose a suitable starting point, in 1982, Rasmusson ([1982](#)) studied anaesthetised *raccoons* at 2, 8, and 16 weeks after normal peripheral input to a region of the primary somatosensory cortex was removed by the amputation of the fifth digit. They reported that:

- at 2 weeks post-amputation, there was almost no response to sensory input in the fifth digit cortical area;

- at 8 weeks, 31 regions in the fifth digit cortical area responded to stimulations of other regions of the hand with approximately one third (10 of 31) localised to stimulation of the fourth digit with normal sized receptive fields;

- at 16 weeks, of 53 responsive regions, 35 had normal sized receptive fields with 27 responding to stimulations of the fourth digit.

The responsiveness of regions in the fifth digit cortical area to stimulation of the fourth digit suggested that some reorganisation was transferring projecting inputs from the fourth digit to these adjacent brain regions. Rasmusson discussed that the reorganisation could either result from the 'unmasking' of pre-existing connections or by the formation of new synapses. As both possibilities were supported by experiments at the time, they concluded by noting that more direct

investigations would be required to confirm the underlying mechanism.

Studies in a multitude of animals continued to report similar results. Wall and Cusick (1984) observed the remapping in the somatosensory cortex from sciatic inputs onto saphenous inputs following transection of the sciatic nerve in the hind-paws of *adult rats*. After the surgical amputation of digit 3, or of both digits 2 and 3 of *adult owl monkeys*, Merzenich et al. (1984) observed that the representation of adjacent digits and palmar surfaces had expanded to occupy most or all of the cortical territories that had originally responded to the amputated digits. Similarly, following the amputation of a single exposed digit on the forelimb in the *flying-fox*, Calford and Tweedale (1988) also observed that the neurons originally mapped to the missing digit now responded to the stimulation of the adjacent regions of the digit, hand, arm, and wing. In the V1 area of *adult monkeys*, Heinen and Skavenski (1991) observed that neurons became visually responsive after normal sensory input was removed by bilateral lesions.

Gilbert and Wiesel (1992) removed visual input by focal binocular retinal lesions in *monkeys* and reported immediate increases in the receptive field size of neurons whose receptive fields were near the edge of the retinal scotoma. Since a large region in the lateral geniculate nucleus (LGN) remained inactive in their study, and the dispersion of LGN afferents to the cortex was found inadequate to account for the cortical recovery, the topographic reorganisation in the cortex was suggested to be caused by synaptic changes intrinsic to the cortex. Pons et al. (1991) observed cortical reorganisation that far exceeded the then assumed possible spatial extent after deafferentation in *adult macaques*, further suggesting axonal sprouting as the underlying mechanism. Finally, while Rajan et al. (1993) confirmed similar reorganisation in the primary auditory cortex using cochlear lesions in *adult cats*, Florence, Taub and Jon H. Kaas (1998) confirmed that it was the growth of intracortical, and not thalamocortical, connections that accounted for the restructuring of sensory maps in the cortex of *adult macaques*. It was Darian-Smith and Gilbert (1994) and Darian-Smith and Gilbert (1995) in 1994, however, who used biocytin (King et al. 1989) labelling of axonal projections to confirm that axonal sprouting of long-range laterally projecting neurons into the Lesion Projection Zone (LPZ) accompanies topological reorganisation in the visual cortex. This work, spurred on by further advancements in imaging technology, has been followed by a number of experiments studying a variety of neurites.

Continuing the use of the peripheral lesioning protocol, Keck, Mrsic-Flogel et al. (2008) used intrinsic signalling and two-photon microscopy to study the changes in the circuitry in V1 area of the adult mouse over a period of months. Coherent with previous reports, they observed

that the initially unresponsive region regained responsiveness over a period of 2 months. In the first month following the lesion, there was a threefold increase in the rate of addition and subtraction of spines inside the LPZ, which corresponded to an almost complete replacement (> 90%) of the initial spines. Newly generated spines in the LPZ were predominantly transient in the first 2 weeks following a lesion. In contrast, many of the spines formed subsequently persisted for extended periods of time, indicating that they carry functional synapses. Overall, the new spines generated inside the LPZ were more likely to persist until the end of the experimental time period (2 months) than control spines, indicating that these structural changes may facilitate and stabilise the observed functional changes. Since Keck, Mrsic-Flogel et al. (2008) focussed on spines, they did not observe changes in axonal circuitry. Accordingly, they discuss that the high availability of axonal contacts in the primary visual cortex of the mouse may be sufficient to enable functional change by alterations in network circuitry at a local scale—by the turnover of dendritic spines alone.

Yamahachi et al. (2009) provided complementary information on axonal sprouting using similar imaging techniques to observe the effects of peripheral lesions in the primary visual cortex in macaques. The confirmed that a rapid turnover of axons by sprouting and pruning, in a process similar to that observed during development, was observed after peripheral lesions in the LPZ. The turnover was most elevated immediately after the lesion, and reduced in subsequent weeks. They documented that the resultant increase in density of axonal terminals in the LPZ correlated with its functional modifications, confirming that axonal turnover also played a role in the repair process.

In two studies in 2011, J. L. Chen, Lin et al. (2011) and Keck, Scheuss et al. (2011) investigated the effects of peripheral lesions on inhibition in the visual cortex. Keck, Scheuss et al. (2011) used similar techniques as in their previous work to study inhibitory neurons in the adult mouse visual cortex. They report that in the subset of inhibitory neurons receiving glutamatergic synapses on their dendritic spines, deafferentation caused a long term loss of these spines. Further, they also observed a reduction in the number of boutons in inhibitory neurons. These two observations together suggested that after deprivation, there is a drop in the excitatory input to inhibitory neurons, along with a reduction in the cell's synaptic output. This results in a lower overall inhibitory drive in the cortex which may trigger functional reorganisation. Chen et al. imaged the dendritic arbours of superficial L2/3 interneurons following deprivation. They report that deprivation increases the turnover of dendritic branch tips three fold, even though net arbour size per cell and average length change per branch tip remained stable due to similar elongations and retractions. Further, they

support past work suggesting that disinhibition enables structural plasticity in adult brain networks (Vetencourt et al. 2008) by discussing that the initial branch tip retractions and the accompanying loss of inhibitory axonal boutons observed immediately after deprivation serve to reduce the local inhibition in the region.

Whereas the aforementioned evidence confirms an inward sprouting of excitatory axons into the LPZ, it was Marik, Yamahachi, McManus et al. (2010) and Marik, Yamahachi, Alten Borgloh et al. (2014) that provided proof of the outgrowth of inhibitory axons from the LPZ. They recorded an increased turnover of inhibitory axons, and although it increased the reach of axons in the cortical space, it also resulted in a decrease in overall axonal density. They also observed axonal growth in the neurons adjacent to the LPZ but in the peri-LPZ, the rate was much less than that in the LPZ and peri-LPZ axons were not observed to sprout into the LPZ.

The proof summarised in Table 1 confirms that the brain retains its capacity for rewiring its circuits from development into adulthood. However, since this evidence is distilled from peripheral lesion experiments, it could be construed that this capacity of rewiring in the brain remains latent to be only triggered by large changes in network activity. To clarify whether this was so, while some peripheral lesion experiments also investigated structural changes in the normally functioning adult brain, other imaging work that focussed only on normal unlesioned adult brains was also carried out (Trachtenberg et al. 2002; Grutzendler, Kasthuri and Gan 2002; A. J. G. D. Holtmaat et al. 2005; De Paola et al. 2006; Stettler et al. 2006; J. L. Chen, Villa et al. 2012; Villa et al. 2016). They have confirmed that the brain is not hard-wired. In fact, similar to synaptic plasticity, they report that the brain continues to tweak its circuits in an experience dependent manner throughout adulthood. This suggests that structural plasticity is also likely to have Hebbian and homeostatic components that allow modification of brain circuits while maintaining stability.

1.2 COMPUTATIONAL MODELLING

Models of structural plasticity have been developed at various levels of detail to investigate the plethora of underlying mechanisms (van Ooyen 2011). Most recently, in 2013, Butz and van Ooyen proposed the Model of Structural Plasticity (MSP) framework that allows the modelling of activity-dependent structural plasticity in single compartment spiking point neurons (Butz and van Ooyen 2013). It is a refinement of earlier models (Dammasch, G. P. Wagner and Wolff 1986; Dammasch, G. P. Wagner and Wolff 1988; Butz, Lehmann et al. 2006; Butz and G.

Table 1: Summary of review of literature on peripheral lesion experiments.

Observation	References
Recovery of neural response in deafferented regions. Inward restoration of activity in LPZ.	Rasmusson (1982), Merzenich et al. (1984), Calford and Tweedale (1988), Heinen and Skavenski (1991), Gilbert and Wiesel (1992), Pons et al. (1991), Rajan et al. (1993) and Florence, Taub and Jon H. Kaas (1998).
Sprouting of axons into the LPZ.	Darian-Smith and Gilbert (1994) and Darian-Smith and Gilbert (1995).
Increase in density of dendritic spines on pyramidal cells in the LPZ.	Keck, Mrsic-Flogel et al. (2008).
Ingrowth of excitatory axonal terminals to the LPZ, resulting in increase in density of axonal terminals in the region.	Yamahachi et al. (2009).
Loss in dendritic spines on inhibitory neurons receiving glutamatergic inputs in LPZ.	Keck, Scheuss et al. (2011).
Reduction in inhibitory boutons in LPZ.	Keck, Scheuss et al. (2011).
Disinhibition in LPZ after deafferentation.	J. L. Chen, Lin et al. (2011) and Keck, Scheuss et al. (2011).
Outgrowth of inhibitory axons from the LPZ.	Marik, Yamahachi, McManus et al. (2010) and Marik, Yamahachi, Alten Borgloh et al. (2014).

Teuchert-Noodt 2006; Butz, Gertraud Teuchert-Noodt et al. 2008; Butz, Van Ooyen and Wörgötter 2009) based on the 'compensation theory' of synaptogenesis (Wolff and G. P. Wagner 1983). The compensation theory stated that neurons may react to deviations in their membrane potential either via electrophysiological responses, action potentials if the membrane threshold potential is crossed, or by slower morphogenetic responses which were suggested to include the 'formation, stabilisation or degradation of presynaptic and postsynaptic "contact offers"' (Wolff and G. P. Wagner 1983).

Based on this, in MSP, each neuron may possess sets of neurites, the growth of which are dependent on the time averaged activity of the
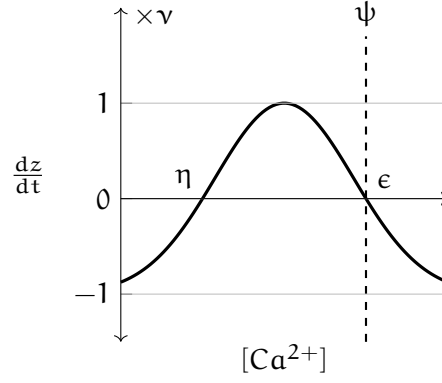
Figure 1: The rate of growth of neurites, dz/dt, is defined as a Gaussian function of the neuron's $[Ca^{2+}]$ (average activity) in MSP. Parameters η, ε and ν define the Gaussian curve, and ψ is the optimal activity required by the neuron.

neuron. This is modelled as the concentration of calcium in neurons, $[Ca^{2+}]$, and is based on two observations:

- $[Ca^{2+}]$ is strongly linked to the growth of neurites (Kater et al. 1988; Al-Mohanna, Cave and Bolsover 1992; Lohmann and Wong 2005; Wong and Ghosh 2002; Brünig et al. 2004; Gasperini et al. 2017; Mikhaylova et al. 2018; Oertner and Matus 2005; Lohmann, Finski and Bonhoeffer 2005);

- $[Ca^{2+}]$ correlates with the average activity of the neuron.

Though the framework is not limited to spiking neurons only—any average measure of activity may be used—for spiking neurons, the $[Ca^{2+}]$ is calculated from neuronal spiking:

$$[Ca^{2+}] = [Ca^{2+}] + \beta, \qquad \text{for each spike} \qquad (1)$$

$$\frac{d[Ca^{2+}]}{dt} = -\frac{[Ca^{2+}]}{\tau_{[Ca^{2+}]}}, \qquad \text{otherwise.} \qquad (2)$$

Here, $\tau_{[Ca^{2+}]}$ is the time constant with which the $[Ca^{2+}]$ decays in the absence of a spike, and β is the constant increase in $[Ca^{2+}]$ caused by each spike.

A Gaussian growth curve describes the rate of growth for each type of neurite (Figure 1), dz/dt, which is defined as:

$$\frac{dz}{dt} = \nu \left(2\exp^{-\left(\frac{[Ca^{2+}]-\xi}{\zeta}\right)^2} - 1 \right)$$

$$\xi = \frac{\eta + \epsilon}{2}, \qquad (3)$$

$$\zeta = \frac{\eta - \epsilon}{2\sqrt{-\ln(1/2)}}$$
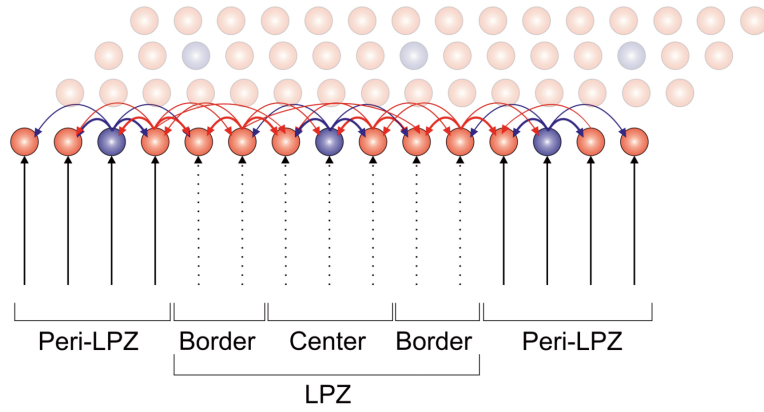
Figure 2: Excitatory (Red) and inhibitory (Blue) neurons are evenly distributed in a two-dimensional sheet in the model developed by Butz and van Ooyen (2013). All neurons receive recurrent inputs from the network, and external inputs. The removal of external inputs to a part of the network results in the formation of the LPZ. (Taken from Butz and van Ooyen (2013), published under a CC-BY license)

Here, ν is a scaling factor, and ξ and ζ together (in terms of η and ϵ) define the width and location of the Gaussian curve on the x-axis. At η and ϵ, $dz/dt = 0$. As documented in later sections, this constraint is used to derive families of growth curves for different neurites.

The formation or removal of synapses depends on the total numbers of 'partner' neurites. Consider an excitatory neuron with two sets of neurites:

- excitatory post-synaptic dendritic neurites: z_{post},

- and excitatory pre-synaptic axonal neurites: z_{pre}.

If, in a network of such neurons, the neuronal activity dictates that two neurons have 'free' pre- and post-synaptic neurites respectively, these free elements may combine to form new synapses. Similarly, if a neuron has z_{conn} neurites of a type engaged in synapses but must retract N of these on account of its activity, it will break N synapses. Free elements borne by neurites, even if released by the breakage of synapses in partner neurons, may immediately form new synapses with new partners. If they remain unconnected, however, they decay over time with the time constant τ_{free}:

$$\frac{dz_{free}}{dt} = -\frac{z_{free}}{\tau_{free}} \tag{4}$$

In the paper, Butz and van Ooyen also demonstrated the use of MSP to propose growth rules for sets of neurites by modelling a peripheral lesion experiment (Figure 2). In this model, each neuron, whether exci-

(a)

(b)
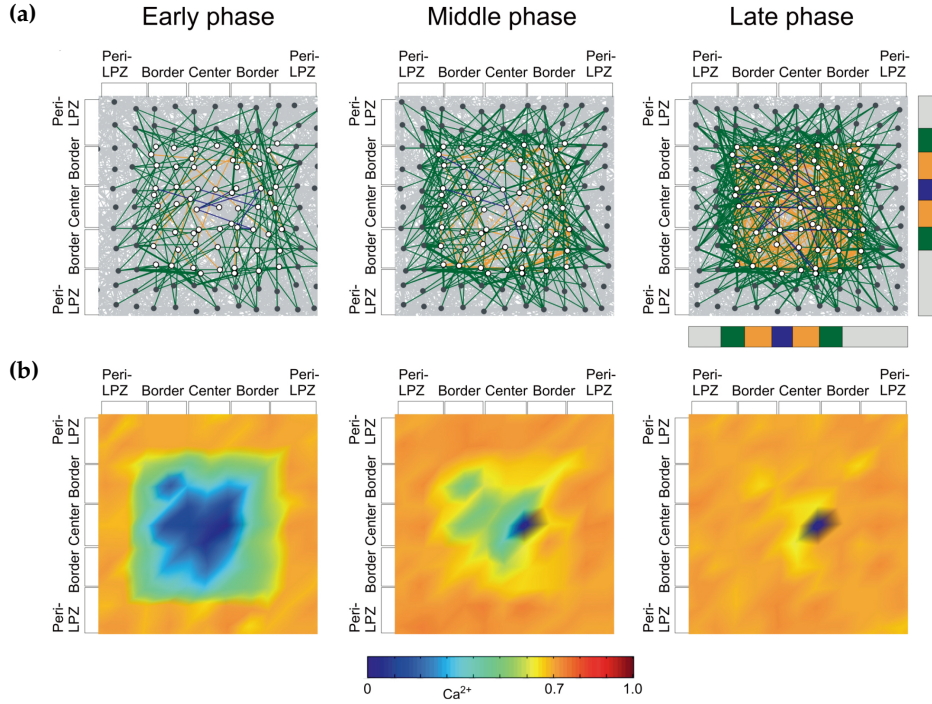
Figure 3: Restoration of activity to neurons and the accompanying reorganisation of synapses in the LPZ in Butz and van Ooyen (Butz and van Ooyen 2013): **(a)** shows the connectivity in the network. Synapses formed after deafferentation that project on to the LPZ are colour labelled. Pre-existing and other connections in grey cover most of the background. Connections from the peri-LPZ are in green, from the border of the LPZ yellow, and from the centre blue. **(b)** shows the $[Ca^{2+}]$ of neurons in the network. Depending on the size of the LPZ, activity may not be restored to all neurons in it. (Taken from Butz and van Ooyen (Butz and van Ooyen 2013), published under a CC-BY license)

tatory or inhibitory, bore both excitatory (z_{post}^{E}) and (z_{post}^{I}) dendritic neurites. Both sets of dendritic neurites on both sets of neurons shared identical Gaussian growth rules. Similarly, for axonal neurites as well, while excitatory and inhibitory neurons only bore excitatory (z_{pre}^{E}) and inhibitory (z_{pre}^{I}) axonal neurites respectively, these still shared identical Gaussian growth rules.

To set up the growth curves, an arbitrary optimal activity level was chosen for the whole population of neurons (ψ). Next, the value of ϵ was set as a 'stable fixed point' by setting its value also to ψ. In this scenario, if a neuron has more activity than necessary, it will retract all neurites to reduce its activity. If it has less activity than required (but more than a minimal amount, η), on the other hand, the neuron will sprout all neurites in an attempt to increase its activity. The formation of new synapses between free elements occurs in a distance dependent manner: neurons closer to each other are more likely to form synapses. The selection of synapses for removal, however, is done randomly.
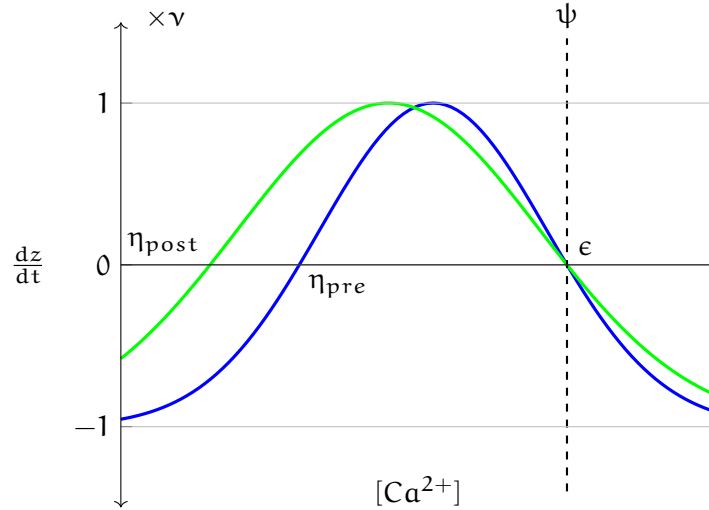
Figure 4: Growth curves for neurites as proposed by Butz and van Ooyen (2013). Green: post-synaptic neurites; Blue: pre-synaptic neurites. Since all neurons had the same preset optimal $[Ca^{2+}]$, ψ, $\epsilon = \psi$ for both growth curves. Butz and van Ooyen (2013) proposed that for activity to be restored to the neurons in the LPZ inwards, from its border to its centre, post-synaptic elements must be formed before, at a lower activity level than, pre-synaptic elements ($\eta_{post} < \eta_{pre}$).

A network with 320 excitatory and 80 inhibitory unconnected neurons spread out in a two-dimensional sheet is initialised in the presence of an external stimulus, and is observed to 'grow' to a stable network. In this state, the network is deafferented to form a LPZ and allowed to repair under the action of the structural plasticity mechanism. As Figure 3 shows, the activity flows into the LPZ due to the ingrowth of axonal projections into the LPZ as documented in experiments. The simulations suggested that these experimental observations could only be reproduced if post-synaptic elements formed before their pre-synaptic counterparts: $\eta_{post} < \eta_{pre}$ (Figure 4).

Table 2 summarises the experimental observations reproduced by Butz and van Ooyen (2013). The simulations of this model do exhibit the ingrowth of excitatory axons to the LPZ. However, because identical growth curves were used for all pre-synaptic neurites, it also exhibits an ingrowth of inhibitory axons unlike reports from experiments. Similarly, because the growth of all post-synaptic neurites on all neuron sets was modulated by identical growth curves, neurons in the LPZ also gained inhibitory dendritic neurites along with excitatory ones contrary to experimental observations. Moreover, since the investigation did not intend to study structural plasticity in any specific brain region or network, the stable network was not derived from experimental data. It, therefore, does not model the adult cortical brain network that this thesis focuses on.

Table 2: Summary of experimental observations reproduced in the model proposed by Butz and van Ooyen (2013).

Experimental observation	Reproduced
Gradual inward restoration of activity in LPZ.	Yes.
Sprouting of axons into the LPZ.	Yes.
Increase in density of dendritic spines on pyramidal cells in the LPZ.	Yes.
Ingrowth of excitatory axonal terminals to the LPZ, resulting in increase in density of axonal terminals in the region.	Yes.
Loss in dendritic spines on inhibitory neurons receiving glutamatergic inputs in LPZ.	No—increase of all synaptic elements in neurons of LPZ.
Reduction in inhibitory boutons in LPZ.	No—increase in inhibitory axonal contacts also.
Disinhibition in LPZ after deafferentation.	No.
Outgrowth of inhibitory axons from the LPZ.	No—ingrowth of inhibitory axons also.

As the core of the model, the use of $\psi = \epsilon$ to set up a 'stable fixed point' in the growth curves merits some discussion. Even though it may be intuitive that a neuron should sprout dendritic (input) elements when it requires more activity (more input), this assumes that the activity of neurons is mediated by their excitatory inputs only. However, it is now established that the activity of individual neurons and their networks is a fine balance of excitation and inhibition (Michael Okun and Ilan Lampl 2008; M. Okun and I. Lampl 2009). Therefore, a neuron can gain activity by gaining excitatory inputs or losing inhibitory ones. Conversely, a neuron can lose activity by retracting excitatory inputs or gaining inhibitory ones. This balance between excitation and inhibition (E-I balance) is not reflected in the growth curves proposed by Butz and van Ooyen (2013). To add to the limitations of this hypothesis, it does not apply to pre-synaptic neurites which may not affect the activity of the neuron they belong to. The only constraint one may apply to the growth curves is that at the optimal activity level, ψ, the rate of growth of all neurites, dz/dt, should be 0. As we see from the growth curves derived by the novel model of peripheral lesioning described in Part ii, both $\eta = \psi$ and $\epsilon = \psi$ satisfy this constraint.

Similar models based on MSP have also been used to study other effects of structural plasticity, such as its effects on the connectivity characteristics of the deafferented network (Butz and van Ooyen 2014; Butz, Steenbuck and van Ooyen 2014a; Butz, Steenbuck and van Ooyen 2014b). The NEST simulator (Diesmann and Gewaltig 2001) now includes a partial implementation of MSP (Diaz-Pier et al. 2016)—it allows for neurons to bear neurites, and it allows for the formation and removal of synapses albeit using random selection only. Unfortunately, since the source code for the work described in Butz and van Ooyen (2013) or subsequent work (Butz and van Ooyen 2014; Butz, Steenbuck and van Ooyen 2014a; Butz, Steenbuck and van Ooyen 2014b) was not based on NEST and has not been made openly available, it has also not yet been replicated.

1.3 CHAPTER CONCLUSIONS

As imaging studies continue to investigate the brain at the microscopic scale, more and more information on its structural plasticity continues to be generated. It is now clear that neurites in the adult brain are continuously formed and removed but the mechanisms underlying this turnover are still being explored. Peripheral lesion experiments provide an appropriate protocol for exploring the effects of sensory deprivation on brain networks. This chapter summarised experimental evidence from a selection of sensory deprivation studies in its first section. By going through the evidence in chronological order, it provided an overview of how the field went from observing structural plasticity indirectly to confirming the formation and removal of neurites and their accompanying synapses.

In the latter half, the chapter provided a overview of the MSP computational modelling framework that was developed to model activity-dependent structural plasticity. Further, it focussed on the most recent model of peripheral lesioning that used this framework to propose activity dependent growth rules for neurites. While the model did provide testable predictions, these were incomplete. This chapter enumerated limitations of the model that made it unsuitable for use in this thesis to justify the development of the novel model documented in Part ii.

MEASURING NETWORK FUNCTION: ASSOCIATIVE MEMORY

Memory is defined as the record of experience represented in the brain (Eichenbaum 2008). Even though this definition of memory is general enough, studies over the years have classified it based on different criteria: by awareness of remembrance and recall, by its term or duration, and by underlying processes (Figure 5).

As introduced in Chapter 1, the goal of this study was to explore the effects that homeostatic structural plasticity based repair has on the function of a cortical network that had been deafferented. Associative memory has been relatively well understood and modelled over the years, and was thus chosen as a convenient network function to investigate.

Associative memory can be broadly defined to include 'any memory about the relationship between two or more items' (Suzuki and Eichenbaum 2006), and studies in fields of psychology and in neuroscience have indicated that multiple regions of the brain are involved in memory storage, consolidation, and recall (Eichenbaum 2008; Cohen et al. 1999; Suzuki and Baxter 2009; Suzuki and Eichenbaum 2006). A detailed discussion of the state of memory research, however, is beyond the scope of this chapter.

The mechanisms underpinning learning, or association, in the brain were first postulated by Hebb:

> When an axon of cell A is near enough to excite B and repeatedly or persistently takes part in firing it, some growth process or metabolic change takes place in one or both cells such that A's efficiency, as one of the cells firing B, is increased (Hebb (1949))

Such a *Hebbian* mechanism, Long-Term Potentiation (LTP), was confirmed in experiments by Bliss and Lømo (1973) in the hippocampus (and later in the cortex by Artola and Singer (1987)) and stimulated the research of plasticity in the brain. Knowledge that brain networks are plastic and undergo alterations gave rise to further questions regarding the stability of these networks (Abraham and Robins 2005). This resulted in the creation of a separate sub-field of plasticity re-
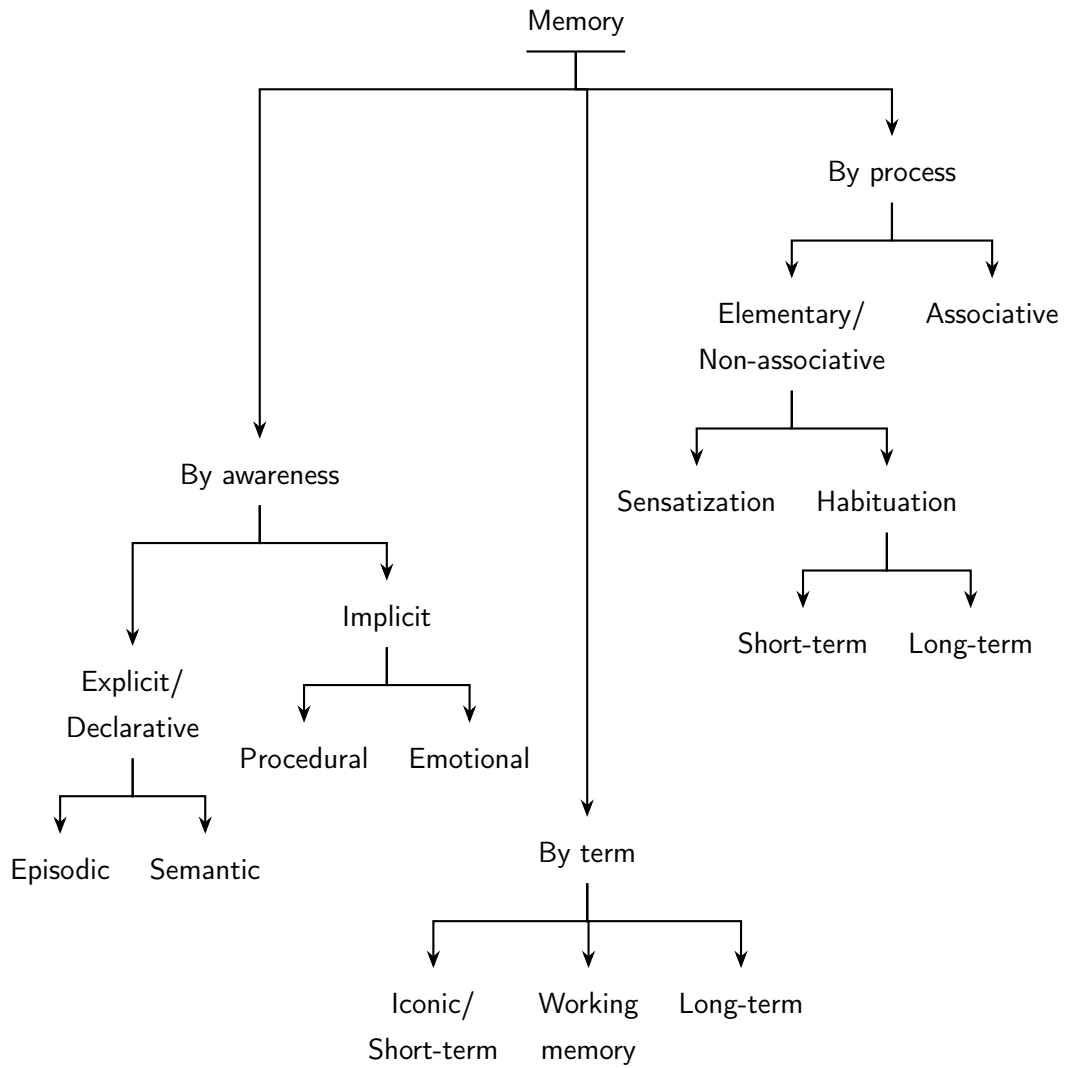
Figure 5: General categorisation of memory in literature. Please see Eichenbaum (2008) for a review.

search dedicated to *homeostatic* plasticity (Turrigiano 1999). Whilst these studies are generally limited to synaptic plasticity, the subject of this study, structural plasticity, is also gradually gaining research focus (van Ooyen and Butz 2017).

Although a number of associative memory models were developed, it was the Associative Net, also commonly called the Willshaw Net, a model of non-holographic distributed associative memory (Willshaw, Buneman and Longuet-Higgins 1969; Willshaw 1971), that served as a starting point for the modelling of associative memory stores. Associative memory was defined in terms of the concept of Classical Conditioning by David Willshaw in his PhD thesis:

> Consider a system in which the event X is causally related to the event Y which follows it. If the event Z occurs coincidentally with X and a mechanism operates, such that subsequently Z on its own will cause Y, then Classical Conditioning is said to have taken place. We employ this analogy by considering the special case when X and Y are identical. Then information has been stored by the mechanism of Classical Conditioning when the information to be stored (Y) and the address to locate it (Z) are together input to the store, so that subsequently the address alone will locate the stored information. This is an associative store. (Willshaw (1971))

In this early model of associative memory, neurons and synapses were both binary, i.e., they could take values of 0 or 1. A simple clipped Hebbian learning rule changed connection weights from 0 to 1 if the input and output units (neurons) were both active for the same input and output pattern pair. The model allowed a myriad of investigations into associative memory, its capacity, connectivity, and performance (Buckingham and Willshaw 1992; Graham and Willshaw 1997; Graham and Willshaw 1999; Graham and Willshaw 1995; Dayan and Willshaw 1991).

Another well known model of associative memory is the Hopfield Network (Hopfield 1982) where synaptic connections are also updated by a Hebbian rule such that 'memory vectors' form the local minima of an energy function. Thus, on the presentation of a partial memory, the system converges to the attractor to recall the stored memory (Hopfield 2007).

Modifications and derivations of these two seminal models have led to much work on associative memory (Palm 1980; Amit and A. Treves 1989; N. Davey and R. Adams 2004; N. Davey, Hunt and R. Adams 2004; N. Davey, Calcraft and R. Adams 2006; Bohland and Minai
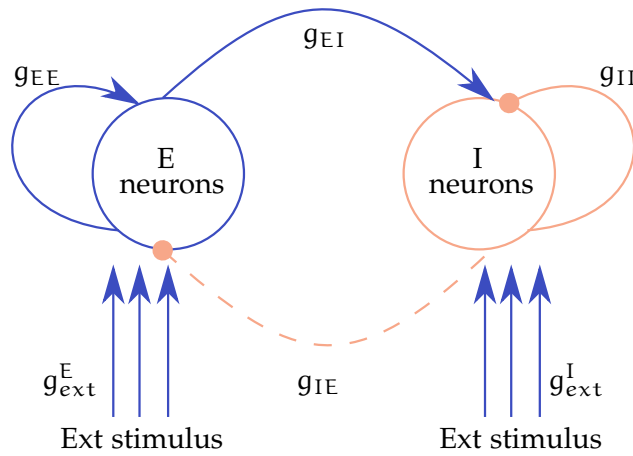
Figure 6: Overview of synapses in Vogels et al. (2011): Excitatory (E) and Inhibitory (I) neurons ($N_E = 4N_I$ (see Table 4)) are initially connected via synapses with a connection probability of ($p = 0.02$). All synapses (EE, EI, II), other than IE synapses, which are modulated by inhibitory spike-timing dependent plasticity, are static with conductances g_{EE}, g_{EI}, g_{II}, respectively. External Poisson spike stimuli are provided to all excitatory and inhibitory neurons via static synapses with conductances g_{ext}^E and g_{Inh}^I, respectively.

2001; Lansner 2009) also in spiking neuronal networks (Anishchenko and Alessandro Treves 2006; W. Chen et al. 2011; Hiratani, Teramae and Fukai 2013), and on neuromorphic hardware (Stöckel et al. 2017). Recently, when investigating a new Spike Timing Dependent Plasticity (STDP) rule for inhibitory synapses, Vogels et al. (2011) demonstrated that their inhibition balanced network exhibited cortical low frequency Asynchronous Irregular (AI) (Brunel 2000) firing and could be used as a store for *attractor-less* associative memories. The biological plausibility of this network model, and the novel implementation of associative memory it proposed made it a good fit for use in this study. The next section includes a brief description of this model of associative memory. The chapter then concludes with a description of the Signal to Noise Ratio (SNR) metric as a measure of associative memory performance and a short discussion.

2.1 VOGELS-SPREKELER MODEL OF ATTRACTOR-LESS ASSOCIATIVE MEMORY

The primary aim of Vogels et al. (2011) was to present a new homeostatic STDP model for inhibitory synapses, based on experimental
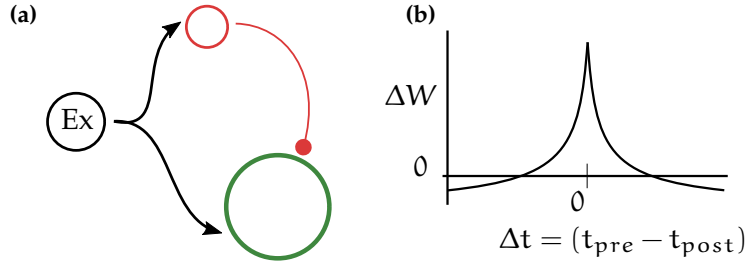
Figure 7: (a): A neuron (green) receives direct excitation and indirect inhibition (red). The inhibitory synapse is modulated by the inhibitory STDP rule such that excitatory and inhibitory post-synaptic currents are balanced. **(b):** Schematic of the symmetric inhibitory STDP rule developed by Vogels et al. (2011). Irrespective of the order of the pre and post-synaptic spikes, their co-incidence facilitates the synapse. Each pre-synaptic spike, however, causes a constant depression. (ΔW is the change in synaptic weight, t_{pre} and t_{post} are spike times for the pre and post-synaptic neuron respectively.)

observations made by Woodin, Ganguly and Poo (2003). In this model, co-incident pre- an post-synaptic spiking results in the strengthening of the involved synapse (Figure 7). Notably, unlike the asymmetric learning rule that governs STDP in excitatory synapses (Bi and Poo 1998; Sjöström and Gerstner 2010), this learning rule is symmetric—the synapse is strengthened irrespective of the order of the pre- and post-synaptic spikes. A constant depression caused by spiking of only the pre-synaptic neuron weakens the synapse.

Formally, to calculate the change in the synaptic weight W_{ij} for a synapse projecting from neuron j to neuron i, each neuron is assigned a synaptic trace x, such that the synaptic trace increases with each spike, $x = x + 1$, and decays otherwise with the time constant τ_{STDP}:

$$\tau_{STDP} \frac{dx}{dt} = -x \tag{1}$$

W_{ij} is then updated for every pre- and post-synaptic event such that:

$$W_{ij} = \begin{cases} W_{ij} + \eta(x_i - \alpha) & \text{for pre-synaptic spikes at time } t_j \\ W_{ij} + \eta x_j & \text{for post-synaptic spikes at time } t_i \end{cases} \tag{2}$$

where η is the learning rate, $\alpha = 2 \times \rho_0 \times \tau_{STDP}$ is the constant depression factor, t_i and t_j are times when neuron i and j spike respectively, and ρ_0 is a constant parameter. Using simulations and mathematical analysis, Vogels et al. (2011) show that the post-synaptic firing rate depends linearly on the strength ρ_0 of the synaptic depression, and in cases where spike-spike correlations may be neglected, the firing rate of the post-synaptic neuron approximates to ρ_0 itself. Thus, the learning rule implements a form of homeostatic plasticity that stabilises the post-synaptic neuron to a target firing rate.
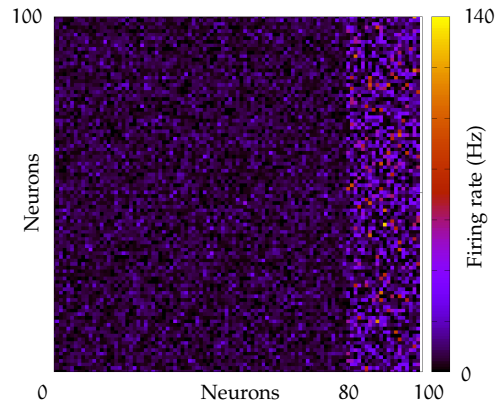
Figure 8: The inhibitory STDP rule developed by Vogels et al. (2011) strengthens inhibitory synapses in the network to maintain it in a low frequency AI regime that is observed in the cortex. (In this and following figures: 100×100 grid shows a snapshot of the firing rate of 10000 neurons in the network. Left: excitatory population of 8000 neurons; Right: inhibitory population of 2000 neurons)

Using single neuron simulations where the neuron receives excitatory and inhibitory inputs, Vogels et al. (2011) showed that the STDP rule strengthens inhibitory synapses until the excitatory and inhibitory post-synaptic membrane currents became approximately balanced. Further, using network simulations (Figure 6), they showed that the inhibitory plasticity mechanism balances a cortical network and maintains it in a low firing AI firing regime. Figure 8 shows a two dimensional top view of the network of neurons in this steady state. The excitatory and inhibitory sets of neurons can be seen on the left and right respectively. Please note that the neurons do not have any spatial relationships in this model—they are placed in this arrangement solely for visualisation purposes.

This network, which is balanced by homeostatic inhibition, was then demonstrated to serve as a store for attractor-less associative memories. Associative memories were stored in the network by strengthening the synapses between a set of excitatory neurons. Although this resulted in an increase in activity of the excitatory neurons forming the associative memory, the inhibitory STDP mechanism increased the efficacy of inhibitory neurons projecting onto these neurons to return the network to its balanced state. Since the strengthened excitatory synapses in the associative memories remain unaffected, these can be recalled by stimulating a subset of the neurons of the stored associative memories. When the recall stimulus is withdrawn, the network returns to its balanced state. This can be observed in Figures 9a and 9b.

(a)

(b)
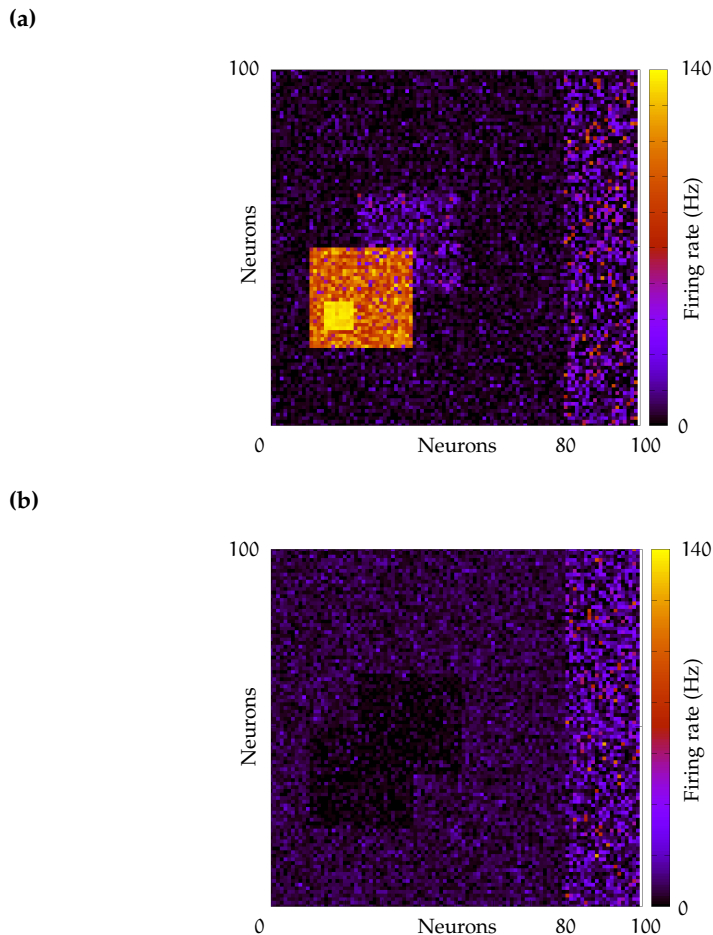
Figure 9: A spiking network balanced by homeostatic inhibitory plasticity serves as a store for attractor-less associative memory (Vogels et al. 2011). **(a)**: Two associative memories are stored in the network by strengthening the excitatory synapses between sets of excitatory neurons. Inhibitory synapses are strengthened by the homeostatic inhibitory STDP mechanism to restore the network to its balanced AI firing regime. When an external recall stimulus is provided to a subset of neurons forming one of the stored associative memories, the lateral excitation enables its recall. **(b):** Under the action of the homeostatic inhibitory STDP mechanism, the network returns to its balanced AI steady state when the external recall stimulus is withdrawn.

The inhibitory STDP rule proposed by Vogels et al. (2011) has been noted to not accurately depict the experimental observations made by Woodin, Ganguly and Poo (2003) (Vogels et al. 2012). Woodin, Ganguly and Poo (2003) identified the underlying mechanism for the increase in synaptic efficacy to be the shift in the reversal potential of post-synaptic GABAergic currents (E_{GPSC}) to more positive values for co-incident pre- and post-synaptic activity. Vogels et al. (2011), however, model the increase in synaptic efficacy as an increase in synaptic conductance. On the other hand, the learning rule does correctly model the constant reduction in synaptic conductance, which

was only observed for repetitive pre-synaptic activity in the absence of post-synaptic activity (Woodin, Ganguly and Poo 2003).

In spite of this observation, the inhibitory STDP rule and the novel model of a cortical balanced network are both important contributions to the field. Even though inhibition has traditionally been relegated to a homeostatic role in the brain, much work needs to be done to improve our understanding of its various mechanisms and effects (Isaacson and Scanziani 2011; Sprekeler 2017). Vogels et al. (2011) also provided the complete set of parameters that were used in the study which enabled the re-implementation of the network model first in the Auryn (Zenke and Gerstner 2014) and later in the NEST (Gewaltig and Diesmann 2007) simulators and verification of their results. The figures used in this chapter were generated from the Auryn implementation made in the initial stages of this study.

## 2.2 SIGNAL TO NOISE RATIO AS A MEASURE OF ASSOCIATIVE MEMORY CAPACITY

Having selected a model of associative memory, it was required to select appropriate metrics to measure its performance in the study. As Graham and Willshaw (1997) document, the performance of a distributed memory store can be described in terms of capacity and information efficiency. The capacity of a memory store is the number of memories that can be stored and recalled at some allowable error rate. The information efficiency is the ratio of the amount of information that can be retrieved from the store to the amount of storage available.

Dayan and Willshaw (1991) suggested the use of the SNR of the associative memory being recalled as the metric to measure the memory capacity of the network. The SNR for an associative memory being recalled is given by:

$$S/N = \frac{(\mu_p - \mu_b)^2}{0.5(\sigma_p^2 + \sigma_b^2)} \tag{1}$$

Here, μ_p and σ_p are the mean and standard deviation of the firing rates of the neurons forming the associative memory being recalled (the signal); and μ_b and σ_b are the mean and standard deviation of the firing rates of the neurons not belonging to the associative memory, therefore forming the background (the noise).

Consider two inputs that are given to a single unit that must distinguish between them—'lows' and 'highs'—based on the 'dendritic sum' it receives. The dendritic sums translate proportionately to the
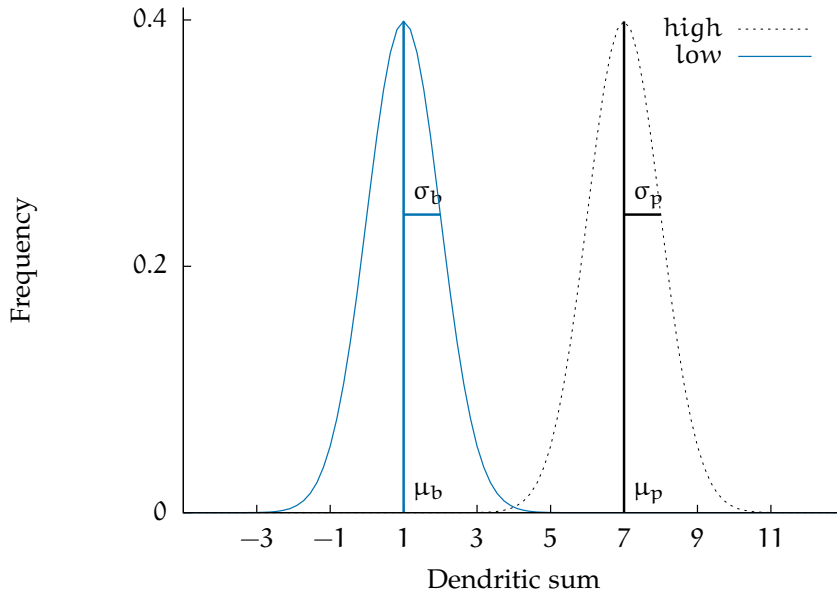
Figure 10: Distributions of 'low' and 'high' dendritic sums.

population firing rates received by the unit and are assumed to exhibit Gaussian distributions. The 'lows' correspond to the background inputs, while the 'highs' correspond to the pattern inputs. The distributions of dendritic sums for the two inputs are both approximately Gaussian—$\mathcal{G}(\mu_b, \sigma_b)$ and $\mathcal{G}(\mu_p, \sigma_p)$ respectively, as illustrated in Figure 10. Then, it will be easy to distinguish between these two signals if:

1. the peaks of the Gaussians are far apart, i.e., $(\mu_p - \mu_b)$ is large, and/or

2. the peaks of the Gaussians are narrow, i.e., the noise in these two signals—σ_p and σ_b—are small.

The formula for the SNR, Equation (1), incorporates both these effects and maximising it should, therefore, enhance separability.

It is non-trivial to say what value of SNR would be sufficient for pattern separation in the brain. Since this study focusses on the *change* in the SNR as a result of deafferentation and network repair, the base value of SNR is chosen to be one that clearly shows the recall of the stored associative memories in the normally functioning network upon visual inspection, for example, in Figure 9.

2.3 CHAPTER CONCLUSIONS

This chapter explains the selection of the storage and recall of associative memories as an appropriate network function for investigation during repair by structural plasticity in this study. A brief overview of memory was given, with focus on associative memory. Next, the use of the new model of a balanced cortical network exhibiting low frequency AI firing characteristics under the action of a novel inhibitory STDP rule (Vogels et al. 2011) was discussed. This model served as a suitable starting point for the study. Additionally, the simulation protocol used in (Vogels et al. 2011) also aided the design of simulation protocols used in the study. Finally, SNR was described as a metric to measure the performance of associative memory stores.

This chapter concludes the description of the current state of the art. The next part of this thesis will document the use of the information gathered here to carry out the study.

Part II

CONTRIBUTIONS TO THE FIELD

PERFORMANCE OF BALANCED NETWORKS AS ASSOCIATIVE MEMORY STORES

To investigate the performance of associative memory after deprivation and repair in this study, it was required to first establish the performance of associative memory in a physiological network model, one that has not experienced sensory deprivation by peripheral lesions.

In this chapter, the performance of the balanced cortical network model proposed by Vogels et al. (2011) as an associative memory store is described. The model was first replicated and verified (as discussed in Part i). Next, where Vogels et al. (2011) limited their discussion to the storage and recall of a pair of overlapping associative memories only, in this study, the performance of the network as an associative memory store was quantified using the Signal to Noise Ratio (SNR) metric (Equation (1)). Additionally, the capacity of the network was also investigated by storing multiple associative memories in it.

The work detailed in this chapter was disseminated as a poster at CNS*2015:

- Ankur Sinha, Neil Davey et al. (2015). 'Structural plasticity and associative memory in balanced neural networks with spike-time dependent inhibitory plasticity'. In: *BMC Neuroscience* 16.1, p. 1. URL: http://www.biomedcentral.com/1471-2202/16/S1/P235.

1.1 SIMULATION PROTOCOL

Since the Auryn simulator (Zenke and Gerstner 2014) was used by Vogels et al. (2011) in their work, it was also used for this stage of the study. Using the same simulation protocol as Vogels et al. (2011) (Figure 11), the network was allowed to stabilise to its Asynchronous Irregular (AI) state after which the excitatory synapses between a randomly selected set of excitatory neurons were strengthened to g_{pat} by a potentiation factor χ to form the Hebbian assembly:

$$g_{pat} = \chi \times g_{EE} \tag{1}$$

where g_{EE} is the synaptic conductance of the excitatory synapse as set up initially in the model.
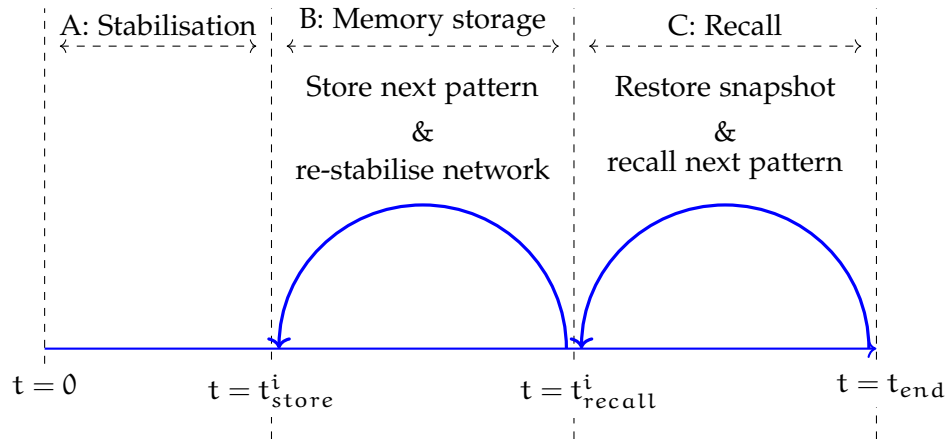
Figure 11: Simulation protocol for associative memory performance simulations: the network is set up with its initial connectivity and allowed to stabilise to its AI regime. Then, at t_{store}^1, an associative memory is stored by strengthening the synapses between a randomly selected set of neurons. The network is again allowed to re-stabilise to its AI state. If needed, more patterns are stored in the network in this way. When the last associative memory has been stored and the network returned to its balanced state a snapshot of the network is saved. Then, the stored associative memories are recalled by providing stimulus to a subset of the neurons forming each pattern. The firing rates of the neurons in the associative memory, forming the pattern, and the rest of the neurons of the population, which form the background, allow the calculation of the SNR. After an associative memory has been recalled at $t = t_{recall}^i$, the network snapshot is restored before the next one is recalled at t_{recall}^{i+1} to ensure that the recalling of an associative memory does not affect future recalls.

The strengthening of lateral excitatory synapses causes an increase in the activity of the network. Therefore, inhibitory synaptic plasticity was allowed to re-establish the AI state of the network before an external stimulus was provided to a randomly selected subset of neurons forming the associative memory for a 1 s period to recall it. The SNR of the associative memory was calculated from the spike data recorded from the network at this time—for the neurons forming the memory, the pattern neurons, and neurons not included in the memory, the background neurons.

Multiple associative memories were also successively stored in the network to investigate its capacity in this study. After the last associative memory had been stored and the network returned to its AI state, each associative memory was recalled and network activity recorded. To ensure that the recall of an associative memory did not affect the subsequent recalls of other associative memories in any way, a snapshot of the network was taken after all associative memories were stored and the network had been restored to its AI state. Each time after an associative memory was recalled and its activity

recorded, the network was reset to its pre-recall state by loading the snapshot. Additionally, during the recall of each pattern, all plasticity was disabled in the network to prevent pattern recall from affecting the network in any way.

1.2 RESULTS

The primary parameter that affects the recall performance of associative memories in the network is the *potentiation factor* (χ) by which the synapses that are part of a stored associative memory are strengthened. The SNR of stored associative memories during recall for different values of χ depends on the activity of the neurons forming the associative memory (the pattern signal) and that of the remaining neurons in the network (the background signal) (Equation (1)). The activity of these neuronal sets, in turn, is modulated by the magnitudes of inhibition and excitation they receive. As more associative memories are stored in the network, the strengthening of involved excitatory synapses increases lateral excitation in the network. This is constantly balanced by the strengthening of corresponding inhibitory projections by the inhibitory Spike Timing Dependent Plasticity (STDP) mechanism to maintain the network in its low frequency AI firing state.

In the case of multiple associative memories that may overlap with each other, two methods of augmenting associative memory synapses can be used that would also affect the performance of the network. In the first 'clipped' method, it is assumed that the maximum possible synaptic strength of synapses involved in associative memories is already attained on the storage of the first associative memory. These synapses, therefore, are not strengthened repeatedly on the storage of later associative memories. In the other 'cumulative' method, on the other hand, this assumption is not made. Thus, in this system, each time an associative memory is stored, all its synapses are reinforced again.

To compare the difference in performance when associative memories are stored using these two methods, a number of associative memories were stored in the network, recalled, and the SNR calculated for $\chi = 5$ (as used in Vogels et al. (2011)). Figure 12a shows the percentage of the excitatory neuron population of 8000 neurons that were recruited by associative memories of 800 neurons each as each pattern is selected, while Figure 12b shows the SNR for the two storage methods as a function of the number of associative memories stored in the network. As expected, the SNR for a lone associative memory was found to be the same in both storage methods. We note this SNR, which was the baseline value that the performance of a
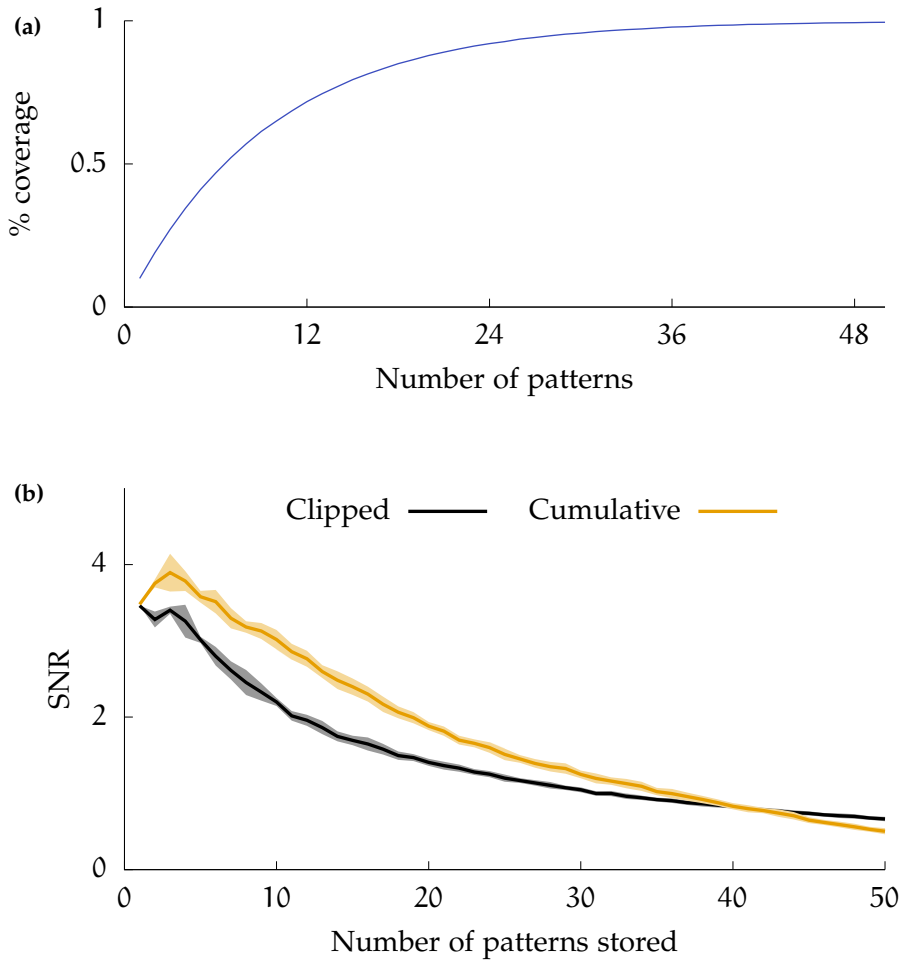
Figure 12: (a): When multiple associative memories consisting of 800 neurons selected randomly from a population of 8000 neurons are repeatedly stored in the network, when the associative memories are allowed to overlap, approximately 40 are sufficient to cover the whole network. At this stage, almost all synapses in the network have been strengthened. **(b):** SNR vs number of associative memories ($\chi = 5$). For both storage methods, as more associative memories are stored the inhibition in the network also increases to match the increased lateral excitation resulting in a decrease in SNR. Since the conductances of synapses shared between multiple associative memories are higher in the cumulative storage method than the clipped storage method, the SNR was initially observed to be higher in this regime. However, as more associative memories are stored and the overlap increases, the network configuration reaches a state where the coupling between synapses in the pattern and background neurons is large enough to result in a lesser SNR for cumulative storage than clipped storage.

deprived network was compared to in later stages of the study. In general, as more associative memories are stored, the SNR deteriorates. This can be explained by analysing the activities of the pattern and background neurons in each case.

Associative memories that do not overlap also do not affect each other's recall performance. When one is recalled, the activity of the other memories remains at baseline levels as part of the background signal. When associative memories overlap, however, the coupling between them may affect their recall performance. The storage of each new associative memory activates previously stored associative memories that it overlaps with, for example, also increasing the inhibition they receive. The increased inhibition hampers their activity during recall. This can be seen in Figures 13a and 14a where, as more associative memories were stored in the network, the firing rates of pattern neurons during recall decreased. On the other hand, the stimulation of an associative memory during recall will also activate the associative memories that it overlaps with—increasing the background activity. This can be observed in Figures 13b and 14b. For higher values of χ, which results in more excitation for each new associative memory stored in the network, the activity of the background neurons also decreases eventually because of the corresponding increase in stabilising inhibition—similar to the pattern neurons.

When associative memories are stored using the cumulative method, overlap among associative memories repeatedly strengthens synapses common to the involved memories. For the storage of the first few associative memories, where there is less overlap, the increased lateral excitation dominates pattern dynamics. Thus, an increase in the pattern activity is observed during recall (Figure 14a). This also translates to a marginally improved SNR (Figure 15b). Thereafter, inhibition dominates to reduce the pattern activity during recall as discussed above. This feature is not observed in the clipped storage case, since synapses common to multiple associative memories are not strengthened repeatedly there.

Given that the excitatory synapses that belong to multiple associative memories have higher conductances in the cumulative storage method than in the clipped one, it is also expected that the SNR for patterns stored using the former will be higher than for patterns stored using the latter. At some stage, however, a lower SNR is observed for cumulative storage than clipped storage (at N = 40 patterns in Figure 12b). This is also ascribed to lower firing rates for pattern neurons in the cumulative storage case for the same number of patterns stored using the same value of χ ($\chi = 5$ for N = 40 patterns in Figure 13a vs Figure 14a). Because the cumulative storage method results in higher
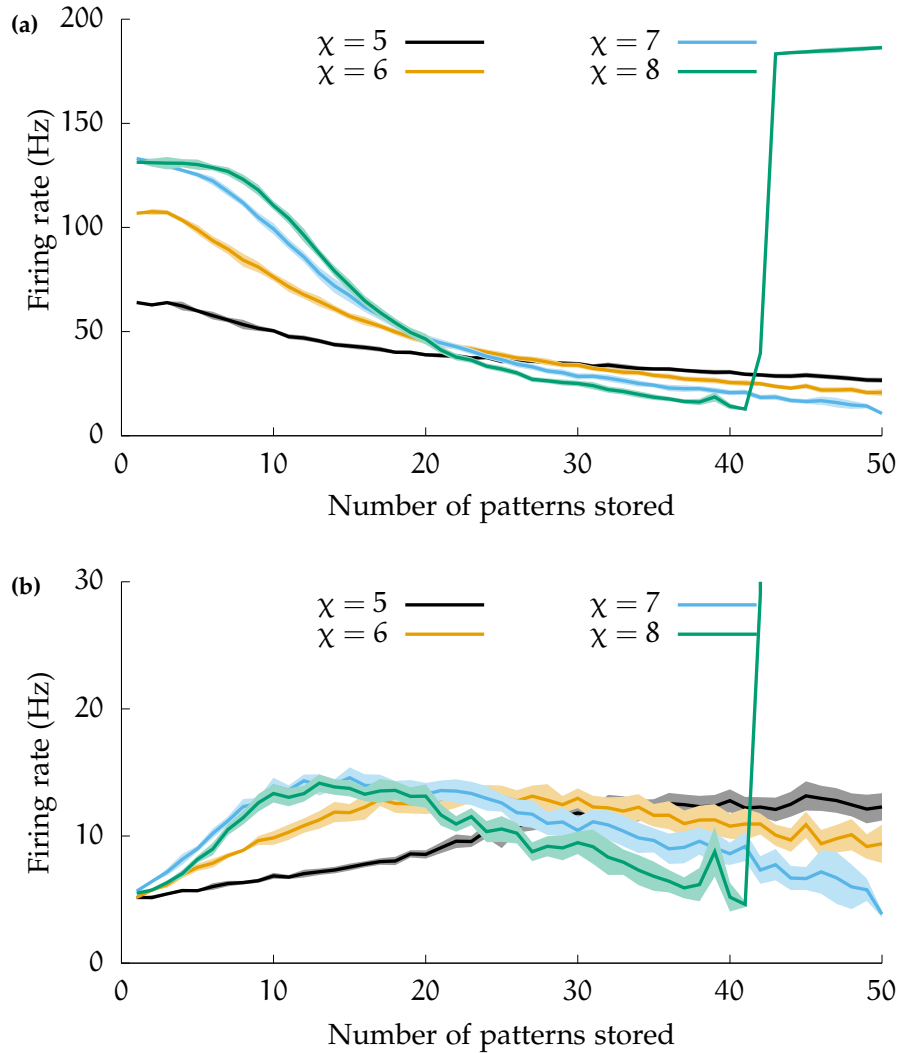
Figure 13: Mean firing rates for neurons during recall with different values of χ, using the clipped learning method. **(a):** pattern neurons; **(b):** background neurons. For χ = 8, when more than 40 patterns are stored in the network, all neurons in the network, the pattern and the background neurons, are activated maximally by the recall stimulus as a result of increased excitatory recurrent connectivity in the network. This represents the limit of the capacity of the network as an associative memory store since in this configuration, the patterns stored in the network cannot be separated from the background activity upon recall.
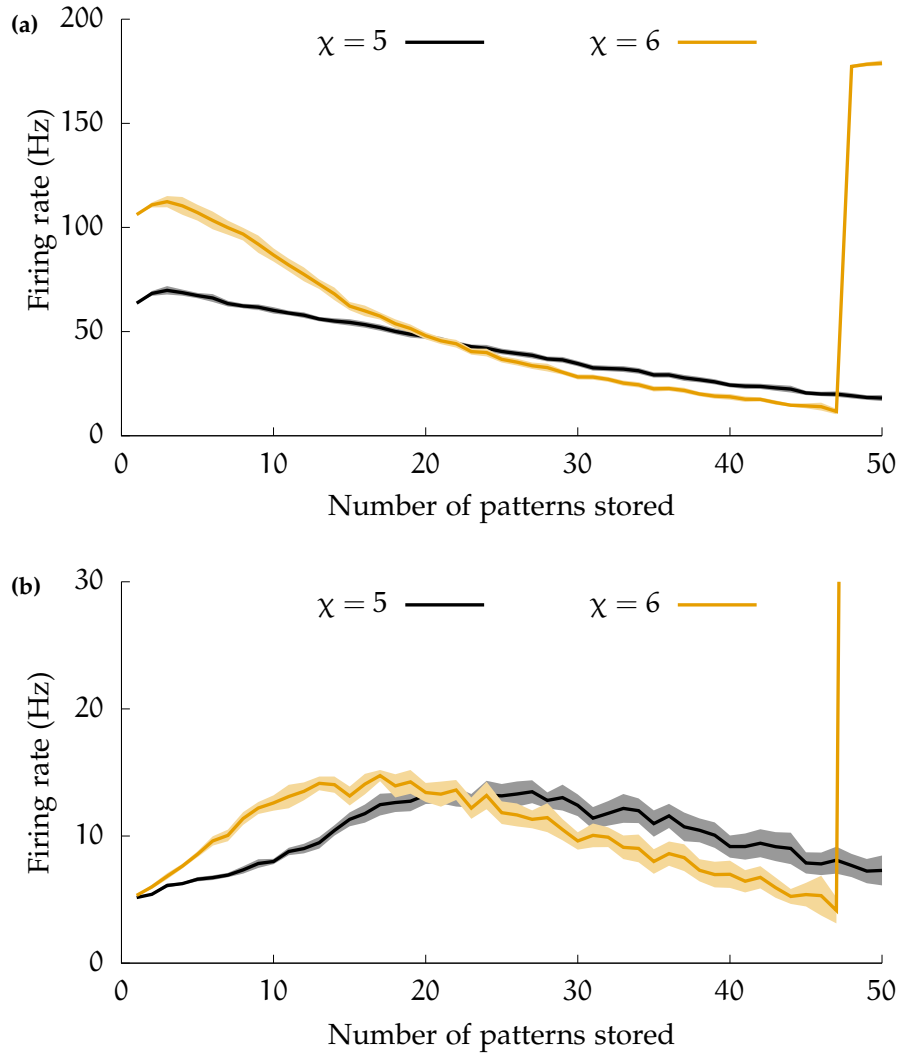
Figure 14: Mean firing rates for neurons during recall with different values of χ, using the cumulative learning method. **(a):** pattern neurons; **(b):** background neurons. Similar to the previous case where clipped storage was used, for χ = 6 here, when more than ~45 patterns are stored in the network, all neurons in the network are activated maximally by the recall stimulus as a result of increased excitatory recurrent connectivity in the network. In this case also, since patterns stored in the network can not be separated from the background activity upon recall, this serves as the storage limit of the network as an associative memory store.

levels of excitation for the storage of the same number of patterns, the magnitude of stabilising inhibition here is also higher.

Having established the differing effects of the different systems of storing multiple associative memory patterns in the network, the effect of the potentiation factor on network performance was studied. The same simulation protocol was repeated with different values of χ. In general, a higher potentiation factor would be expected to increase the SNR of a pattern. This was confirmed for both clipped and cumulative storage (Figures 15a and 15b). As can also be seen, for all values of χ, the trend of SNR remained the same as more patterns were stored in the network.

A notable observation in both Figures 15a and 15b is that the SNR drops to 0 as a high number of patterns is stored in the network. The firing rates of pattern and background neurons during recall explain this phenomenon (Figures 13a, 13b, 14a and 14b). As the figures show, during recall, all neurons in the network fire at high firing rates close to their maximum (200 Hz) indicating that the lateral excitatory connectivity in the excitatory neurons of the network is high enough to cause them all to fire when the recall stimulus is applied. Thus, stored associative memories can no longer be recalled in the network. Therefore, though a higher value of χ may result in a higher SNR with fewer patterns, it results in worse performance as the number of patterns increases and it also limits the capacity of the network to recall stored patterns.

Furthermore, as larger values of χ result in more recurrent excitation in the network, the re-establishment of its AI state after the storage of new associative memories also requires larger increases in conductances of its IE synapses by the inhibitory STDP mechanism. If IE synapses have attained their maximum value (the maximum value for IE conductances is a free parameter that can be set in the model) no corresponding increase in inhibition will occur to settle the network back into its AI firing regime when more associative memories are stored in it. The upper limit for the value of χ that may be used, therefore, depends on the maximum value of IE synapse conductance permitted in the network, and represents the storage limit of the network. This storage limit, a function of χ and the maximum possible IE conductance value, was not tested in the study. Instead, the scope of the study was limited to regimes where the network could be restored to the AI state after the storage of a new associative memory.
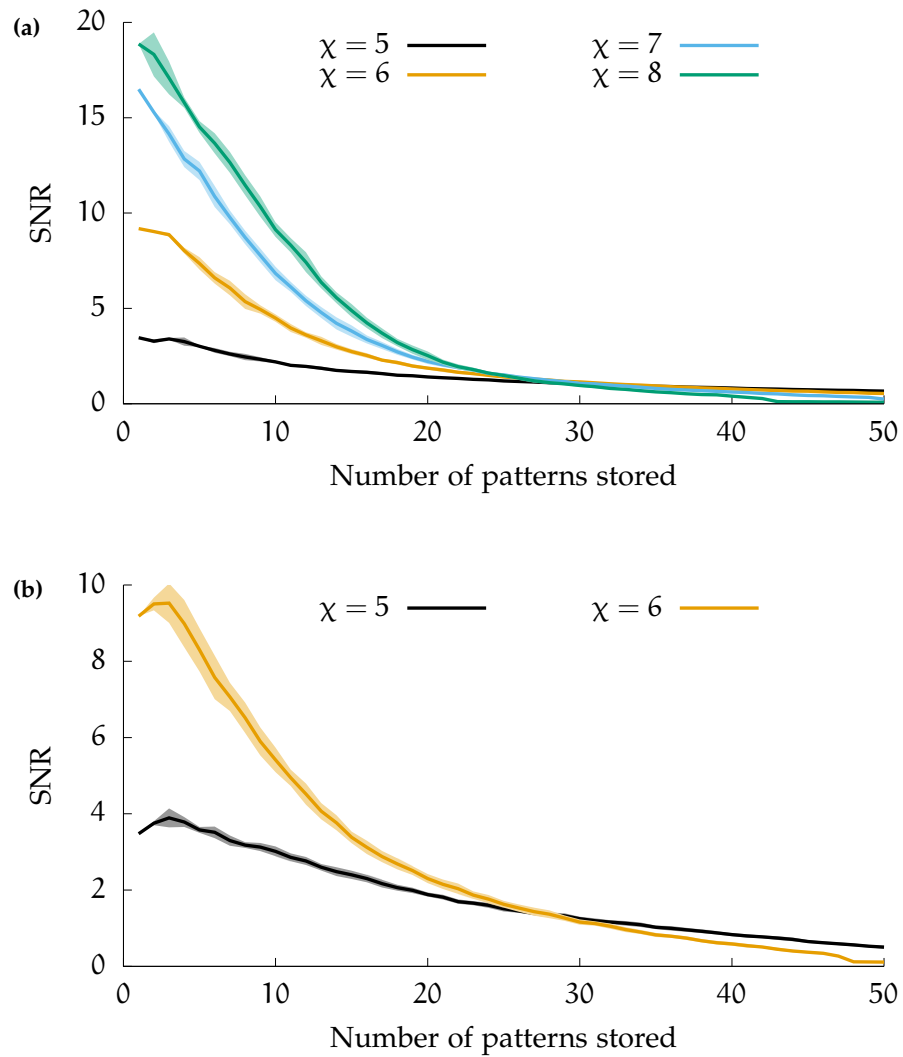
Figure 15: SNR vs number of patterns for different potentiation factors. **(a):** using the clipped method; **(b):** the cumulative method.

1.3   CHAPTER CONCLUSIONS

This chapter described the initial stages of this study where the performance of associative memories in a normal, undeafferented network was quantified. It documented the SNR of recalling an associative memory stored in the balanced cortical network model. It also included information suggesting that the storage of multiple associative memories in a network where they may overlap with each other results in a deterioration of their performance. Lastly, it explored the effect that the magnitude of augmentation of synapses to form associative memories may have on its recall.

The simulations here, however, represent only a very limited, simplified version of a brain network, sufficient for this study, and the results generated here, therefore, must be limited to this scope. The brain, of course, is far more complex and its neurons are capable of functioning as a store for associative memories without performance degradation over extended periods of time—years if not complete lifetimes.

2

MODELLING POST-DEAFFERENTATION REPAIR IN BALANCED NETWORKS

The previous chapter established the capacity of the cortical Asynchronous Irregular (AI) network to store and recall associative memories. To investigate how sensory deprivation and subsequent repair affects this function, a model of peripheral lesioning and structural plasticity mediated network reorganisation was required. As discussed in Chapter 1, whereas the Model of Structural Plasticity (MSP) framework does allow for modelling structural plasticity, a model of peripheral lesioning and subsequent repair adequate for this study was unavailable. Thus, a novel model of network repair after peripheral lesioning was developed. This chapter documents the new model.

Until this juncture, the study had used the Auryn simulator (Zenke and Gerstner 2014). However, Auryn, which uses a traditional connection matrix data structure to implement synaptic connections, did not include the necessary features required to model structural plasticity using the MSP. Specifically, the formation and removal of synapses during simulation was not trivial. At the same time, features required to implement the MSP framework were being added to the NEST simulator (Diaz-Pier et al. 2016; Kunkel, Morrison et al. 2017) which uses more flexible data structures that allow for connectivity changes during simulation (Kunkel, Potjans et al. 2011; Kunkel, Schmidt et al. 2014). Thus, it was decided to migrate the model to the NEST simulator.

The work documented in this chapter was disseminated in the following:

- Ankur Sinha, Christoph Metzner, Neil Davey et al. (2019b). 'Growth Rules for the Repair of Asynchronous Irregular Neuronal Networks after Peripheral Lesions'. In: *bioRxiv*. DOI: 10.1101/810846. eprint: https://www.biorxiv.org/content/early/2019/10/21/810846.full.pdf. URL: https://www.biorxiv.org/content/early/2019/10/21/810846

- Ankur Sinha, Christoph Metzner, Neil Davey et al. (2019a). 'Growth rules for repair of asynchronous irregular network mod-

Table 3: Neuronal parameters.

| Parameter	Symbol	Value
LIF parameters		
Refractory period	t_{ref}	5 ms
Reset potential	V_{reset}	-60 mV
Threshold potential	V_{th}	-50 mV
Capacitance	C	200 pF
Leak conductance	g_L	10 nS
Leak reversal potential	E_L	-60 mV
Inhibitory reversal potential	E_{inh}	-80 mV
Excitatory reversal potential	E_{exc}	0 mV
Excitatory time constant	τ_{exc}	5 ms
Inhibitory time constant	τ_{inh}	10 ms
$[Ca^{2+}]$ increase per spike	β	0.1
$[Ca^{2+}]$ decay time constant	$\tau_{[Ca^{2+}]}$	50 s
External inputs		
Poisson spike input to all neurons	r_{ext}	10 Hz
External projections to E neurons	g_{ext}^E	8 nS
External projections to I neurons	g_{ext}^I	12 nS

els following peripheral lesions'. In: *BMC Neuroscience* 20. ISSN: 1471-2202

2.1 EXTENDED NEURON MODEL FOR STRUCTURAL PLASTICITY

Neurons are modelled as leaky integrate and fire (LIF) conductance based point neurons with exponential conductances (Meffin, Burkitt and Grayden 2004), the membrane potentials of which are governed by:

$$C\frac{dV}{dt} = -g_L(V - E_L) - g_{exc}(V - E_{exc}) - g_{inh}(V - E_{inh}) + I_e \quad (1)$$

where C is the membrane capacitance, V is the membrane potential, g_L is the leak conductance, g_{exc} is the excitatory conductance, g_{inh} is the inhibitory conductance, E_L is the leak reversal potential, E_{exc} is the excitatory reversal potential, E_{inh} is the inhibitory reversal potential, and I_e is an external input current. Incoming spikes induce a post-
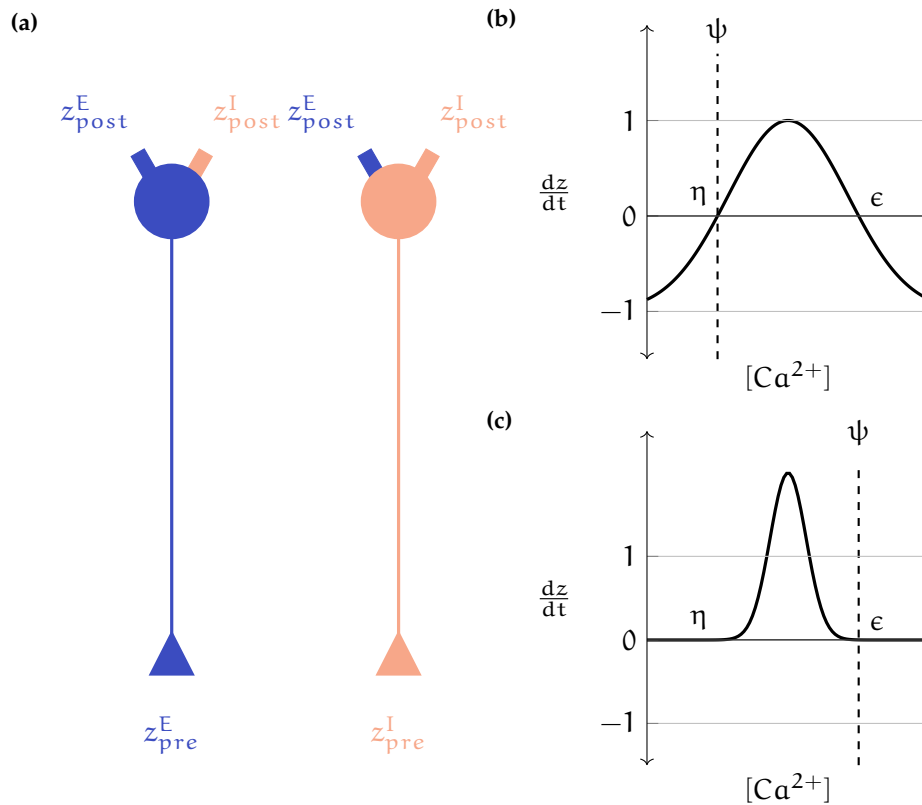
Figure 16: Gaussian growth curves modulate the rate of turnover of synaptic elements ($\frac{dz}{dt}$) in a neuron as a function of its $[Ca^{2+}]$: **(a)** Excitatory: Blue; Inhibitory: Red; All neurons possess excitatory and inhibitory post-synaptic elements (z_{post}^E, z_{post}^I) but excitatory and inhibitory neurons can only bear excitatory and inhibitory pre-synaptic elements, respectively (z_{pre}^E, z_{pre}^I); **(b)** and **(c)**: Example Gaussian growth curves (growth curves for all neurites are derived in Chapter 3). Constants η and ϵ control the width and positioning of the growth curve on the x-axis. ω (see Equation 1) controls the positioning of the growth curve on the y-axis. ν (see Equation 1) is a scaling factor. ψ is the optimal $[Ca^{2+}]$ for the neuron. The minimum and maximum values of dz/dt can be analytically deduced to be $-\nu\omega$ and $\nu(2-\omega)$ respectively (See Methods). The relationship between η, ϵ, and ψ regulates the activity dependent dynamics of neurites.

(b) $\psi = \eta = 5.0, \epsilon = 15.0, \nu = 1.0, \omega = 1.0, -\nu\omega = -1.0, \nu(2-\omega) = 1.0$. Here, new neurites are formed when the neuronal activity exceeds the required level and removed when it falls below it. **(c)** $\eta = 5.0, \psi = \epsilon = 15.0, \nu = 1.0, \omega = 0.001, -\nu\omega = -0.001, \nu(2-\omega) = 1.999$. Here, the growth curve is shifted up along the y-axis by decreasing the value of ω. New neurites are formed when the neuronal activity is less than the homeostatic level and removed (at a very low rate) when it exceeds it.

synaptic change of conductance that is modelled by an exponential waveform following the equation:

$$g(t) = \bar{g} \exp\left(-\frac{t - t_s}{\tau_g}\right) \tag{2}$$

where τ_g is the decay time constant and $\bar{g}$ is the maximum conductance as the result of a spike at time t_s. Table 3 enumerates the constants related to the neuron model.

Both Auryn (Zenke and Gerstner 2014) and NEST (Jordan, Mørk et al. 2019) include implementations of the LIF neuron model, but they vary in their underlying architecture and implementation. Auryn uses the simple forward Euler integration method, whereas NEST makes use of the Runge-Kutta-Fehlberg integration method via the GNU Scientific Library (GSL) (Galassi et al. 2002). The integration time step (dt) for each simulator can be set during the compilation of the simulator and is documented in Table 4.

As shown in Figure 16a, following the MSP framework, each neuron in the model possesses sets of both pre- and post-synaptic synaptic elements, the total numbers of which are represented by (z_{pre}) and (z_{post}) respectively. Excitatory and inhibitory neurons only possess excitatory (z_{pre}^E) and inhibitory axonal elements (z_{pre}^I) respectively, but they can each host both excitatory and inhibitory dendritic elements ($z_{post,E}, z_{post,I}$) (since the number of neurites must be a non-negative integer, the floor value of the continuous variable is used for connectivity updates). Similarly, the rate of change of each type of synaptic element, (dz/dt), is modelled as a Gaussian function of the neuron's 'Calcium concentration' ($[Ca^{2+}]$). The Gaussian function was generalised by including a new parameter ω:

$$\frac{dz}{dt} = \nu\left(2\exp^{-\left(\frac{[Ca^{2+}]-\xi}{\zeta}\right)^2} - \omega\right)$$
$$\xi = \frac{\eta + \epsilon}{2}, \tag{3}$$
$$\zeta = \frac{\eta - \epsilon}{2\sqrt{-\ln(\omega/2)}}$$

Here, ν is a scaling factor, ξ and ζ (in terms of η and ϵ) define the width and location of the Gaussian curve on the x-axis, while ω controls the location of the curve on the y-axis ($0 < \nu$, $0 < \eta < \epsilon$, $0 < \omega < 2$).

The $[Ca^{2+}]$ represents the time averaged activity of the neuron, and is given by:

$$[Ca^{2+}] = [Ca^{2+}] + \beta, \qquad\qquad \text{if } V \geqslant V_{th} \tag{4}$$
$$\frac{d[Ca^{2+}]}{dt} = -\frac{[Ca^{2+}]}{\tau_{[Ca^{2+}]}}, \qquad\qquad \text{otherwise.} \tag{5}$$

Here, $\tau_{[Ca^{2+}]}$ is the time constant with which the $[Ca^{2+}]$ decays in the absence of a spike, and β is the constant increase in $[Ca^{2+}]$ caused by each spike.

Given that $([Ca^{2+}] > 0)$, (dz/dt) is bound as:

$$
\min\left(\frac{dz}{dt}\right) = -\nu\omega \quad \text{for} \quad ([Ca^{2+}] \to \infty)
$$
$$
\max\left(\frac{dz}{dt}\right) = \nu(2 - \omega) \quad \text{for} \quad \left([Ca^{2+}] = \left(\frac{\eta + \epsilon}{2}\right)\right) \tag{6}
$$

Using $(\omega = 1)$ generates the growth curves proposed by the MSP where the maximum and minimum values of dz/dt are equal in magnitude to ν. This implies that the maximum rates of formation $(dz/dt > 0)$ and retraction $(dz/dt < 0)$ are equal. Varying ω removes this constraint. Neurites may now be modelled with different maximal rates of formation and retraction.

Within these bounds, as shown in the example Gaussian curves in Figures 16b and 16c, (dz/dt) is:

$$
\begin{aligned}
&> 0 \quad \text{for} \quad \eta < [Ca^{2+}] < \epsilon \\
&= 0 \quad \text{for} \quad [Ca^{2+}] = \{\eta, \epsilon\} \\
&< 0 \quad \text{for} \quad [Ca^{2+}] < \eta \quad \cup \quad [Ca^{2+}] > \epsilon
\end{aligned} \tag{7}
$$

If, based on its activity, a neuron has more synaptic elements of a particular type (z) than are currently engaged in synapses $(z_{connected})$, the free elements (z_{free}) can participate in the formation of new synapses at the next connectivity update step:

$$
z_{free} = \lfloor (z - z_{connected}) \rfloor \tag{8}
$$

However, if they remain unconnected, they decay at each integration time step with a constant rate τ_{free}:

$$
\frac{dz_{free}}{dt} = -\tau_{free} z_{free} \tag{9}
$$

On the other hand, a neuron will lose z_{loss} synaptic connections if the number of a synaptic element type calculated by the growth rules (z) is less than the number of connected synaptic elements of the same type $(z_{connected})$:

$$
z_{loss} = \lfloor (z_{connected} - z) \rfloor \tag{10}
$$

Growth curves for all neurites are derived in the next chapter, Chapter 3.
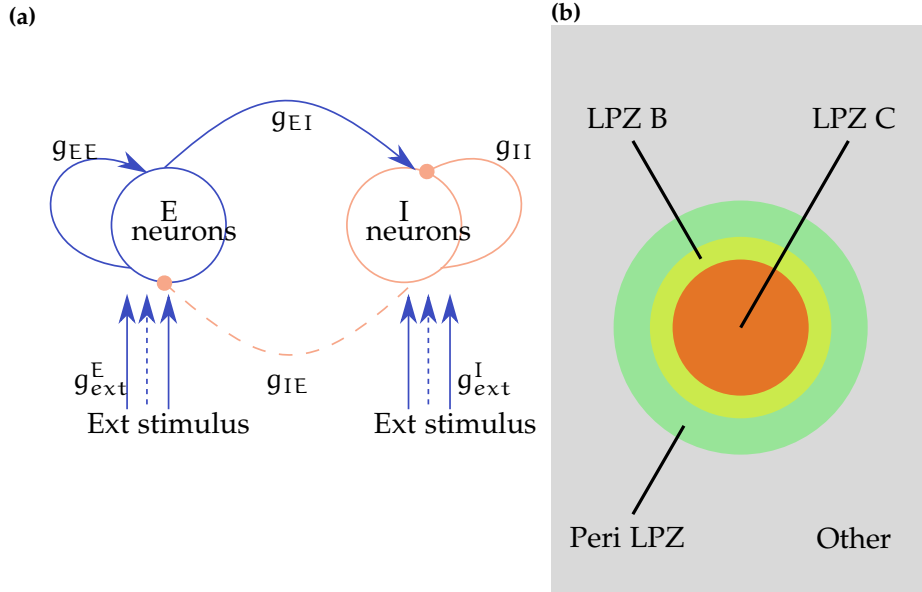
Figure 17: Overview of the model: **(a)** Excitatory (E) and Inhibitory (I) neurons ($N_E = 4N_I$ (see Table 4)) are initially connected via synapses with a connection probability of ($p = 0.02$). All synapses (EE, EI, II), other than IE synapses, which are modulated by inhibitory spike-timing dependent plasticity, are static with conductances g_{EE}, g_{EI}, g_{II}, respectively. All synapse sets are modifiable by the structural plasticity mechanism. External Poisson spike stimuli are provided to all excitatory and inhibitory neurons via static synapses with conductances g_{ext}^E and g_{Inh}^I, respectively. To simulate deafferentation, the subset of these synapses that project onto neurons in the Lesion Projection Zone (LPZ) (represented by dashed lines in the figure) are disconnected. **(b)** Spatial classification of neurons in relation to the LPZ: LPZ C (centre of LPZ) consists of 2.5 % of the neuronal population; LPZ B (inner border of LPZ) consists of 2.5 % of the neuronal population; Peri-LPZ (outer border of LPZ) consists of 5 % of the neuronal population; Other neurons consist of the remaining 90 % of the neuronal population. (Figure not to scale)

2.2 NETWORK MODEL AND SIMULATION PROTOCOL

The cortical network model, when used only as an associative memory store, did not require neurons to be distributed in space. The connectivity of the network was generated from the probability of connection formation (p) that was constant for each neuron. However, since the peripheral lesion experiments this study relies on deprivation of sets of neurons that are spatially close to each other, the cortical model was extended to distribute its neurons in a two-dimensional grid (Figure 17b).

Each neuron is placed using a Gaussian distribution centred at its calculated grid location (col, row) that is obtained from its 'id' i (NEST assigns neurons in a population of N neurons ids incrementally:
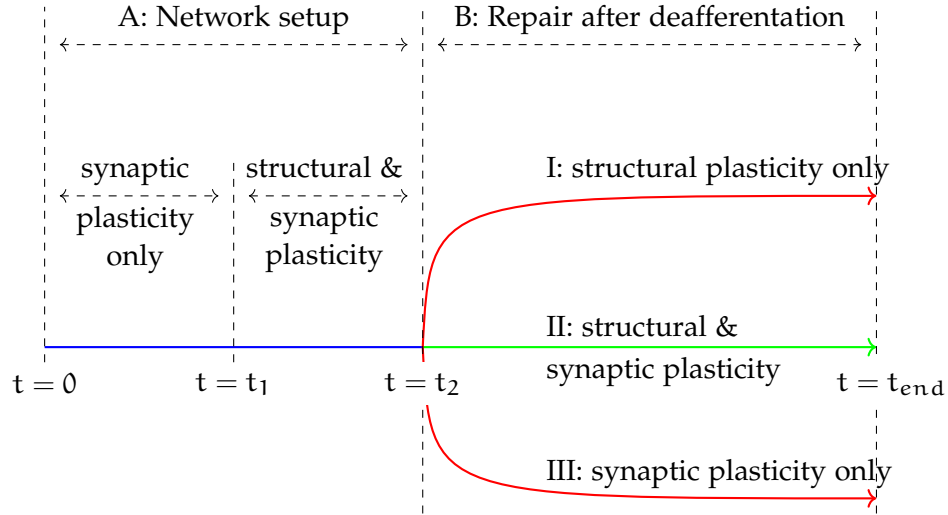
Figure 18: The simulation runs in 2 phases. Initially, the setup phase ($0\,\mathrm{s} < t < t_2$) is run to set the network up to the balanced AI state. At ($t = t_2$), a subset of the neuronal population is deafferented to simulate a peripheral lesion and the network is allowed to organise under the action of homeostatic mechanisms until the end of the simulation at ($t = t_{end}$). Each homeostatic mechanism can be enabled in a subset of neurons to analyse its effects on the network after deafferentation.

$(I, I + 1, \ldots, I + (N - 1)))$. Thus for a neuron with id i in a population starting at I:

$$\mathrm{row} = \lfloor (i - I)/N_{\mathrm{cols}} \rfloor \tag{1}$$

$$\mathrm{col} = (i - I)\%N_{\mathrm{rows}} \tag{2}$$

$$y = G(\mathrm{row} * \mu_d, \sigma_d) \tag{3}$$

$$x = G(\mathrm{col} * \mu_d, \sigma_d) \tag{4}$$

where $\lfloor \ldots \rfloor$ denotes the floor value, % denotes the modulo function, N_{rows} and N_{cols} are the number of rows and columns in the grid, and $G(\mu, \sigma)$ is the Gaussian distribution with mean μ and standard deviation σ. $\mu_d = \mu_d^E$ is the mean distance between two adjacent excitatory neurons, and $\sigma_d = \sigma_d^E$ is the standard deviation used for G. Inhibitory neurons are similarly scattered such that they are evenly dispersed among the excitatory neurons. To prevent any edge effects from affecting the simulation, the plane is wrapped around to form a toroid. Table 4 summarises the parameters used to arrange the neurons.

Since neurons are now spatially distributed, the cortical network model was further extended such that neurons nearer to each other are more likely to form synapses. This was done by choosing the initial set of partners for neurons based on a probability of synapse formation,

p_{form}, which is a Gaussian function of the distance between the pair, d:

$$p_{form} = \hat{p} \exp^{-\left(d/(w\mu_d^E)\right)^2} \tag{5}$$

Here, $\hat{p} \in \{\hat{p}_E, \hat{p}_I\}$ is the maximum probability, μ_d^E is the mean distance between two adjacent excitatory neurons, and $w \in \{w_E, w_I\}$ is a multiplier that controls the spatial extent of new synaptic connections.

Previous research indicates that lateral connections in the primary visual cortex are organised in a 'Mexican hat' pattern. Whereas experimental work does support the presence of the 'Mexican hat' pattern (B.-h. Liu et al. 2011; Haider, Häusser and Carandini 2013), anatomical research suggests that inhibitory connections are more localised than excitatory ones, contradicting the traditional use of shorter excitatory and longer inhibitory connections in computer models (Stepanyants et al. 2009). Analysis of the local cortical circuit of the primary visual cortex suggests that the 'Mexican hat' pattern can either be generated by narrow but fast inhibition, or broad and slower inhibition that may be provided by longer axons of GABAergic basket cells (Kang, Shelley and Sompolinsky 2003; Rudiger et al. 2013). Investigations into the maintenance of the 'Mexican hat' pattern are beyond the scope of this study. Therefore, this study was limited to the traditional model of longer inhibitory connections and shorter local excitatory connections by using a larger multiplier for inhibitory synapses, w_I, than for excitatory synapses, w_E, ($w_E < w_I$).

After the neurons and connectivity of the network model had been initialised, the simulation was divided into multiple phases, as shown in Figure 18.

2.2.1 *Initial network stabilisation to physiological state*

The network is first permitted to stabilise to its balanced AI state ($t = t_2$ in Figure 18). In this iteration of the model, this phase consists of two simulation regimes. Initially, only inhibitory synaptic plasticity is activated to stabilise the network ($t < t_1$ in Figure 18). As this state is considered the normal physiological state of our network model, the network parameters obtained at this point are set as the steady state parameters of neurons and synapses in the network. The optimal activity of each neuron, ψ, is set to the activity achieved by the neuron at this point, and its growth curves are initialised in relation to it. The mean conductance for new IE synapses is also set as the mean conductance of the IE synapses obtained at this stage.

The homeostatic structural plasticity mechanism is then activated in the network at this point ($t = t_1$ in Figure 18) to verify that the network continues to remain in its balanced AI state in the presence of both homeostatic mechanisms.

2.2.2 *Simulation of peripheral lesion*

Next (at $t = t_2$ in Figure 18), the external Poisson spike train inputs are disconnected from excitatory and inhibitory neurons that fall in the Lesion Projection Zone (LPZ) to simulate a peripheral lesion in the network. For analysis, the neuronal plane is classified into four regions:

- LPZ C: the centre of the LPZ (Red in Figure 17b).

- LPZ B: the inner border of the LPZ (Yellow in Figure 17b).

- P LPZ: peri-LPZ, the outer border of the LPZ (Green in Figure 17b).

- Other neurons: neurons further away from the LPZ (Grey in Figure 17b).

2.2.3 *Network reorganisation*

The deafferented network is permitted to reorganise itself under the action of the active homeostatic mechanisms until the end of the simulation ($t = t_{end}$ in Figure 18). By selectively activating the two homeostatic mechanisms in different simulation runs, the model also allows the investigation of their effects on the network in isolation.

All synapses in the network, except the connections that project the external stimulus onto the neuronal population, are subject to structural plasticity (Figure 17a). Free excitatory pre-synaptic and excitatory post-synaptic elements can combine to form excitatory synapses (EE, EI). Analogously, inhibitory pre-synaptic and inhibitory post-synaptic elements can plug together to form inhibitory synapses (II, IE). The set of possible partners for a neuron, therefore, comprises of all other neurons in the network that have free synaptic elements of the required type. The probability of forming a synapse, p_{form}, is calculated for all possible partners as reported in Equation (5)—partners closer to the neuron have higher values of p_{form}, and are more likely to be chosen for synapse formation. Partners are chosen

stochastically based on their p_{form} values until either all prospective partners have been exhausted or if z_{free} partners have been picked.

New synapses that are added to the network are initialised with conductances similar to that of existing synapses in the balanced network. Their conductance values are taken from a Gaussian distribution centred at the mean conductance for that synapse type. Since new synapses can, therefore, be weaker or stronger than existing ones, this prevents the same set of synapses from being modified in each connectivity update.

In spite of them being plastic, the same method is also used for IE synapses. IE synapses are initialised with zero conductances at the start of the simulation and modify their strengths based on STDP (Vogels et al. 2011). When the network has achieved the balanced AI state, these conductances also settle at higher values. If new IE synapses formed after this point by structural plasticity were to be initialised to zero conductances, they would be most likely to be selected for deletion repeatedly as the weakest ones. STDP does not modulate inactive synapses either—synapses between pairs of neurons that have both been rendered inactive by deafferentation will not be weakened, and may not be lost. Therefore, to ensure the turnover of a diverse set of IE synapses also, new connections of this type are supplied with conductances similar to that of existing stable IE synapses in the balanced network.

Experiments suggest that the stability of synapses is proportional to their efficacy (Knott, A. Holtmaat et al. 2006; Trachtenberg et al. 2002). Taking this into account, as another extension, the probability of deletion of a synapse, p_{del}, was calculated as a function of its conductance g:

$$p_{del} = \exp^{-\left(\frac{g}{(2g_{th})}\right)^2} \tag{6}$$

Here, g_{th} is a threshold conductance value calculated during the simulation, synapses stronger than which are considered immune to activity dependent changes in stability. They are removed from the list of options from which synapses are considered for deletion and are therefore, not considered for deletion at all. The probability of deletion, p_{del}, is calculated for the remaining synapses. From this remaining set, synapses are stochastically selected for deletion based on their p_{del} values until either all prospective synapses have been tested or if z_{loss} synapses have been obtained.

For simplicity, for static excitatory synapses that all have similar conductances (EI, EE), this method of deletion is not used. Instead, for these, z_{loss} connections are randomly selected for deletion from the set of available candidates. Whereas II synapses are also static,

the deletion of an inhibitory synapse by the loss of an inhibitory post-synaptic element can occur by the removal of either an IE or an II synapse. Therefore, to permit competition between II and IE synapses for removal, weight based deletion is applied to both these synapse sets.

The numbers of synaptic elements are updated at every simulator integration time step internally in NEST. Connectivity updates to the network, however, require updates to internal NEST data structures and can only be made when the simulation is paused. Since this increases the computational cost of the simulation, these updates are only made at 1 s intervals. Gathering data on conductances, connectivity, and neuronal variables like $[Ca^{2+}]$ also require explicit NEST function calls while the simulation is paused. Therefore, the required data is written to files only at regular intervals. Table 5 summarises the various synaptic parameters used in the simulation.

2.3 CHAPTER CONCLUSIONS

This chapter documented the new model of peripheral lesioning that was developed for the purpose of this study. It extends the MSP framework to permit the use of a more general set of Gaussian growth curves for neurites. Other additions, such as the synaptic weight dependent deletion of synapses, and the use of a cortical balanced AI network model as the physiological initial state, also lend more biological plausibility to it.

As a simplified representation, however, this model necessarily suffers from various limitations. For example, although the use of simple conductance based point neurons (Meffin, Burkitt and Grayden 2004) is sufficient for this network study, perhaps even necessary for its tractability (Izhikevich 2004), it also limits it. Unlike in the brain where calcium is compartmentalised in neurons (Yuste, A. Majewska and Holthoff 2000), a single compartment point neuron model only allows one value of $[Ca^{2+}]$ for all neurites in a neuron. Thus, each of the neurons in this MSP based model can only either sprout or retract a type of neurite at a point in time. This is not the case in biology where different parts of the neuron can undergo structural changes independently of each other. Point neurons also lack morphology, and this model is therefore unable to explicitly include the directional formation or removal of synapses. Axonal and dendritic arbors are also not explicitly modelled and the directional turnover of synapses that represents axonal sprouting emerges merely from the numbers of connecting partner neurites. Additionally, whereas it was enough for

neurons in the model to be distributed in a two dimensional grid to include a spatial component, this is clearly not true for the brain.

Computational modelling of structural plasticity in general, is limited by the lack of supporting simulation tools. Most current simulators are designed for network modelling of synaptic plasticity, where synaptic efficacy changes while connectivity remains constant, but not structural plasticity. Even the NEST simulator (Jordan, Mørk et al. 2019), where the internal data structures are sufficiently flexible to allow for modification of synapses during simulation (Jordan, Ippen et al. 2018), currently includes a limited implementation of the MSP algorithm (Diaz-Pier et al. 2016). To incorporate the missing pieces—spatial information and different network connectivity modification strategies, for example—it was required to repeatedly pause simulations to make connectivity updates. This is far less efficient than NEST handling these changes in connectivity internally during continuous simulation runs and added a large overhead to the computational costs of our simulations. The development of companion tools for modelling structural plasticity is however, gradually gaining traction (Nowke et al. 2018) with discussions to allow NEST to communicate with stand alone structural plasticity tools via interfaces such as Connection Set Algebra (Djurfeldt 2012) ongoing.

However, for the purposes of this thesis, the model presented in this chapter represents something that is much better than anything that has gone previously. The ability to model structural plasticity, albeit with considerable computational cost, is facilitated and allows the investigation reported in the next chapter.

Table 4: Network simulation parameters.

Parameter	Symbol	Value
Simulation parameters		
Integration time step	dt	0.1 s
Structural plasticity update interval		1 s
Network parameters		
Number of E neurons	N_E	8000
Number of I neurons	N_I	2000
Dimension of 2D E neuron lattice		100×80
Dimension of 2D I neuron lattice		50×40
Mean distance between E neurons	μ_d^E	150 µm
STD of position for E neurons	σ_d^E	15 µm
Mean distance between I neurons	μ_d^I	300 µm
STD of position for I neurons	σ_d^I	15 µm
Neurons in LPZ C		2.5 %
Neurons in LPZ B		2.5 %
Neurons in P LPZ		5 %
Remaining neurons		90 %
Initial network sparsity	p	0.02
Initial out-degree	n_{out}	p × total possible targets
Simulation stages		
Synaptic plasticity only		1500 s
Synaptic and structural plasticity		500 s
Network deafferented at		2000 s

Table 5: Synapse parameters.

Parameter	Symbol	Value
Unit conductance	$\bar{g}$	$0.5\,\text{nS}$
EE synapse conductance	g_{EE}	$\bar{g}$
EI synapse conductance	g_{EI}	$\bar{g}$
II synapse conductance	g_{II}	$10\bar{g}$
IE synapse conductance	g_{IE}	Vogels-Sprekeler STDP
STDP rule time constant	τ_{STDP}	$20\,\text{ms}$
Target constant	α_{STDP}	0.12
STDP learning rate	η_{STDP}	0.05
Width multiplier: excitatory synapses	w_E	8
Width multiplier: inhibitory synapses	w_I	24
Maximum probability of formation: excitatory synapses	$\hat{p}_E$	0.8
Maximum probability of formation: inhibitory synapses	$\hat{p}_I$	0.3
Conductance threshold for deletion: inhibitory synapses	g_{th}	

ACTIVITY DEPENDENT STRUCTURAL DYNAMICS OF SYNAPTIC ELEMENTS

The previous chapter was limited to the description of the new model of peripheral lesioning developed as part of this study. In the current chapter, the use of this model to investigate the activity dependent growth rules of various neurites is documented.

The investigation was carried out in multiple stages. First, the effects of deafferentation on the network were investigated—in a scenario where structural plasticity is disabled so that the network does not undergo any repair. Next, different growth curves were tested for the various neurites in the network to enable structural plasticity. The characteristics of the resulting simulations were compared to the time course of repair reported in experiments (Table 1).

The work documented in this chapter was disseminated in the following:

- Ankur Sinha, Christoph Metzner, Neil Davey et al. (2019b). 'Growth Rules for the Repair of Asynchronous Irregular Neuronal Networks after Peripheral Lesions'. In: *bioRxiv*. DOI: 10.1101/810846. eprint: https://www.biorxiv.org/content/early/2019/10/21/810846.full.pdf. URL: https://www.biorxiv.org/content/early/2019/10/21/810846

- Ankur Sinha, Christoph Metzner, Neil Davey et al. (2019a). 'Growth rules for repair of asynchronous irregular network models following peripheral lesions'. In: *BMC Neuroscience* 20. ISSN: 1471-2202

3.1 EFFECTS OF DEAFFERENTATION ON THE BALANCED CORTICAL NETWORK

Before activating structural plasticity in the model, the effects of deafferentation on the cortical balanced Asynchronous Irregular (AI) network, which is already stabilised by the inhibitory homeostatic synaptic plasticity mechanism, were investigated. Figure 19 shows
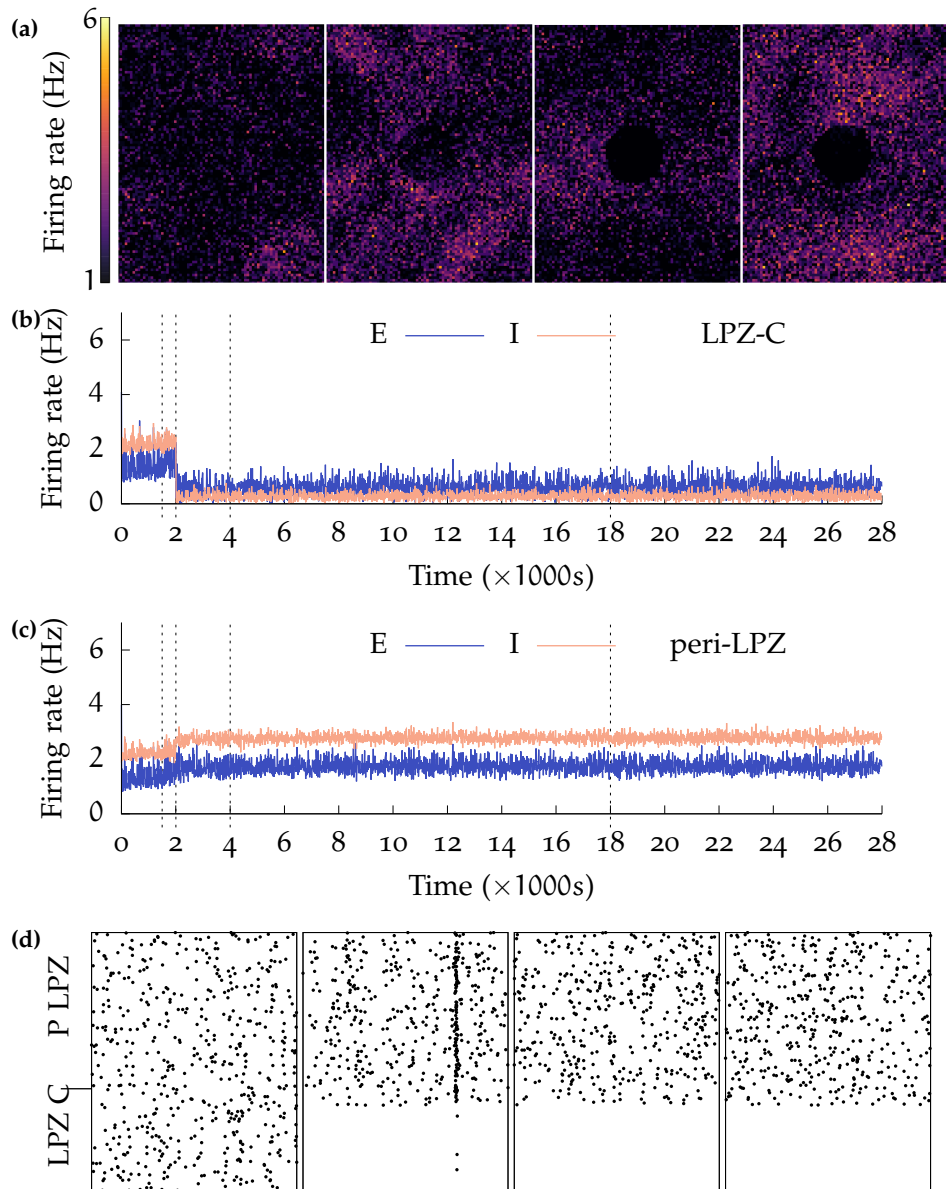
Figure 19: Network spiking rates after deafferentation without structural plasticity: (Mean firing rates of neurons are calculated over a 2500 ms window): **(a)** shows the firing rates of the whole excitatory population at $t = \{1500\,s, 2001.5\,s, 4000\,s, \text{ and } 18\,000\,s\}$. These time-points are marked by dashed lines in the next graphs. **(b)** shows mean firing rate of neurons in centre of the Lesion Projection Zone (LPZ) (LPZ-C); **(c)** shows mean firing rate of neurons in outer periphery of the LPZ (peri-LPZ); **(d)** shows spike times of neurons in the LPZ C and peri-LPZ over a 1 s period at $t = \{1500\,s, 2001.5\,s, 4000\,s, \text{ and } 18\,000\,s\}$.

the mean firing rates of the network over time in the presence of homeostatic inhibitory synaptic plasticity only.

The expected effect of deafferentation on the network—removal of external excitatory inputs—was a loss in activity. Although this was the case for neurons in the LPZ, a slight increase in activity was observed in neurons outside the LPZ (Figures 19b and 19c). This suggests that in this inhibition dominated network model, deafferentation results in a net loss of excitation in neurons of the LPZ but a net loss of inhibition is experienced by neurons outside it. Thus, for the neurons of the network to return to their pre-deprivation activity levels, while neurons in the LPZ must gain net excitation, neurons outside the LPZ must gain net inhibition. As the next sections will document, this has important implications on the activity dependent growth rules of various neurites.

As can also be seen in Figure 19, synaptic plasticity alone is unable to restore activity to deprived neurons in the LPZ. In this regime, where there are no changes in network connectivity, the neurons in the LPZ remain inactive in normal functioning of the network. Neurons outside the LPZ continue to fire. In essence, the LPZ is lost to the network, which continues to function without it.

3.2 ACTIVITY DEPENDENT GROWTH CURVES FOR POST-SYNAPTIC STRUCTURES

Having established that the homeostatic synaptic plasticity mechanism in the network is insufficient to restore activity to neurons of the LPZ, structural plasticity was activated in the subsequent simulations. The activity dependent growth curves for dendritic (post-synaptic) structures were investigated first since these form the input elements that accept neuronal inputs to modulate the activity of neurons.

All neurons in the LPZ, excitatory and inhibitory, show near zero activity after deafferentation due to a net loss in excitatory input (Figure 19). As summarised in Table 1, experimental studies report that these neurons gain excitatory synapses on newly formed dendritic spines (Keck, Mrsic-Flogel et al. 2008) and lose inhibitory shaft synapses (J. L. Chen, Villa et al. 2012) to restore activity after deprivation. The increase in lateral excitatory projections to these neurons requires them to gain excitatory dendritic elements to serve as contact points for excitatory axonal collaterals. At the same time, inhibitory synapses can be lost by the retraction of inhibitory dendritic elements. This suggests that new excitatory post-synaptic elements should be
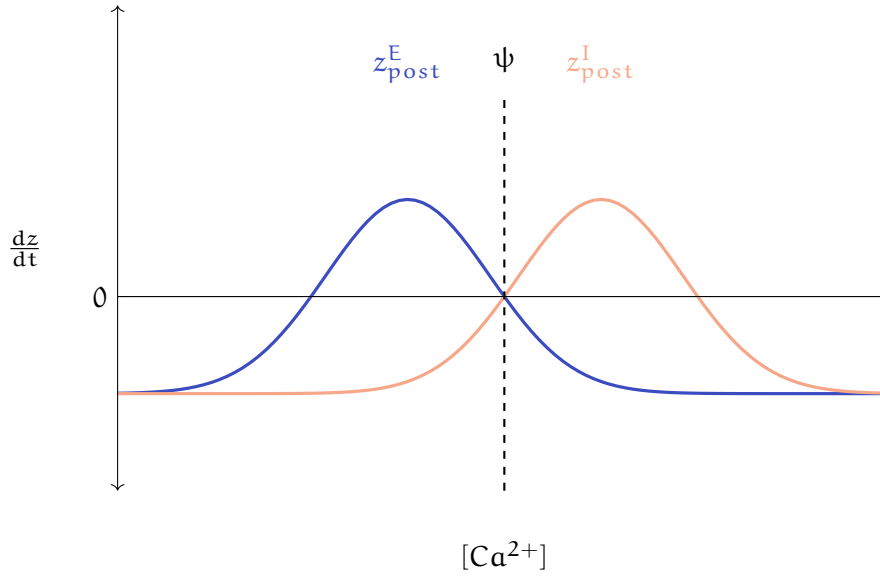
Figure 20: Activity-dependent dynamics of *post-synaptic* elements (dz/dt) as functions of a neuron's time averaged activity ($[Ca^{2+}]$): The balance between excitation and inhibition (E-I balance) received by a neuron may be disturbed by a change in either of the two types of input. Post-synaptic elements of a neuron react to deviations in activity from the optimal level (ψ) by countering the changes in excitatory or inhibitory inputs to restore the E-I balance. For both excitatory and inhibitory neurons, excitatory post-synaptic elements sprout when the neuron experiences a reduction in its activity, and retract when the neuron has received extra activity. Inhibitory post-synaptic elements for all neurons follow the opposite rule: they sprout when the neuron has extra activity and retract when the neuron is deprived of activity.

formed and inhibitory ones removed when neuronal activity is less than its optimal level (($[Ca^{2+}] < \psi$) in Figure 20):

$$\frac{dz_{post}^{E}}{dt} > 0 \quad \text{for} \quad [Ca^{2+}] < \psi$$

$$\frac{dz_{post}^{I}}{dt} < 0 \quad \text{for} \quad [Ca^{2+}] < \psi \tag{1}$$

Unlike neurons in the LPZ that suffered a net loss of excitation, neurons outside it appeared to suffer a net loss of inhibition, which indicates that they must gain inhibitory and lose excitatory inputs to return to their balanced state. Hence, the formation of new inhibitory dendritic elements and the removal of their excitatory counterparts occurs in a regime where neuronal activity exceeds the required amount (($[Ca^{2+}] > \psi$) in Figure 20):

$$\frac{dz_{post}^{E}}{dt} < 0 \quad \text{for} \quad [Ca^{2+}] > \psi$$

$$\frac{dz_{post}^{I}}{dt} > 0 \quad \text{for} \quad [Ca^{2+}] > \psi \tag{2}$$

The constraints described by Equations (1) and (2) can be satisfied by Gaussian growth rules for excitatory and inhibitory dendritic elements, with $\epsilon_{post}^{E} = \psi$ and $\eta_{post}^{I} = \psi$, respectively (Figure 20). Given the distinct characteristics of excitation and inhibition, the two growth rules were treated independently and the parameters governing them were tuned iteratively over multiple simulation runs. For example, sufficiently high values for the rate of formation of inhibitory dendritic elements had to be selected for excitatory neurons to prevent the build up of excessive excitation (Table 7).

3.2.1 *Selected post-synaptic growth curves stabilise individual neurons*

Experiments suggest that not just networks, but also individual neurons in the brain maintain a finely tuned balance between excitation and inhibition (Michael Okun and Ilan Lampl 2008; M. Okun and I. Lampl 2009; Isaacson and Scanziani 2011). This raised the question whether the complementary nature of the selected excitatory and inhibitory post-synaptic growth rules is sufficient to ensure stability at the level of single neurons.

Since the state of each neuron is tightly coupled to the states of other neurons in the network, a neuron was modelled in isolation to investigate how its input connectivity would be affected by changes in activity as per the selected post-synaptic growth curves (Figure 21a). The neuron is initialised with an input connectivity similar to a neuron from the network in its steady state: it has the same number of excitatory (z_{post}^{E}) and inhibitory (z_{post}^{I}) dendritic elements and receives the same mean conductances through them (g_{EE}, g_{IE}). Thus, the $[Ca^{2+}]$ of the neuron in this state represents its optimal activity ($\psi = [Ca^{2+}]$ at $t = 0\,s$ in Figure 21b). In this scenario, the net input conductance received by the neuron (g_{net}), which modulates its activity, can be estimated as the difference of the total excitatory (g_{EE}) and inhibitory (g_{IE}) input conductances.

$$g_{net} = z_{post}^{E} g_{EE} - z_{post}^{I} g_{IE} \qquad (3)$$

The activity of the neuron is then varied by an external sinusoidal current stimulus (Figure 21b). In addition, the deviation of the neuron's excitatory (Δg_{E}), inhibitory (Δg_{I}), and net input conductance (Δg_{net}) from baseline levels due to the formation or removal of dendritic elements under the action of the growth curves is recorded (Figure 21c). It was found that modifications of the input connectivity of the neuron resulted in alterations to its excitatory and inhibitory
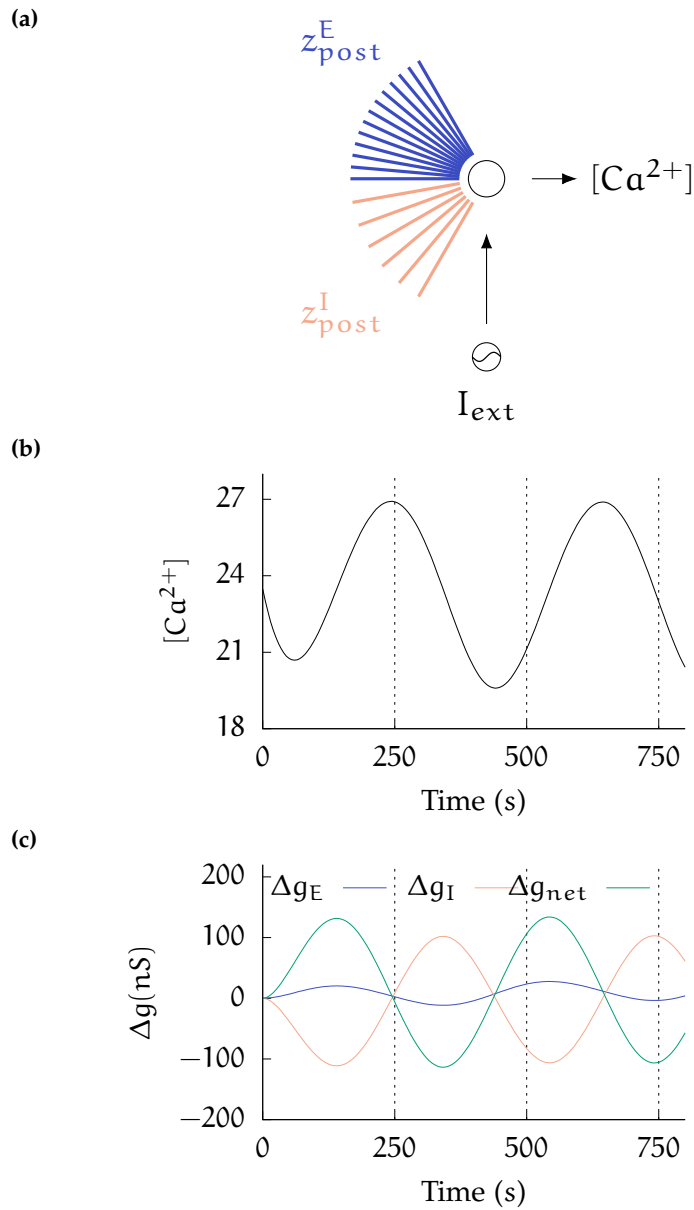
Figure 21: Input conductances in single neuron simulations show the homeostatic effect of the post-synaptic growth rules: **(a)** A neuron in its steady state receives excitatory (g_E) and inhibitory (g_I) conductance inputs through its excitatory (z_{post}^E) and inhibitory (z_{post}^I) dendritic elements, respectively, such that its activity ($[Ca^{2+}]$) is maintained at its optimal level (ψ) by its net input conductance (g_{net}). **(b)** An external sinusoidal current stimulus (I_{ext}) is applied to the neuron to vary its activity from the optimal level. **(c)** Under the action of the selected post-synaptic growth curves, the neuron modifies its dendritic elements to change its excitatory (Δg_E) and inhibitory (Δg_I) conductance inputs such that the net change in its input conductance (Δg_{net}) counteracts the change in its activity: an increase in $[Ca^{2+}]$ due to the external stimulus is followed by a decrease in net input conductance through the post-synaptic elements and vice versa (dashed lines in Figures 21b and 21c).
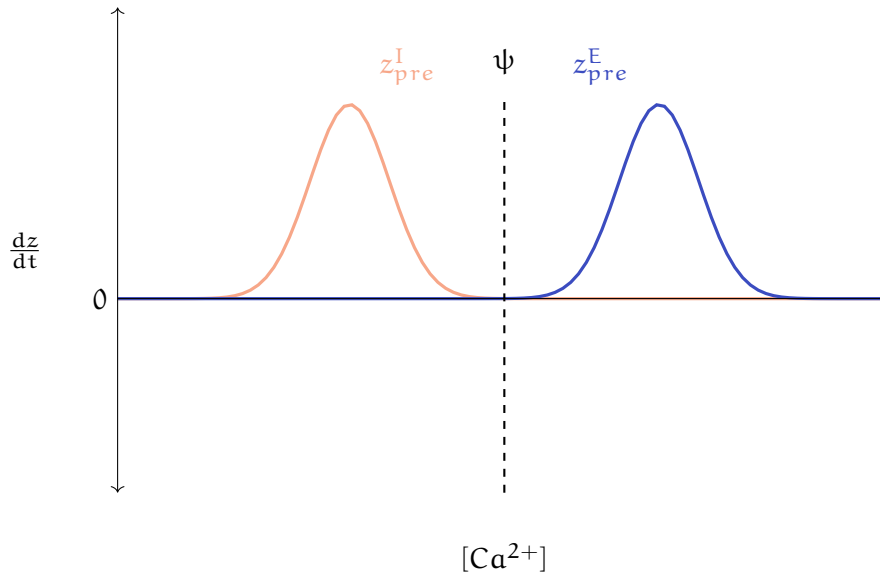
Figure 22: Activity-dependent dynamics of *pre-synaptic* elements (dz/dt) as functions of a neuron's time averaged activity ($[Ca^{2+}]$): In excitatory neurons, axonal sprouting is stimulated by extra activity. In inhibitory neurons, on the other hand, deprivation in activity stimulates axonal sprouting. Synaptic elements that do not find corresponding partners to form synapses (free synaptic elements) decay exponentially with time. These graphs are for illustration only. Please refer to Table 7 for parameter values.

input such that the net change in its input conductance counteracts changes in its activity: an increase in $[Ca^{2+}]$ due to the external stimulus is followed by a decrease in net input conductance through the post-synaptic elements and vice versa (dashed lines in Figures 21b and 21c). These simulation results show that even though the activity dependent growth rules of excitatory and inhibitory post-synaptic elements are derived from data gathered from network studies, they also serve a homeostatic function in single neurons.

3.3 ACTIVITY DEPENDENT GROWTH CURVES FOR PRE-SYNAPTIC STRUCTURES

While the activity dependent formation and degradation of post-synaptic elements provides a homeostatic mechanism for the stabilisation of activity in single neurons and the network, the increase in excitatory or inhibitory input received by a neuron also relies on the availability of pre-synaptic counterparts. Activity dependent growth rules for excitatory (z^Epre) and inhibitory (z_{pre}^I) pre-synaptic elements were initially derived using the same methods that were used for post-synaptic elements.

Within the LPZ, the increase in excitation requires a corresponding increase in the supply of excitatory pre-synaptic elements. Yamahachi et al. (2009) report a sizeable increase in the formation and removal of axonal structures in and around the LPZ, while Marik, Yamahachi, McManus et al. (2010) document a marked addition of lateral projections from neurons outside the LPZ into it. Whereas an increase in post-synaptic elements within the LPZ may contribute to repair, an inflow of activity from the periphery of the LPZ to its centre has been observed in multiple experiments (Darian-Smith and Gilbert 1994; Keck, Mrsic-Flogel et al. 2008; Marik, Yamahachi, McManus et al. 2010), pointing to the inwards sprouting of excitatory axonal projections from outside the LPZ as the major driver of homeostatic rewiring. For this sprouting of excitatory projections from the non-deafferented area into the LPZ, the increase in activity in neurons outside the LPZ must stimulate the formation of their excitatory axonal elements:

$$\frac{dz_{pre}^{E}}{dt} > 0 \quad \text{for} \quad [Ca^{2+}] > \psi \tag{1}$$

Conversely, neurons outside the LPZ with increased activity need access to inhibitory pre-synaptic elements in order to receive the required additional inhibitory input. Deafferentation studies in mouse somatosensory cortex (Marik, Yamahachi, McManus et al. 2010) report more than a 2.5 fold increase in the lengths of inhibitory axons projecting out from inhibitory neurons in the LPZ two days after the peripheral lesion. This outgrowth of inhibitory projections preceded and was faster than the ingrowth of their excitatory analogues (Marik, Yamahachi, McManus et al. 2010; Marik, Yamahachi, Alten Borgloh et al. 2014). In the model, the experimentally observed outward protrusion of inhibitory axons from the LPZ requires that the formation of inhibitory pre-synaptic elements is driven by reduced neuronal activity:

$$\frac{dz_{pre}^{I}}{dt} > 0 \quad \text{for} \quad [Ca^{2+}] < \psi \tag{2}$$

To validate the derived pre-synaptic growth curves, shown in Figure 22, the complete set of possible pre-synaptic growth curves was tested. These are labelled **G0, G1, G2, G3, G4,** and **G5** and illustrated in Figure 23:

- **G0**: control case where there are no growth curves, achieved by setting $\nu = 0$,

- **G1**: both inhibitory and excitatory neurites sprout when activity is more than required,

- **G2**: (selected growth curves shown in Figure 22 fall in this family) inhibitory neurites sprout when activity is less than

optimal, but excitatory neurites sprout when activity is more than required,

- **G3**: excitatory neurites sprout when activity is less than optimal, but inhibitory neurites sprout when activity is more than required,

- **G4**: both excitatory and inhibitory neurites sprout at optimal activity, and

- **G5**: both inhibitory and excitatory neurites sprout when activity is less than optimal.

As summarised in Table 6, only the derived pre-synaptic growth curves reproduce all experimentally reported features of the repair process. Although a few other pre-synaptic growth curves did allow simulations to show an increase in activity in the LPZ and a loss of activity outside it, the networks in these simulations did not re-balance to a stable state.

Similar to the post-synaptic growth rules, the pre-synaptic growth rules for excitatory and inhibitory neurons were also treated separately and their parameters were tuned iteratively over repeated simulations. Since inhibitory neurons form only one-fifth of the neuronal population, and only a small number of these fall into the LPZ, in this study, simulations require the growth rates of inhibitory axonal elements to be high enough to stabilise the large number of hyperactive neurons outside the LPZ (Table 7).

Figures 28a and 28b show the rewiring of axonal projections from an excitatory neuron in the peri-LPZ and an inhibitory neuron in the centre of the LPZ, respectively. Following the growth functions derived above, our simulations correctly reproduce the inward sprouting of excitatory axons into the LPZ and the outward sprouting of inhibitory axons from the LPZ that is observed during the repair process.

3.4 A NEW MODEL OF RECOVERY IN SIMPLIFIED CORTICAL AI NETWORKS AFTER PERIPHERAL LESIONS

Figures 24 and 25 provide an overview of the activity in the network observed in simulations using the derived activity dependent growth curves. The network is initially balanced by the homeostatic inhibitory Spike Timing Dependent Plasticity (STDP) mechanism, which results in establishing its physiological state where it displays low frequency AI firing similar to cortical neurons (Vogels et al. 2011) (t < 1500 s
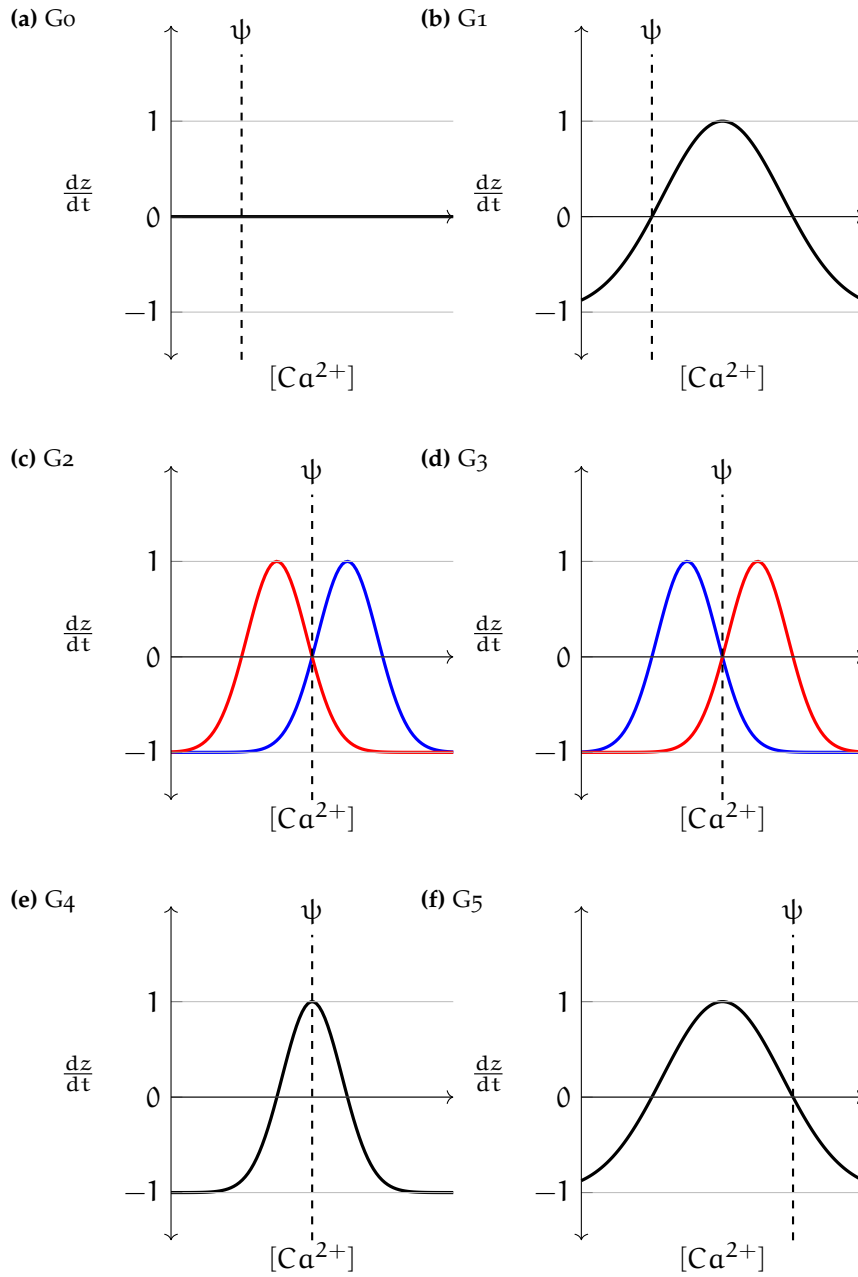
**Figure 23:** Axonal growth curves investigated in the study. (Where applicable, Red: inhibitory, Blue: excitatory)

	G0	G1	G2	G3	G4	G5
Initially remains stable	Y	Y	Y	Y	N	Y
LPZ gains activity	Y	Y	Y	N	NA	N
Outside LPZ loses activity	Y	Y	Y	NA	NA	NA
Returns to balanced state	N	N	Y	NA	NA	NA
LPZ B restores before LPZ C	NA	NA	Y	NA	NA	NA
Ingrowth of excitatory projections	NA	NA	Y	NA	NA	NA
Outgrowth of inhibitory projections	NA	NA	Y	NA	NA	NA
Disinhibition in LPZ	NA	NA	Y	NA	NA	NA

Table 6: Summary of axonal growth curve hypotheses tested in the model. Each row represents a feature that is observed in experiments:
1. Initially remains stable: the network should remain stable without deafferentation; **2. LPZ gains activity**: increase in activity of LPZ neurons to pre-deafferentation levels; **3. Outside LPZ loses activity**: decrease in activity of neurons outside the LPZ to pre-deafferentation levels; **4. Returns to balanced state**: the network should return to its balanced stable state after activity of all neurons has been restored to pre-deafferentation levels; **5. LPZ B restores before LPZ C**: activity should be restored to the LPZ B neurons before the LPZ C neurons; **6. Ingrowth of axonal projections**: there should be ingrowth of excitatory axons to the LPZ; **7. Outgrowth of inhibitory projections**: outgrowth of inhibitory axons from the LPZ should stabilise neurons outside the LPZ; **8. Disinhibition in LPZ**: disinhibition should be observed in the LPZ neurons.
Each column represents a set of growth curves (illustrated in Figure 23):
G0: no growth curves (no sprouting or retraction); **G1**: both inhibitory and excitatory neurites sprout when activity is more than required; **G2**: inhibitory neurites sprout when activity is less than optimal, but excitatory neurites sprout when activity is more than required; **G3**: excitatory neurites sprout when activity is less than optimal, but inhibitory neurites sprout when activity is more than required; **G4**: both excitatory and inhibitory neurites sprout at optimal activity. **G5**: both inhibitory and excitatory neurites sprout when activity is less than optimal;
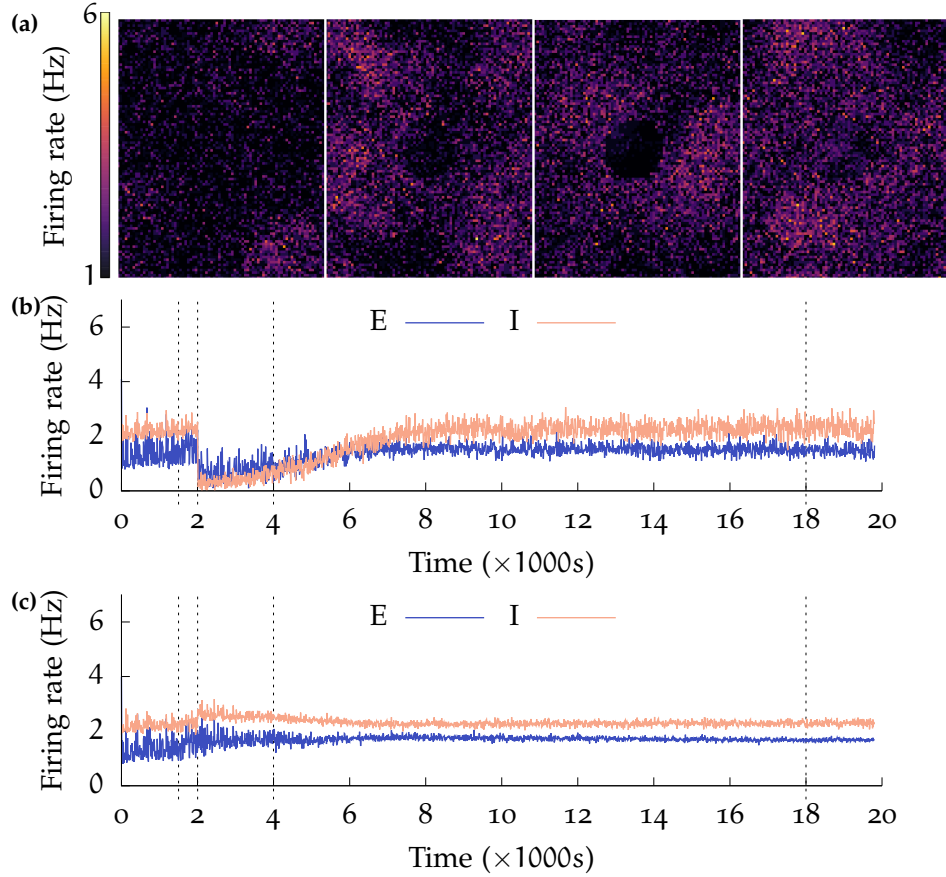
Figure 24: Recovery of activity over time (mean firing rates): (Mean firing rates of neurons are calculated over a 2500 ms window): **(a)** shows the firing rates of the whole excitatory population at t = {1500 s, 2001.5 s, 4000 s, and 18 000 s}. These are marked by dashed lines in the next graphs. **(b)** shows mean firing rate of neurons in LPZ-C; **(c)** shows mean firing rate of neurons in peri-LPZ; The network is permitted to achieve its balanced AI low frequency firing regime under the action of inhibitory synaptic plasticity (t ⩽ 1500 s). The structural plasticity mechanism is then activated to confirm that the network remains in its balanced AI state (panel 1 in Figure 24a). At (t = 2000 s), neurons in the LPZ are deafferented (panel 2 in Figures 24a and 25b are at t = 2001.5 s) and the network allowed to repair itself under the action of the structural plasticity mechanism (panels 3 (t = 4000 s) and 4 (t = 18 000 s) in Figures 24a and 25b).
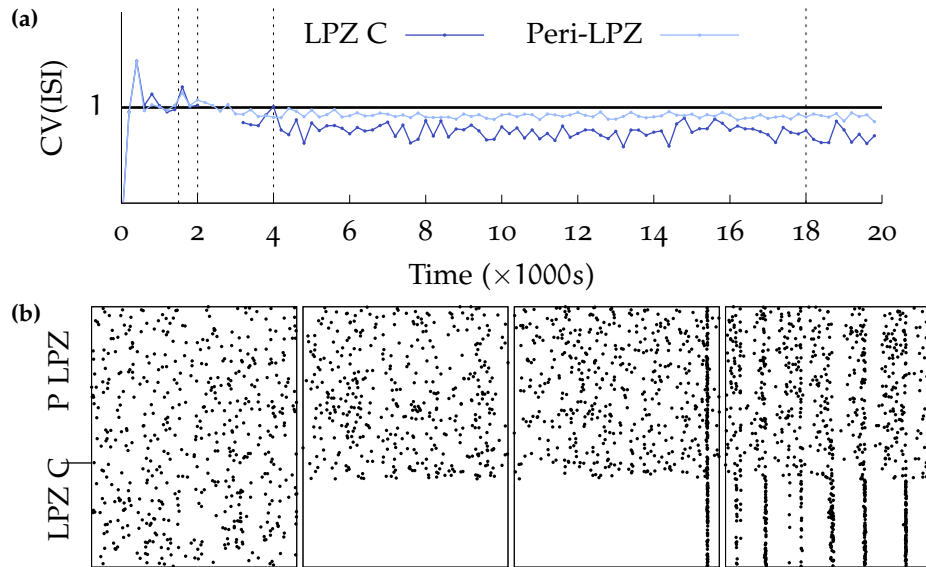
Figure 25: Recovery of activity over time (firing characteristics): (Mean firing rates of neurons are calculated over a 2500 ms window): **(a)** shows the coefficient of variation (CV) of the inter-spike intervals of neurons in the LPZ-C and peri-LPZ. The graph is discontinuous because ISI CV is undefined in the absence of spikes in the LPZ C; **(b)** shows spike times of neurons in the LPZ C and peri-LPZ over a 1 s period at $t = \{1500\,s, 2001.5\,s, 4000\,s,$ and $18\,000\,s\}$. The network is permitted to achieve its balanced AI low frequency firing regime under the action of inhibitory synaptic plasticity ($t \leqslant 1500\,s$). The structural plasticity mechanism is then activated to confirm that the network remains in its balanced AI state (panel 1 in Figure 24a). At ($t = 2000\,s$), neurons in the LPZ are deafferented (panel 2 in Figures 24a and 25b are at $t = 2001.5\,s$) and the network allowed to repair itself under the action of the structural plasticity mechanism (panels 3 ($t = 4000\,s$) and 4 ($t = 18\,000\,s$) in Figures 24a and 25b).

in Figures 24b, 24c and 25a, and panel 1 in Figures 24a and 25b). Once this AI state is achieved, homeostatic structural plasticity is enabled, and it is confirmed that the network maintains its balanced state under the combined action of the two homeostatic mechanisms ($1500\,s < t < 2000\,s$ in Figures 24b, 24c and 25a). At ($t = 2000\,s$), the network is deafferented by removing external inputs to neurons in the LPZ.

In line with experimental findings, the immediate result of deafferentation is the loss of activity in neurons of the LPZ. Neurons outside the LPZ, on the other hand, show an increase in activity ($t = 2000\,s$ in Figure 24c). The change in activity caused by deafferentation stimulates neurite turnover in neurons of the network in accordance with the proposed activity dependent growth rules ($t > 2000\,s$). Over time, activity is gradually restored in the network to pre-deafferentation levels ($t = 18\,000\,s$ in Figures 24b and 24c, and panel 4 in Figures 24a and 25b).

Even though the mean activity of neurons within and outside the LPZ returns to pre-deprivation levels, the network reorganization by structural plasticity leads to synchronous spiking in neurons in the LPZ, instead of the AI firing observed during the pre-deprivation stages in simulations (t > 4000 s in Figure 25a, and panels 3 and 4 in Figure 25b). This predicted effect of network rewiring on the temporal characteristics of neural activity should be an interesting subject for future experimental studies. Furthermore, the observed lack of AI activity in the LPZ is expected to have functional implications; this is another promising topic for future theoretical work.

Figure 26 shows the time course of rewiring of excitatory and inhibitory connections to excitatory neurons in the centre of the LPZ that result from these growth curves in simulation runs. As described in experimental studies, the loss of activity by neurons in the LPZ is followed by an increase in excitatory input connections and a transient reduction in inhibitory input connections. Specifically, as also found in these experiments, the increase in excitatory inputs is dominated by an ingrowth of lateral projections from outside the LPZ. Both of these features can be seen in Figures 26a and 26b. As shown in Figure 27, neurons directly outside the LPZ lose excitatory and gain inhibitory input connections to reduce their activity back to their optimal values. Furthermore, in line with experimental observations, a significant contribution to the new inhibitory inputs to these neurons is provided by new inhibitory projections from within the LPZ. Given the small number of inhibitory neurons in the LPZ, however, their inhibitory projections were found to be insufficient to stabilise the large number of neurons outside the LPZ in simulations runs. Hence, inhibitory projections are also recruited from inhibitory neurons outside the LPZ.

Figures 28a and 28b show the rewiring of axonal projections from an excitatory neuron in the peri-LPZ and an inhibitory neuron in the centre of the LPZ, respectively. Following the growth functions derived above, simulations correctly reproduce the inward sprouting of excitatory axons into the LPZ and the outward sprouting of inhibitory axons from the LPZ that is observed during the repair process.

## 3.5 SYNAPTIC AND STRUCTURAL PLASTICITY ARE BOTH NECESSARY FOR REPAIR

In my model, network rewiring after deafferentation of the LPZ occurred in the presence of both activity-dependent structural plasticity and inhibitory synaptic plasticity. These results show that both types of homeostatic plasticity can co-exist during successful network repair, but they do not indicate their respective contributions to restoring ac-

(a)

(b)

(c)

(d)
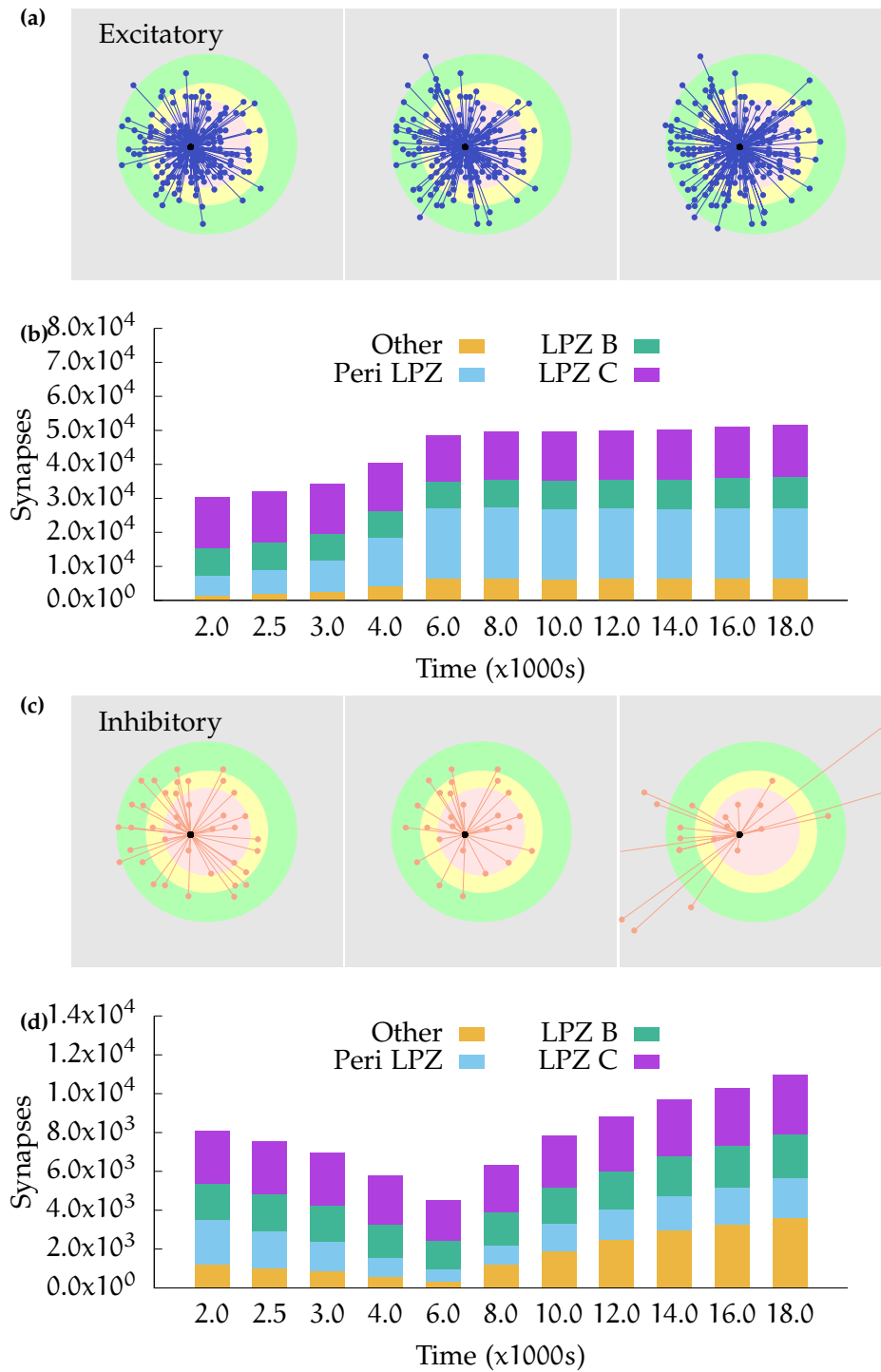
Figure 26: Input connectivity of excitatory neurons in the centre of the LPZ: **(a)** and **(c)** show incoming excitatory and inhibitory projections to the same randomly chosen neuron in the centre of the LPZ at different stages of the simulations. From left to right: t = 2000 s, t = 4000 s, and t = 18 000 s. **(b)** and **(d)** show total numbers of incoming excitatory and inhibitory projections to these neurons from different regions at different points in time. Following the proposed growth rules for post-synaptic elements and consistent with experimental reports, the deprived neurons in the LPZ C gain lateral excitatory inputs from neurons outside the LPZ. Also in line with biological observations, they temporarily experience disinhibition after deafferentation. However, as these neurons gain activity from their new lateral excitatory inputs, the number of their inhibitory input connections increases again in order to restore the E-I balance.
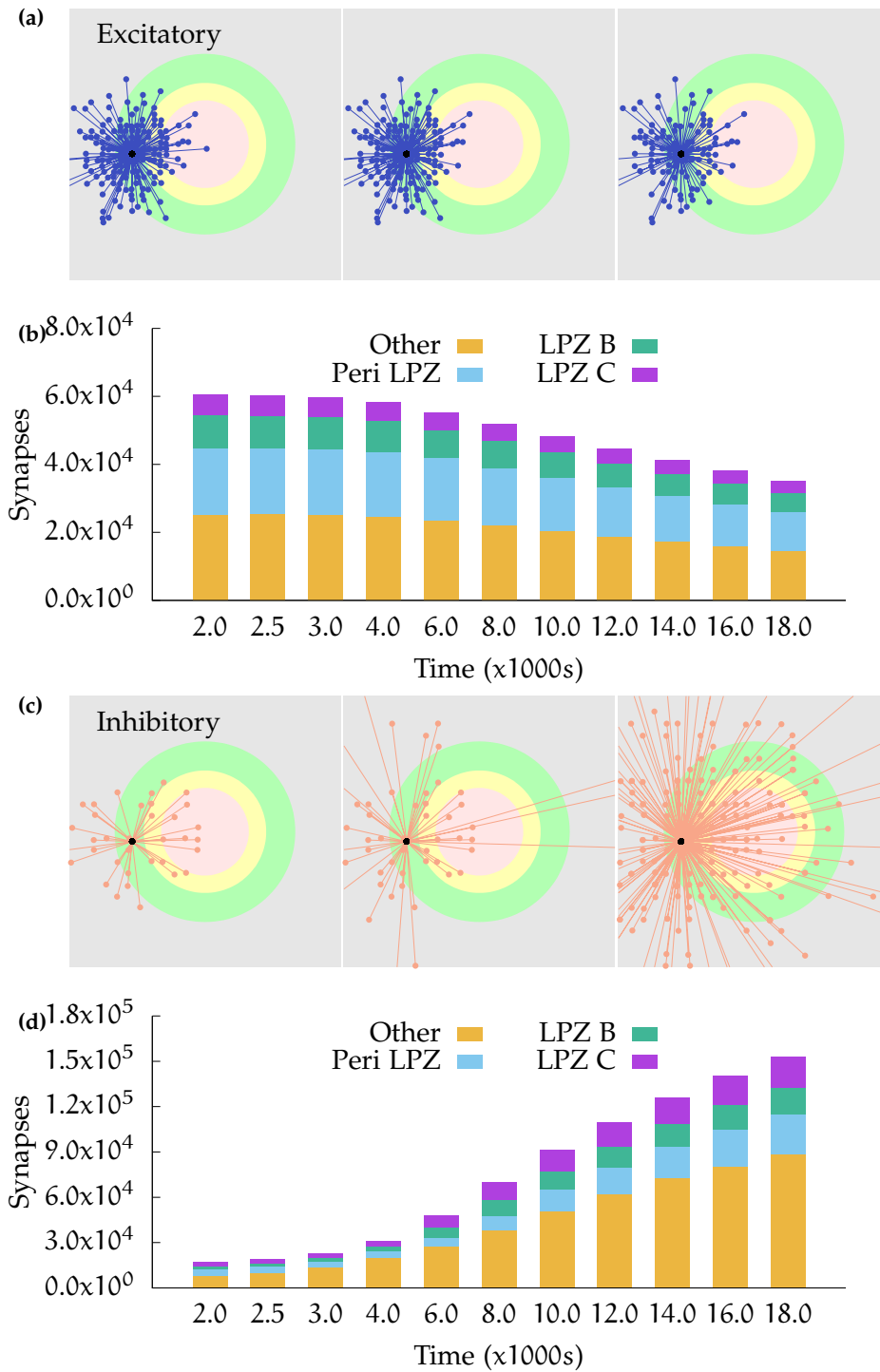
Figure 27: Input connectivity of excitatory neurons in the peri-LPZ: **(a)** and **(c)** show the incoming excitatory and inhibitory projections to the same randomly chosen neuron in the peri-LPZ at different stages in the simulation. From left to right: t = 2000 s, t = 4000 s, and t = 18 000 s. **(b)** and **(d)** show total numbers of incoming excitatory and inhibitory projections to these neurons from different regions at different points in time. In contrast to neurons in the LPZ, neurons outside the LPZ experience an increase in activity in these simulations. As a result of the growth rules, these neurons lose excitatory inputs and gain inhibitory ones so that their activity is reduced back to pre-lesion levels.
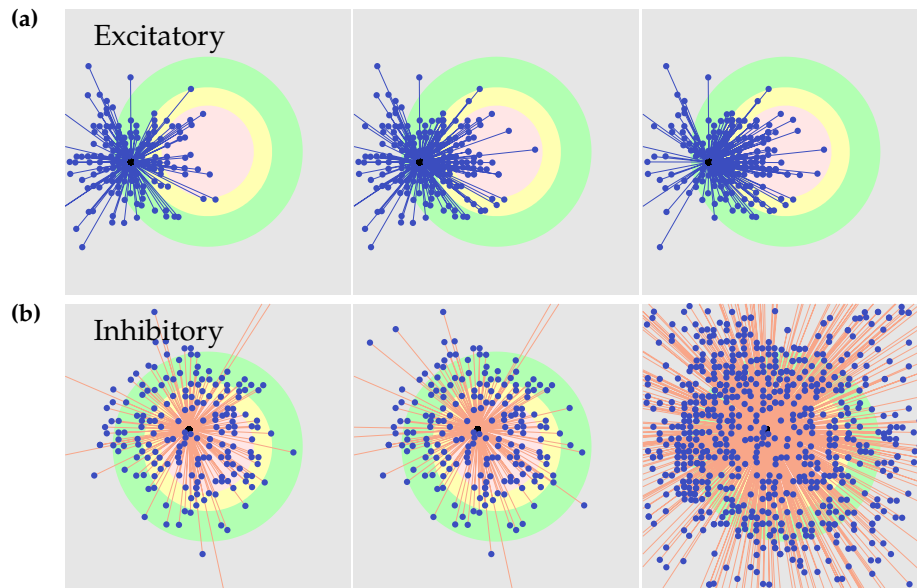
Figure 28: Outgoing neuronal projections: **(a)** shows the outgoing (axonal) projections of an excitatory neuron in the peri-LPZ. **(b)** shows the outgoing (axonal) projections of an inhibitory neuron in the LPZ C. From left to right: t = 2000 s, t = 4000 s, and t = 18 000 s. As per the suggested growth rules for pre-synaptic elements, excitatory neurons produce new pre-synaptic elements and sprout axonal projections when they experience extra activity, while inhibitory neurons form new pre-synaptic elements and grow axons when they are deprived of activity. As a consequence and in line with experimental data, following deafferentation of the LPZ, excitatory neurons in the peri-LPZ sprout new outgoing projections that help transfer excitatory activity to neurons in the LPZ. Also in accordance with experimental work, inhibitory neurons inside the LPZ form new outgoing connections that transmit inhibition to neurons outside the LPZ.

tivity in the network. Section 3.1 documented that inhibitory synaptic plasticity alone, although able to re-balance neurons outside the LPZ by increasing the strength of their inhibitory inputs, fails to restore activity in the deprived neurons in the LPZ even after small peripheral lesions (Figures 29a and 29d). Although the homeostatic inhibitory synaptic plasticity on its own leads to a reduction in conductances of the inhibitory synapses projecting onto neurons in the LPZ, this is not sufficient to reactivate them. The stabilisation of activity in the neurons outside the LPZ, however, is successful due to the strengthening of IE synapses by STDP. In the absence of network rewiring by structural plasticity, this leads to a network where the neurons outside the LPZ retain their functionality while the LPZ is effectively lost. This indicates that the larger deviations from the desired activity that result from deafferentation in the balanced network model require the reconfiguration of network connectivity by structural plasticity to re-establish a functional balance.
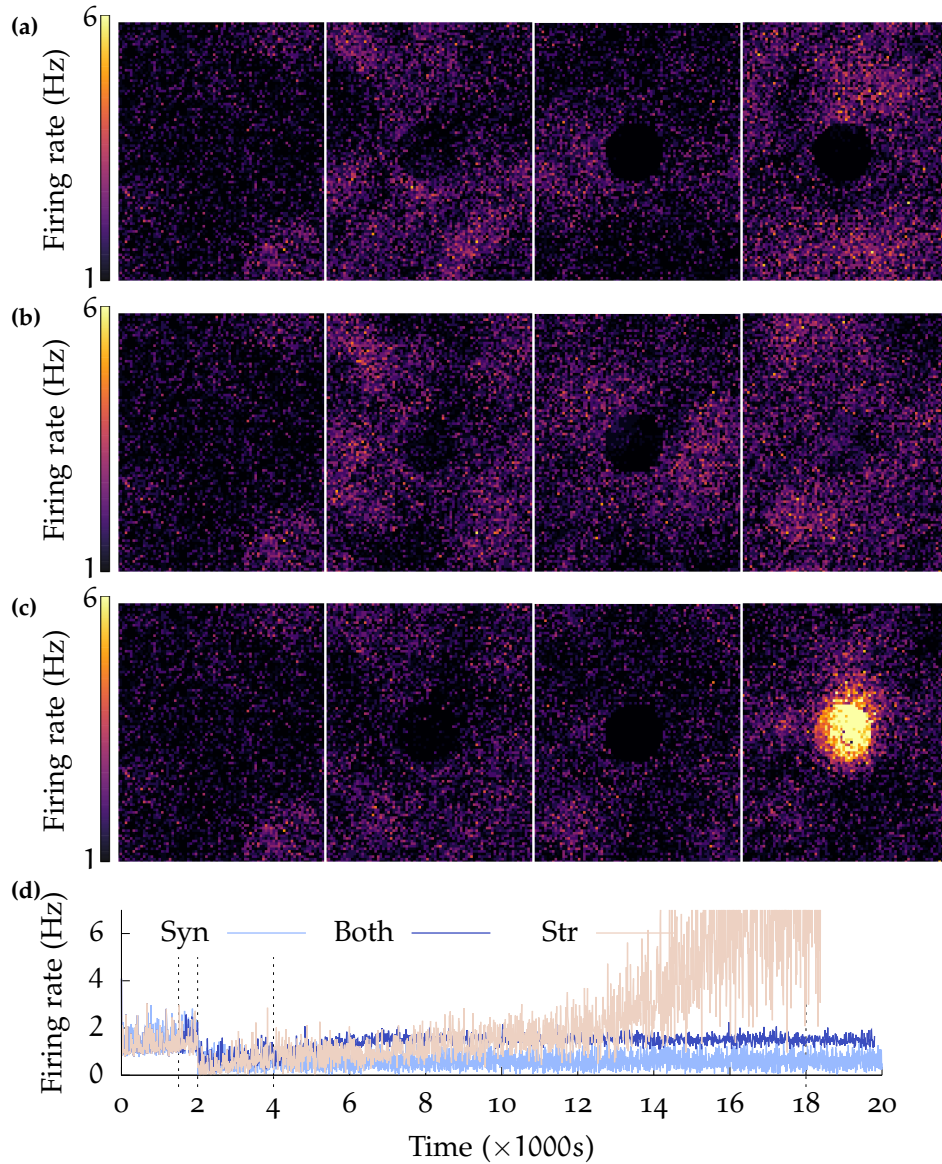
Figure 29: Both structural and synaptic plasticity are required for restoration of activity after deafferentation: **(a), (b), (c)** show firing rate snapshots of neurons at t = 1500 s, 2001.5 s, 4000 s, 18 000 s. **(a)** Synaptic plasticity only: after the network has settled in its physiological state by means of synaptic plasticity, structural plasticity is not enabled. With only synaptic plasticity present, the network is unable to restore activity to neurons in the LPZ. Neurons outside the LPZ return to their balanced state, but the neurons in the LPZ are effectively lost to the network. **(b)** Both structural and synaptic plasticity are enabled: neurons in the LPZ regain their low firing rate as before deafferentation. **(c)** Structural plasticity only: after the network has settled in its physiological state by means of synaptic plasticity, homeostatic synaptic plasticity is turned off and only structural plasticity is enabled. With only structural plasticity present, activity returns to neurons in the LPZ but does not stabilise in a low firing rate regime. The firing rate of these neurons continues to increase and, as a result, these neurons continue to turn over synaptic elements. This cascades into increased activity in neurons outside the LPZ, further causing undesired changes in network connectivity. **(d)** shows the mean population firing rates of neurons in the centre of the LPZ for the three simulation configurations. (Panel 1 is identical in all three simulation configurations because the same parameters are used to initialise all simulations.)

Simulations where homeostatic synaptic plasticity was disabled, on the other hand, also failed to re-establish the balanced state of the network before the peripheral lesion (Figures 29c and 29d). Though the activity of the deprived neurons in the LPZ initially increased back to pre-lesion levels, under the action of structural plasticity only, the network eventually started exhibiting abnormally high firing rates instead of settling in the desired low firing rate regime. These results suggest that inhibitory synaptic plasticity is required to finely tune inputs to neurons so that the network can achieve its balanced state.

Thus, the simulations run in this study predict that both homeostatic processes are required for successful repair—structural plasticity for larger changes in network connectivity and synaptic plasticity for the fine tuning of conductances that establishes stable activity in the network. These results support the idea that multiple plasticity mechanisms work in harmony to sustain functional brain networks at varying time scales.

3.6   CHAPTER CONCLUSIONS

This chapter documented the derivation of activity dependent growth curves of various neurites using simulations of the newly developed model of peripheral lesioning that was reported in Chapter 2.

First, simulations of the new model suggest that deafferentation does not necessarily result in the loss or even a decrease of activity in all neurons of the network. Neurons outside the LPZ experienced a gain in activity because of a net loss in inhibition in these simulations. This prediction should be tested in future experiments that investigate neuronal activity just outside the LPZ.

Secondly, simulation results suggest that although the network may restore its mean activity, the temporal fine structure of the activity, and in particular the AI firing characteristic of the network are permanently disturbed by deafferentation. This change in firing patterns of the network also merits experimental validation, especially given its implications for network function. Synchronous firing in the network may not be evident in studies of the mapping between peripheral inputs and network activity. However, in combination with the change in network connectivity, it can affect network function, such as the storage and recall of associative memory. Given that the inhibitory STDP mechanism is unable to maintain the network in its AI regime following repair by structural plasticity, the deviation from the AI firing regime is likely caused by the alteration of network connectivity during the repair process. Indeed, as Figure 26b shows, neurons in the

LPZ C region gain a significant number of lateral excitatory connections from neurons outside the LPZ ($< 1 \times 10^4$ before deafferentation at t = 2000s vs 3×10^4 at the end of the repair process at t = 18000s) greatly increasing their excitatory input connectivity. This is in line with previous work that indicates that synchronisation may occur in networks of excitatory and inhibitory neurons when the number of inputs being received by neurons is more than a critical value (Börgers and Kopell 2003; Brunel 2000; Qu et al. 2013; Golomb and Hansel 2000; Nowotny and Huerta 2003; Papadopoulou et al. 2011). The precise relationship between network sparsity and population firing dynamics in a network balanced by the inhibitory STDP mechanism used here, however, does not appear to have been ascertained yet.

Thirdly, the results from simulations suggest different growth rules for different types of neurite (Figures 20 and 22). In spite of being derived from network lesion experiments that were not aimed at studying the relation between activity and neurite turnover (Marik, Yamahachi, McManus et al. 2010; J. L. Chen, Lin et al. 2011; Yamahachi et al. 2009; Hickmott and Steen 2005; Keck, Mrsic-Flogel et al. 2008; Keck, Scheuss et al. 2011; Trachtenberg et al. 2002; Marik, Yamahachi, Alten Borgloh et al. 2014), other work seems to support these proposals. The growth rule for excitatory dendritic elements is coherent with results from an experimental study in hippocampal slice cultures. In their study, Richards et al. (2005) note that reduced neuronal activity resulted in the extension of glutamate receptor-dependent processes from dendritic spines of CA1 pyramidal neurons. Furthermore, the predicted growth function for inhibitory dendritic elements is supported by a study by Knott, Quairiaux et al. (2002), which reports an increase in inhibitory inputs to spines in adult mice after their activity was increased by whisker stimulation.

On the pre-synaptic side, axonal turnover and guidance has been investigated in much detail, and is known to be a highly complex process incorporating multiple biochemical pathways (Goodhill 2013; Lowery and Van Vactor 2009). The hypothesis regarding excitatory pre-synaptic structures is supported by a report by Perez et al. (1996) who find that CA1 pyramidal cells, which become hyper-excitable following hippocampal kainate lesions, sprout excitatory axons that may contribute to the epileptiform activity in the region. For inhibitory pre-synaptic elements, Schuemann et al. (2013) report that enhanced network activity reduced the number of persistent inhibitory boutons over short periods of time (30 minutes) in organotypic hippocampal slice cultures. However, these experiments also found that prolonged blockade of activity (over seven days) did not affect inhibitory synapses, contrary to the reports from peripheral lesion studies (J. L. Chen, Villa et al. 2012; Keck, Scheuss et al. 2011).

Indirect evidence on the temporal evolution of inhibitory projections to neurons in the LPZ further supports the inhibitory growth rules suggested in this chapter (Figure 26d). Whereas an initial disinhibition aids recovery in these deprived neurons, as activity is restored, a subsequent increase in inhibition is seen to re-establish the E-I balance in the deafferented region in the simulations. This is in line with observations that the pharmacological reduction of inhibition re-activates structural plasticity in the visual cortex (Vetencourt et al. 2008). These simulations, therefore, support the proposed role of inhibition as control mechanism for the critical window for structural plasticity (Rosier et al. 1995; Massie et al. 2003; Garraghty, LaChica and J H Kaas 1991; Hensch 2005; Fagiolini and Hensch 2000; Versendaal et al. 2012).

Finally, these simulation results indicate that the suggested growth rules, despite being derived from network simulations, can contribute to the stability of activity in individual neurons (Figure 21). Since structural plasticity and synaptic plasticity are not independent processes in the brain, this is not a wholly surprising result. Structural plasticity of the volumes of spines and boutons underlies the modulation of synaptic efficacy by synaptic plasticity. Thus, given that synaptic plasticity mechanisms can stabilise the firing of individual neurons (Turrigiano 2008; Keck, Keller et al. 2013), it follows that structural plasticity mechanisms could also be involved. Further, extending from the functional coupling of synaptic and structural plasticity, these simulations also required both structural and synaptic plasticity for successful network repair (Figure 29). Thus, the results obtained here lend further support to the notion that multiple plasticity mechanisms function in a cooperative manner in the brain.

These proposals are limited by the various shortcomings, assumptions, and constraints that apply to the model that were discussed in the previous chapter. In addition, whereas simulations were sufficient to indicate the families of growth curves that apply to neurites, an exhaustive exploration of the parameter space of growth curves for individual neurites was hindered by the computational costs of simulation. Where simulations without structural plasticity merely took hours on 128 processing cores on the UH High Performance Cluster, the activation of structural plasticity increased the computing time to the maximum available—a full week. This required additional constraints to be included to reduce the parameter space to be explored.

These simulation results do not imply that these are the only activity dependent growth rules that can underlie the turnover of neurites. Given the variety of neurons in the brain, many families of growth rules may apply to neurons. For example, as discussed previously, Butz and van Ooyen (2013) proposed a different set of growth rules

using a model of peripheral lesioning in fast spiking neurons that did not investigate the low firing AI state. Different growth rules could therefore apply to brain regions with different neuronal types and firing characteristics.

Table 7: Growth rule parameters.

Parameter	Symbol	Value
Optimal $[\text{Ca}^{2+}]$	ψ	
Excitatory neurons		
Scaling factor: pre-synaptic structures (z_{pre}^{E})	ν_{pre}^{E}	15×10^{-4}
Vertical shift	ω_{pre}^{E}	1×10^{-2}
X-axis parameters	$(\eta_{pre}^{E}, \epsilon_{pre}^{E})$	$(\psi, 1.75 \times \psi)$
Decay rate	$\tau_{pre,free}^{E}$	0.01
Scaling factor: excitatory post-synaptic structures ($z_{post,E}^{E}$)	$\nu_{post,E}^{E}$	3×10^{-5}
Vertical shift	$\omega_{post,E}^{E}$	4×10^{-1}
X-axis parameters	$(\eta_{post,E}^{E}, \epsilon_{post,E}^{E})$	$(0.25 \times \psi, \psi)$
Decay rate	$\tau_{post,E,free}^{E}$	0.01
Scaling factor: inhibitory post-synaptic structures ($z_{post,I}^{E}$)	$\nu_{post,I}^{E}$	3×10^{-4}
Vertical shift	$\omega_{post,I}^{E}$	4×10^{-2}
X-axis parameters	$(\eta_{post,I}^{E}, \epsilon_{post,I}^{E})$	$(\psi, 3.5 \times \psi)$
Decay rate	$\tau_{post,I,free}^{E}$	0.01
Inhibitory neurons		
Scaling factor: pre-synaptic structures (z_{pre}^{I})	ν_{pre}^{I}	3×10^{-2}
Vertical shift	ω_{pre}^{I}	4×10^{-4}
X-axis parameters	$(\eta_{pre}^{I}, \epsilon_{pre}^{I})$	$(0.25 \times \psi, \psi)$
Decay rate	$\tau_{pre,free}^{I}$	0.01
Scaling factor: excitatory post-synaptic structures ($z_{post,E}^{I}$)	$\nu_{post,E}^{I}$	3×10^{-5}
Vertical shift	$\omega_{post,E}^{I}$	4×10^{-1}
X-axis parameters	$(\eta_{post,E}^{I}, \epsilon_{post,E}^{I})$	$(0.25 \times \psi, \psi)$
Decay rate	$\tau_{post,E,free}^{I}$	0.01
Scaling factor: inhibitory post-synaptic structures ($z_{post,I}^{I}$)	$\nu_{post,I}^{I}$	3×10^{-5}
Vertical shift	$\omega_{post,I}^{I}$	4×10^{-1}
X-axis parameters	$(\eta_{post,I}^{I}, \epsilon_{post,I}^{I})$	$(\psi, 3.5 \times \psi)$
Decay rate	$\tau_{post,I,free}^{I}$	0.01

4

# NETWORK REORGANISATION AND ASSOCIATIVE MEMORY

The novel model of peripheral lesioning discussed in the previous chapter allowed for the investigation of the primary research question outlined at the start of the study: how does network repair affect the storage and recall of associative memory stored in the network?

The simulation protocol used in this stage of the study was similar to previous protocols (Figure 30). Initially, the network is allowed to stabilise to its balanced Asynchronous Irregular (AI) state under the action of only homeostatic synaptic plasticity. When this steady state has been achieved, an associative memory is stored in the network by strengthening the lateral excitatory synapses between a randomly selected set of excitatory neurons. This normally functioning network is then subjected to a peripheral lesion by deafferenting neurons in a region to form the Lesion Projection Zone (LPZ). As the network undergoes repair using the activity dependent growth curves derived in the previous chapter, the recall performance of the associative memory is measured.

To quantify the effect of the deafferentation and repair, the analysis was divided into three stages. First, the recall performance of associative memories stored in a normally functioning network was established. Next, the recall performance of the associative memories after deafferentation but without repair was quantified to investigate the effects of sensory deprivation. Finally, the recall performance of the associative memories during the repair process was noted.

The proportion of the associative memory that is deafferented is also expected to affect its recall performance. If more neurons of the associative memory fall in the LPZ, fewer neurons are available to receive projections that may recall the stored memory. This effect of the overlap between LPZ and neurons of the associative memory was also tested.

The work documented in this chapter has been submitted to CNS*2020 for consideration.
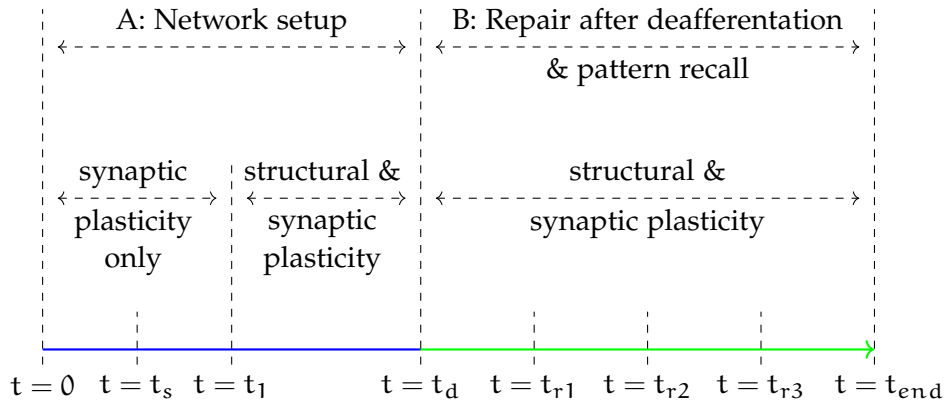
Figure 30: The simulations in 2 phases. Initially, the setup phase ($0\,\mathrm{s} < t < t_d$) is run to set the network up to the balanced AI state. Here, the network is allowed to stabilise to its AI state under the action of synaptic plasticity only. Then, at ($t = t_s$), an associative memory is stored in the network by strengthening the excitatory synapses between a randomly selected set of excitatory neurons. The network is again allowed to stabilise to its AI state under the action of synaptic plasticity only ($t = t_1$). This represents the physiological state of the network. Neuronal parameters obtained at this point are used as the steady-state/homeostatic parameters for neurons. Structural plasticity is then enabled to verify that the network remains in its stable balanced AI state. At ($t = t_d$), a subset of the neuronal population is deafferented to simulate a peripheral lesion and the network is allowed to repair under the action of homeostatic mechanisms. At regular intervals ($t = \{t_{r1}, t_{r2}, t_{r3}, \dots\}$), the stored associative memory is recalled by providing external stimulus to a randomly selected set of neurons that form it. While neurons from the pattern that fall in the LPZ may be selected for this stimulus, given that they have been deafferented, they will not receive any. During each recall, both plasticity mechanisms are disabled to prevent changes in network connectivity. They are re-enabled a short period after each recall when the network has returned to its steady state.

4.1 REVISITING RECALL PERFORMANCE WITHOUT DEAFFERENTATION

Although the recall performance of stored associative memories in a physiological network was already established in Chapter 1, the extensions made to the cortical network model necessitated a reconfirmation of these metrics. Specifically, in the new implementation of the model in NEST, neurons are spatially distributed and connectivity is distance dependent—neurons closer to each other are now more likely to form synapses. If more associative memory neurons are selected from the region that would form the LPZ, a higher proportion of associative memory neurons would be closer to each other. As a result, the associative memory would include more lateral excitatory synapses that would be strengthened to store it. This section documents results
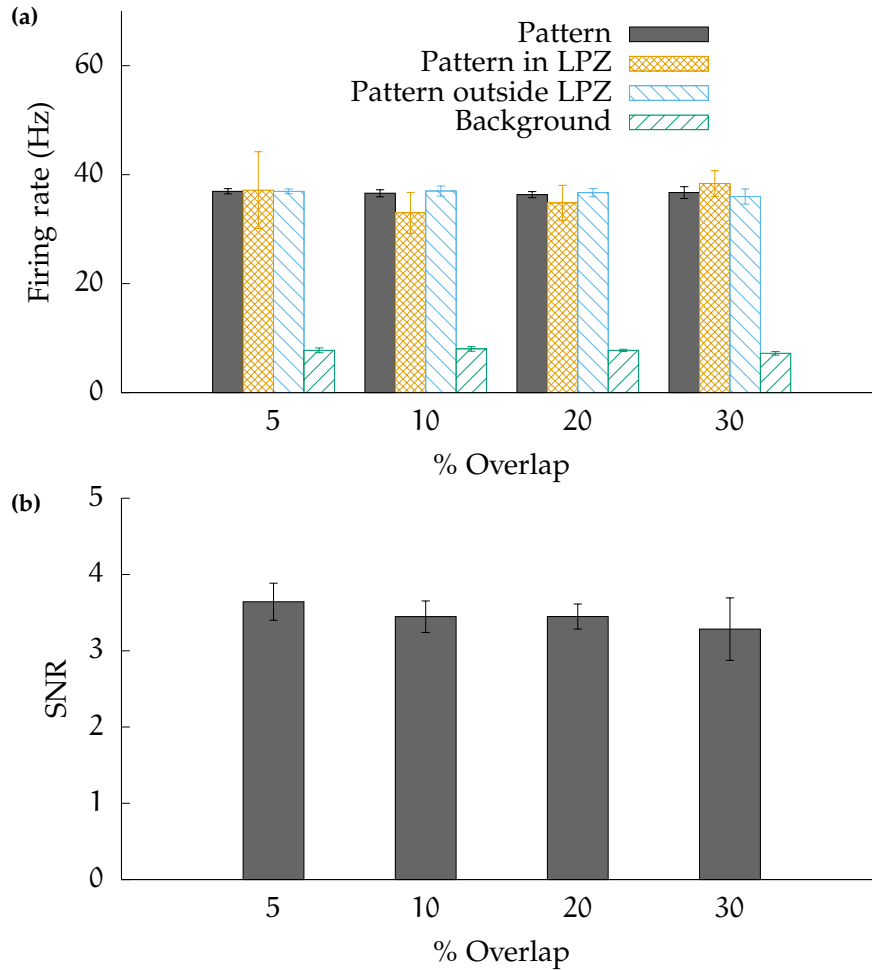
Figure 31: Recall performance for different proportions of the associative memory falling in the LPZ without deafferentation (the % of overlap is the % of neurons of the associative memory that fall in the LPZ): In the absence of deafferentation, during recall: **(a)** firing rates of neurons forming the associative memory inside and out of the LPZ remained similar for different proportions of the associative memory falling in the LPZ. The overall firing rates of the neurons forming the pattern and background also remained similar. **(b)** as a result, the Signal to Noise Ratio (SNR) obtained also did not vary too much. (Here, the mean and standard deviation were calculated over $n = 5$ simulations for each level of overlap.)

from simulations that explored the effects of selecting different numbers of associative memory neurons from the pre-selected central LPZ region on the recall performance of the associative memory.

As shown in Figure 17b, 5% of the total population of neurons in the network at the centre of the grid are pre-selected for deafferentation to form the LPZ. Using the same configuration as Vogels et al. (2011), the associative memories stored in the network consist of 10% of the excitatory population. This sets the upper limit for the proportion of associative memory neurons that could fall in the LPZ at 50%. At this value, all excitatory neurons of the LPZ would be included in the associative memory. However, in simulations of the normally functioning network where more than 30% of associative memory neurons were selected from the LPZ, the firing of these associative memory neurons in the LPZ was not re-stabilised to the balanced state by the homeostatic inhibitory plasticity mechanism. Because of this, the upper limit of neurons selected from the LPZ for inclusion in the associative memory was reduced to 30%.

After the network had stabilised to its balanced AI state, whereas the firing rates of associative memory neurons in the LPZ were initially found to be slightly higher than those outside the LPZ, during recall, when the network had re-stabilised, the mean firing rates of the associative memory neurons both in and outside the LPZ and the background neurons remained in the same range (Figure 31a). Similar to earlier simulations, this is attributed to the homeostatic inhibitory plasticity mechanism that strengthens inhibitory projections on to the neurons of the associative memory to match their excitation and balance their activity. As a result, the SNR during recall was also not observed to be affected significantly by different spatial organisation and connectivity of the associative memory neurons (Figure 31b).

4.2 EFFECT OF DEAFFERENTATION ON RECALL PERFORMANCE

In this section we deafferent neurons that fall in the pre-selected LPZ, but do not activate the repair process. Although the selection of more neurons for the associative memory from the LPZ did not affect the recall performance without the peripheral lesion, after deafferentation, an observable deterioration in recall performance was observed (Figure 32). Neurons of the associative memory that fall in the LPZ do not receive any recall stimulus. Their contribution to the recall of the associative memory, therefore, will be less than that in a normally functioning network. This effect can be seen in Figure 32a. As more associative memory neurons are selected from the LPZ, the activity of
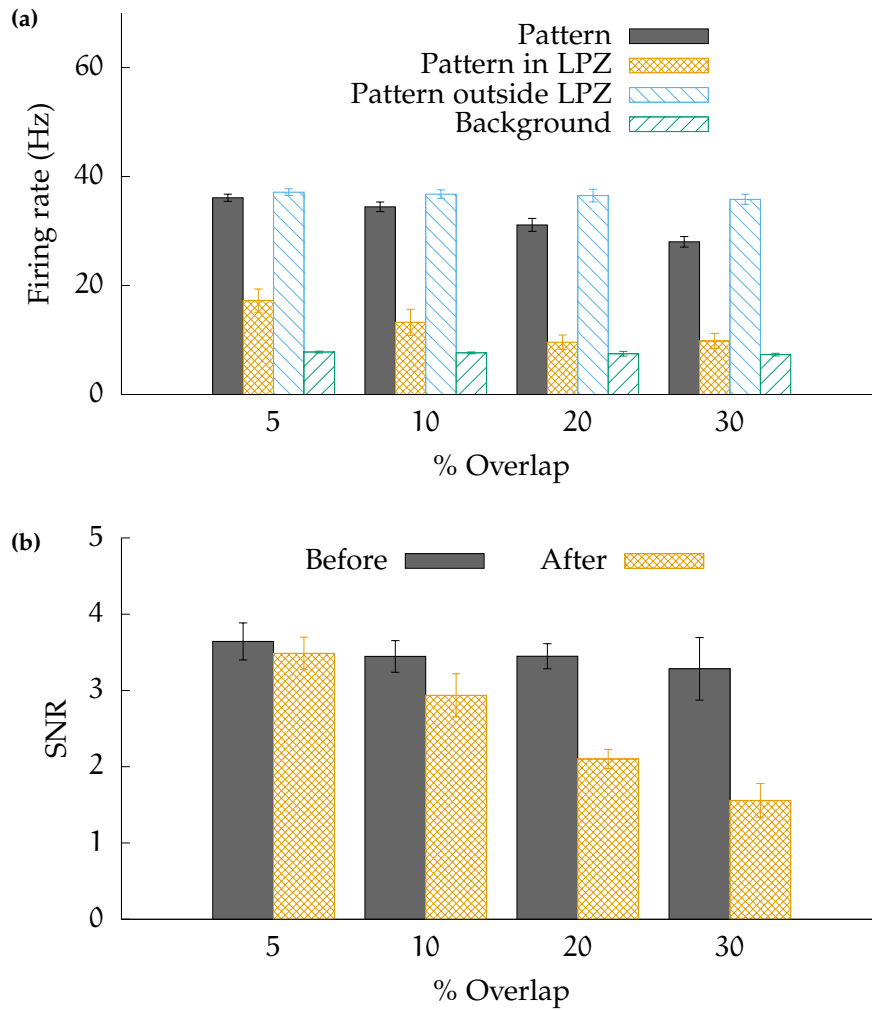
Figure 32: Recall performance for different proportions of the associative memory falling in the LPZ after deafferentation but before repair (the % of overlap is the % of neurons of the associative memory that fall in the LPZ): When the network is deafferented, neurons that are included in the associative memory from the LPZ do not receive the recall stimulus. As more neurons from the associative memory are selected from the LPZ, less stimulus is projected on the associative memory during recall. Thus: **(a)** the firing rates of these neurons reduces, also reducing the mean firing rate of the associative memory; the firing rates of associative memory neurons outside the LPZ remains largely unaffected. **(b)** as the background firing rate also remains unaffected by the peripheral lesion, the SNR of the recalled associative memory drops. (Student's independent two sample t-test, SNR before vs after deafferentation: 5% overlap: $P = 0.312$; 10% overlap: $P = 0.0118$; 20% overlap: $P = 4.6\exp(-7)$; 30% overlap: $P = 3.42\exp(-5)$) (Statistics were calculated over $n = 5$ simulations for each level of overlap. The Shapiro-Wilk test was used to test for normality, and Levene's test was used to analyse the variance of samples.)
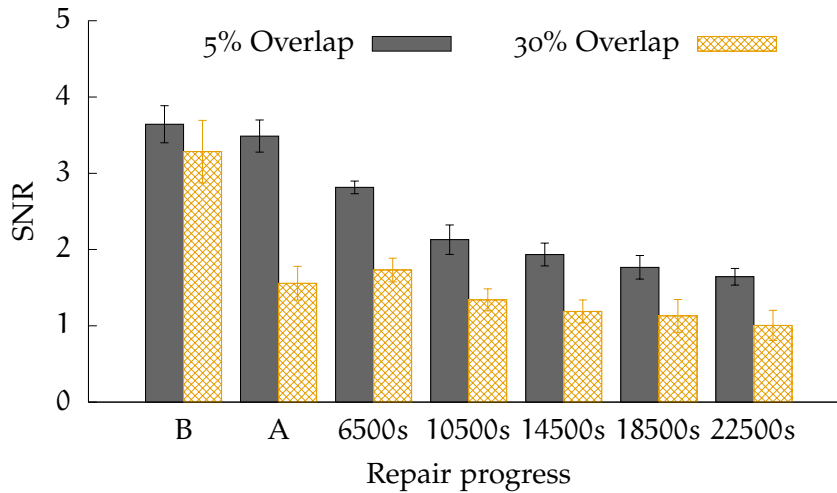
Figure 33: Recall performance during repair with 5% and 30% of the associative memory falling in the LPZ. The network is deafferented at t = 4000 s. **B**: before deafferentation; **A**: after deafferentation but before repair. Even though activity in the network is restored, the SNR of the stored associative memory during recall does not return to pre-deprivation levels. (Student's independent two-sample t-test, SNR before deafferentation vs SNR at t = 22500s: 5% overlap: P = 1.59 exp(−7); 30% overlap: P = 1.98 exp(−5)) (Statistics were calculated over n = 5 simulations for each level of overlap. The Shapiro-Wilk test was used to test for normality, and Levene's test was used to analyse the variance of samples.)

these neurons when the associative memory is recalled is less, and so is the resulting mean firing rate of the complete associative memory.

The firing rate of associative memory neurons outside the LPZ remains stable in the range of parameters tested here. This indicates that these neurons receive sufficient stimulus to maintain their recall performance. Similarly, the mean firing rate of neurons forming the background network also appears to be unaffected by the deafferentation. The combined result of the unaffected background activity and the fall in mean firing rate of the associative memory neurons due to a loss of recall stimulus to the subset of neurons falling in the LPZ results in a reduction of the recall performance (Figure 32b).

4.3   EFFECT OF NETWORK REPAIR ON RECALL PERFORMANCE

Having established the recall performance of stored associative memories in a normal network and a deafferented network, the final stage of the analysis studied recall performance during repair by structural plasticity (Figures 33 and 34). The associative memory is stored in the network at t = 1500 s and the network is deafferented at t = 4000 s. At regular intervals in the simulation, plasticity was disabled and the
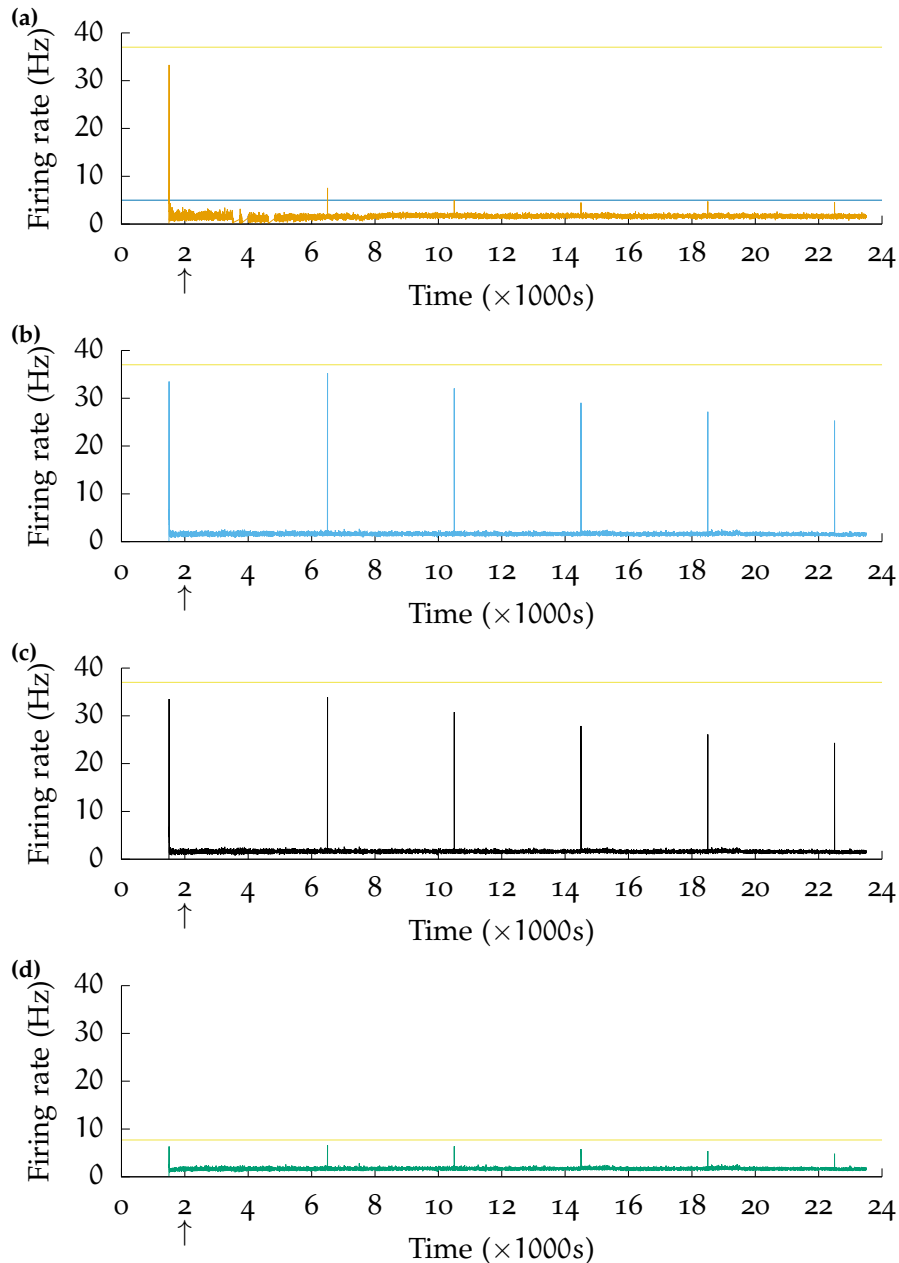
Figure 34: Mean firing rates of associative memory and background neurons in an example simulation (5% of associative memory overlaps with the LPZ): **(a)** associative memory neurons in the LPZ; **(b)** associative memory neurons outside the LPZ; **(c)** all associative memory neurons; **(d)** all background neurons. **Arrow** indicates time in simulation when network was deafferented. **Yellow** horizontal lines: mean firing rate during recall in a normal network; **Blue** horizontal lines: mean firing rate during recall after deafferentation before repair; Where they overlap or were close together, the blue line has been omitted for clarity. The first spike in activity shows the storage of the associative memory. Subsequent spikes show recall of the associative memory. In the absence of deprivation, the activity levels of associative memory neurons in and outside the LPZ are similar during recall (Figure 31a). As can be seen here, however, after deprivation, the activity of associative memory neurons in the LPZ does not recover.

associative memory recalled. The spikes in firing rates after $t = 4000\,s$ in Figure 34 are as a result of these recalls.

As Figure 33 shows, the recall performance of the stored associative memory does not return to pre-deprivation levels. For networks with less overlap between the associative memory and the LPZ (5%), the recall performance continues to deteriorate as the network undergoes repair. In this case, the associative memory is recalled better in the absence of structural plasticity based repair (point A vs $t = 22500s$). For networks with more overlap (30%), where the recall performance is already low after deafferentation, recall performance remains similar during repair. In neither case was the recall performance improved after repair.

Since the lateral excitatory synapses between neurons forming the associative memory have higher conductances than the synapses connecting the background neurons, in the model, they are less likely to be removed. Thus, it is likely that the associative memory still exists in the network and the recall stimulus that is still received by the neurons of the associative memory outside the LPZ can be transferred to other neurons of the associative memory in the LPZ. However, as Figure 34 shows, the firing rates of associative memory neurons outside the LPZ are also reduced during recall, along with the firing rates of the neurons forming the background. This decrease could result from the large increase in inhibition in the network as the repair process proceeds (discussed in Chapter 3). The drastic drop in the firing rates of the associative memory neurons inside the LPZ suggests that the transfer of excitation laterally, from the now less active associative memory neurons outside the LPZ, to them does not compensate for the loss in projecting recall stimulus. Thus, whereas alterations in lateral connectivity by the repair process may restore activity to neurons of the LPZ, changes in connectivity related to the stored associative memories result in reduced activity in associative memory neurons in and outside the LPZ, which results in reduced recall performance.

Although deafferentation was localised in this study to model a peripheral lesion, neurons forming the associative memory were randomly selected to model distributed associative memories both in and outside the LPZ. The spatial configuration of the neurons forming the associative memory, however, can affect its recall performance in multiple ways. First, as documented in this chapter, the proportion of associative memory neurons falling in the LPZ affects its recall performance. Next, in this model where connectivity is dependent on the distances between neurons, the spatial clustering of associative memory neurons influences the lateral connectivity of the Hebbian assembly. If the neurons forming the associative memory are clustered close together, the lateral excitatory connectivity between them will

be higher. To investigate this second factor, different magnitudes of clustering must be analysed for different proportions of associative memory neurons falling in the LPZ, expanding the exploration space to two dimensions. Given the computational costs of simulating the model, the scope of the current study was limited to investigating the effects of varying amounts of randomly selected associative memory neurons falling in the LPZ only. A more complete analysis of the spatial characteristics of stored associative memories and their role in mediating recall performance is noted here as future work.

It is also noteworthy that in a normally functioning brain network, the characteristics of the recall stimulus would be expected to be similar to the general input the network receives. Thus, if the associative memory neurons and their recall stimulus are distributed over the network, the effects of the deafferentation would also perhaps be similarly distributed. Since the model is based on peripheral focal lesion experiments, the deafferentation was also modelled here as a localised loss of external input. At this level of abstraction, the background external input that is modelled here using simple feed-forward projections may be interpreted as a combination of input projections from different sources. The deafferented input in this interpretation may represent a localised projection perhaps from one of the sources that experiences a lesion whereas the recall stimulus may be understood to consist of inputs from other uninjured sources. The effects of such input regimes on the network repair and associative memory recall performance were beyond the scope of this study. Nevertheless, these research questions can be studied by making minor extensions to the model developed in this study. Multiple input projections may be modelled by splitting the external input into different populations combinations of which may be lesioned to model a variety of deafferentation regimes. Furthermore, the spatial characteristics of deafferentation may also be explored by varying the clustering of neurons that are selected for deprivation.

Finally, another factor that may affect the performance of the stored associative memories in the network, with and without deafferentation, is the method used to store them in the network. Here, associative memories were stored by a 'one shot' learning process where the synapses of the associative memory were strengthened together to form the Hebbian assemblies. In the brain, however, such associations would be formed via plasticity mechanisms. The inclusion of plasticity in the excitatory neuron population along with the structural and homeostatic synaptic plasticity mechanism considerably increases the complexity of the model and the accompanying analysis necessary to isolate their individual effects. In general, the addition of more plasticity and other mechanisms to bring the model closer to biology

is also noted here as future work that may be undertaken using the model as a starting point.

4.4 CHAPTER CONCLUSIONS

This chapter documented the final stage of the study where the newly developed model was used to investigate the effects of network repair by structural plasticity on associative memory stored in the network. The simulations indicate that though the associative memory may remain in the network, their recall performance is not retained after injury. Indeed, they suggest that associative memories that have only a small proportion of neurons falling in the LPZ may continue to perform better if the network were not modified by structural plasticity at all. Further work is needed to explore if there are methods, such as recall or retraining of associative memories as discussed in the next chapter, that may maintain or improve the recall performance.

The prohibitive computational costs of running simulations of the model make the investigation of the effects of repair on overlapping associative memories intractable. However, as reported in Chapter 1, increased overlap between associative memories also caused a loss in performance. Therefore, it is unlikely that the storage of multiple overlapping associative memories would aid performance.

In the next, final chapter of the dissertation, the contributions to knowledge, the results, the limitations, and a plethora of open questions that could not be investigated are discussed.

CONCLUSIONS AND FUTURE WORK

An expert is a man who has made all the mistakes which can be made, in a narrow field.

Niels Bohr

The aim of this thesis was to contribute to a better understanding of functional changes in brain regions that undergo re-organization by homeostatic structural plasticity after experiencing peripheral lesioning. Specifically, this thesis focussed on the recall performance of associative memories stored in adult cortical networks during repair after sensory deprivation by a focal peripheral lesion. The following questions were addressed:

> How does repair by activity-dependent structural plasticity affect the function of a neuronal network as an associative memory store?

> How can neurites in a cortical network react to changes in the host neuron's activity to allow the restoration of stable activity in a deafferented network?

To address these questions, a novel spiking network model of peripheral lesioning and repair was developed. This model was then used to investigate the recall performance of associative memory in the network. The development of the model, the results obtained from its simulations, their limitations, and directions for future research will be summarised in this chapter.

5.1 CONTRIBUTIONS TO THE FIELD

The initial research for the study, summarised in Part i, identified relevant information from a review of published literature. Since the information on the repair of networks after focal peripheral lesions was gathered from experiments that reported on network characteristics,

two existing computational spiking network models were chosen to form the foundation of this study:

- the model of a balanced Asynchronous Irregular (AI) spiking cortical network which was demonstrated to act as a store for attractor-less associative memories (Vogels et al. 2011),

- the Model of Structural Plasticity (MSP) framework that allows for the modelling of structural plasticity in spiking neuronal models, demonstrated by the reproduction of a peripheral lesioning study (Butz, Van Ooyen and Wörgötter 2009; Butz and van Ooyen 2013).

These models dictated the choice of tools that were to be used in the study. Initially, the Auryn simulator (Zenke and Gerstner 2014), and later the NEST simulator (Kunkel, Morrison et al. 2017; Diesmann and Gewaltig 2001; Peyser et al. 2017; Linssen et al. 2018; Jordan, Mørk et al. 2019) were chosen as appropriate modelling software that would enable the modelling of a peripheral lesioning experiment. As part of the study, contributions were made to both these tools. Notably, the symmetric inhibitory Spike Timing Dependent Plasticity (STDP) rule used in Vogels et al. (2011) was added to the NEST simulator, and improvements were made to NEST's implementation of the MSP in collaboration with the NEST development team. These contributions resulted in my inclusion as a co-author in scientific publications for these NEST releases:

- Susanne Kunkel, Abigail Morrison et al. (2017). *NEST 2.12.0*. DOI: `10.5281/zenodo.259534`

- Alexander Peyser et al. (2017). *NEST 2.14.0*. DOI: `10.5281/zenodo.882971`

- Charl Linssen et al. (2018). *NEST 2.16.0*. DOI: `10.5281/zenodo.1400175`

- Jakob Jordan, Håkon Mørk et al. (2019). *NEST 2.18.0*. DOI: `10.5281/zenodo.2605422`. URL: `https://doi.org/10.5281/zenodo.2605422`

As detailed in the chapters in Part ii, the study was divided into multiple stages. In the first stage of the study, reported in Part ii: Chapter 1, it was established that a normally functioning balanced cortical network is capable of storing multiple overlapping patterns that can then later be recalled. It was observed that the recall performance of the associative memories reduces as more and more of them are stored in the network. It was also noted that the network has a finite capacity to store associative memories. Depending on

the magnitude by which synapses that were part of an associative memory were strengthened, after a number of memories were stored, the homeostatic inhibitory synaptic plasticity mechanism was unable to balance the increased excitation.

The next stage of the study involved the use of a model of peripheral lesioning to study the effects of deafferentation and repair on the recall performance of associative memory. Here, whereas the MSP framework was found the be sufficient, the model of peripheral lesioning developed by Butz and van Ooyen (2013) was not. The limitations of their model were discussed in Part i: Chapter 1. A novel model of peripheral lesioning was, therefore, developed that correctly simulates the time course of repair observed in experimental work (Part ii: Chapters 2 and 3). The development of this model required the investigation of the activity dependent growth of neurites by structural plasticity. Results from simulations suggest that for both pre- and post-synaptic neurites, excitatory and inhibitory neurites have to react to changes in activity in opposite ways for activity to be restored to the Lesion Projection Zone (LPZ) by the experimentally observed ingrowth of excitatory and outgrowth of inhibitory projections. Further, in spite of these growth rules being obtained from the reproduction of network level changes, single neuron simulations indicate that the growth rules for post-synaptic neurites also stabilise individual neurons by countering changes in the balance between excitation and inhibition (E-I balance).

The final stage of the study, detailed in Part ii: Chapter 4, used the novel model of peripheral lesioning and repair to investigate the recall performance of associative memories during the repair process. Here, simulations suggest that even though activity is restored to the deafferented neurons of the LPZ, the performance of the associative memory is not maintained. The recall performance of the stored associative memory continues to deteriorate throughout the repair process. In contrast, the simulations suggest that the recall performance of the associative memory is better if no structural plasticity based repair takes place at all.

The research from these stages of the study was disseminated in the following publications:

- Ankur Sinha, Neil Davey et al. (2015). 'Structural plasticity and associative memory in balanced neural networks with spike-time dependent inhibitory plasticity'. In: *BMC Neuroscience* 16.1, p. 1. URL: http://www.biomedcentral.com/1471-2202/16/S1/P235

- Ankur Sinha, C. Metzner et al. (2017). 'The effect of homeostatic structural plasticity on associative memory in a network with

spike-time dependent inhibitory synaptic plasticity.' In: *BMC Neuroscience, 18(Suppl.1)*. DOI: `10.1186/s12868-017-0370-3`

- Ankur Sinha, Christoph Metzner, Roderick Adams et al. (2018). 'The combined effect of homeostatic structural and inhibitory synaptic plasticity during the repair of balanced networks following deafferentation'. In: *BMC Neuroscience* 19.2, pp. 129–130. ISSN: 1471-2202. DOI: `10.1186/s12868-018-0451-y`

- Ankur Sinha, Christoph Metzner, Neil Davey et al. (2019a). 'Growth rules for repair of asynchronous irregular network models following peripheral lesions'. In: *BMC Neuroscience* 20. ISSN: 1471-2202

- Ankur Sinha, Christoph Metzner, Neil Davey et al. (2019b). 'Growth Rules for the Repair of Asynchronous Irregular Neuronal Networks after Peripheral Lesions'. In: *bioRxiv*. DOI: `10.1101/810846`. eprint: `https://www.biorxiv.org/content/early/2019/10/21/810846.full.pdf`. URL: `https://www.biorxiv.org/content/early/2019/10/21/810846` (Manuscript has been submitted for peer review).

An abstract detailing the final stages of the study has also been submitted to CNS*2020 for consideration.

Although not directly related to the study, the complexity of tools used in computational neuroscience also encouraged me to resurrect the NeuroFedora initiative. It is a volunteer driven initiative to provide a Free/Open Source (FOSS) Fedora Linux (RedHat 2008) based Operating System for use in Computational Neuroscience. It includes a plethora of commonly used simulators and analysis tools that can be easily installed using the default Fedora package manager. A downloadable, ready to use ISO installation image is also available. NeuroFedora was presented to the research community as a poster at CNS*2019:

- Ankur Sinha, Luis Bazan et al. (2019). 'NeuroFedora: a ready to use Free/Open Source platform for Neuroscientists'. In: *BMC Neuroscience* 20. ISSN: 1471-2202. URL: `https://neuro.fedoraproject.org`

An abstract reporting on the progress that has been made in NeuroFedora the past year has been submitted to CNS*2020 for consideration. NeuroFedora was also presented by a team member to the Free/Open Source community at the Open Research Tools and Technologies Devroom at FOSDEM.

5.2   DISCUSSION AND FUTURE WORK

Whereas the study did answer the intended research question, a number of open questions remain that present avenues for future research. In addition, various limitations that arise from the research method and other practical considerations also present avenues for improvements. In this section I will attempt to outline these for each stage of the study.

In a computational modelling study, it is paramount to choose the right level of abstraction for the model. A number of factors suggested that the use of simple single compartment point neurons was sufficient here. First, the experimental evidence that this study relies on primarily provides network metrics on the growth of neurites during the repair process. The MSP framework also uses similar sources of evidence to allow modelling of neurite growth in simplified spiking neuron models only. In addition, the investigation of associative memory as network function also implied that a network model rather than a detailed neuron model was to be used. Thus, the model of associative memory developed by Vogels et al. (2011) provided an appropriate starting point. Not only did it model a biologically plausible cortical network, it was also demonstrated to function as an associative memory store. Even though different point neuron models were investigated, no clear advantage was seen in using a more featured neuron model, such as the Adaptive Exponential Integrate and Fire neuron model (Brette and Gerstner 2005) or Izhikevich (Izhikevich and Desai 2003) model, that would add to the computational cost of simulation instead of the simple leaky integrate and fire model used by Vogels et al. (2011).

The first stage of the study, where the performance of a normal network as an associative memory store was investigated, presented a few technical challenges. The Auryn simulator that was used by Vogels et al. (2011) allows the user to make snapshots of the network that may be loaded to continue simulations. This was particularly useful in simulations where multiple overlapping associative memories were stored and recalled in succession so that their recall performance may be analysed. The design of the simulator, however, does not lend itself to the implementation of the MSP framework or connectivity changes during simulation. On the other hand, whereas the NEST simulator does permit implementation of the MSP framework and updates in network connectivity during simulation, it is not currently possible to make snapshots of simulations. In later stages of the simulation, a workaround for NEST was to disable plasticity, both structural and synaptic, when associative memories were recalled during repair, and to let the network re-stabilise to its balanced state. Although this

ensured that neither the connectivity nor the inhibitory synaptic plasticity based synapses were affected by the recall of memories, various changes in the internal states of simulation variables would still occur. Thus, the addition of the ability to make complete snapshots of simulations in the NEST simulator remains an open research question. As we will see, NEST also presented other challenges in later stages of the study.

As the storage of associative memory was only used as a proxy to study network function, even at its first stage, the study did not delve into the details of the storage of associative memory in cortical networks. As an example, whereas the role of inhibitory neurons is traditionally limited to a homeostatic one, preliminary analysis showed that storage of associative memories in the excitatory population also resulted in changes in activity in inhibitory neurons. With inhibitory plasticity recently gaining research focus (Sprekeler 2017), perhaps investigating the effects of the inclusion of excitatory neurons and their inhibitory counterparts to store associative memories would be an interesting study. Of course, in general, more faithful modelling of cortical networks by the inclusion of heterogeneous neuronal populations, multiple plasticity mechanisms, and other biological realities as they are discovered remains an open research field (Zenke, Agnes and Gerstner 2015).

Similarly, the inhibitory STDP rule that was developed by Vogels et al. (2011) was also not investigated in detail. It has since been noted that whereas the changes in the synaptic efficacies of inhibitory synapses by the rule are correct, the rule does not model the correct mechanisms responsible for this change (Vogels et al. 2012). The experimental results that reported STDP in GABAergic synapses, that the mathematical model was meant to be based on, identified the underlying mechanism for increase in synaptic efficacy to be the shift in the reversal potential of post-synaptic GABAergic currents (E_{GPSC}) to more positive values for co-incident pre- and post-synaptic activity, but a reduction in synaptic conductance was only observed for repetitive pre-synaptic activity in the absence of post-synaptic activity (Woodin, Ganguly and Poo 2003).

In the next stage of the study, structural plasticity was to be added to the model. As discussed in Part ii: Chapter 2, the use of a single compartment point neuron model introduced certain constraints on the study. The development of a multi compartment version of the MSP framework to remove these constraints, however, is not a trivial undertaking and was deemed beyond the scope of the study. Thus, it is an area yet to be explored. The development of companion tools to improve the simulation of structural plasticity using the current version of the MSP also remains a potential undertaking. In its cur-

rent form, NEST only includes a partial implementation of the MSP. Due to the design of the NEST simulator, for example, one cannot introduce distance dependent connectivity updates in simulations. As a workaround, neurons in the model were provided with spatial information explicitly in the Python simulation code. Further, since the efficient routines for connection updates provided in the NEST kernel could not be used, it was required to extract information for each neuron from the paused simulation, calculate the necessary connection updates in native Python, and push these changes back to the simulation before its resumption. The additional routine calls here greatly increase the computation cost. Additionally, the increased data transfer cost of repeatedly explicitly synchronising the information between the computing nodes using the Message Passing Interface (MPI) was a bottle neck that could not be circumvented.

This stage of the study concluded with the development of a novel model of peripheral lesioning. To the best of my knowledge, whereas models of peripheral lesioning do exist, most notably models developed by Butz and van Ooyen using the MSP framework, this model is the first spiking network model of peripheral lesioning and subsequent repair in an adult cortical balanced network. Various features were included in the model to increase its biological plausibility. Though new synapses are formed between neurons based on the distance between them in the MSP already, as explained earlier, this is not currently included in the NEST implementation. Apart from re-implementing this feature, the new model also takes into account the relationship between synaptic stability and synaptic efficacy—stronger synapses are less likely to be lost (Knott, A. Holtmaat et al. 2006; Trachtenberg et al. 2002)—and removes synapses based on their synaptic weights. Further, changes to the MSP were also made to permit the use of more general families of Gaussian growth curves.

As reported in Part ii: Chapter 3, the development of the new model included the investigation of the activity dependent growth rules for various types of neurites. Although the high computational costs prevented the use of a complete grid search to ascertain the parameters governing the growth rules, a systematic heuristic based exploration revealed growth curves that do seem to be supported by existing research work (Richards et al. 2005; Knott, Quairiaux et al. 2002; Perez et al. 1996; Schuemann et al. 2013). The multiple hypotheses suggested by this study, however, remain to be experimentally verified. An important future study would be to explore if the activity dependent growth rules of neurites vary between the adult brain, as derived by our model, and the developing brain which has been the subject of much experimental research.

Along with the growth curves, simulations also exhibited features that lead to more open questions. First, simulation results suggested that focal peripheral lesions may affect the activity of neurons in different ways depending on the location of the neuron in relation to the LPZ. Where neurons in the LPZ would lose their external stimulus and suffer a loss in excitation, neurons on the outer periphery were noted to show increased activity—because of a net loss of inhibition. Whereas similar 'edge effects' have been documented in other studies in the context of thalamocortical dysrhythmia that may underlie tinnitus (Llinás et al. 2005; De Ridder et al. 2007), to the best of my knowledge, this observation has not yet been studied directly in peripheral lesion experiments. Second, the time course of inhibition in the simulations matches indications from experiments that suggest its role in structural plasticity. The LPZ experiences disinhibition after deafferentation and as activity returns to its neurons, inhibition increases to re-stabilise their activity. This is in line with experiments that suggest that disinhibition enables changes in synaptic connectivity (Vetencourt et al. 2008; Rosier et al. 1995; Massie et al. 2003; Garraghty, LaChica and J H Kaas 1991; Hensch 2005; Fagiolini and Hensch 2000; Versendaal et al. 2012). Finally, also coherent with the current state of the art that suggests that multiple homeostatic mechanisms are required to stabilise brain networks at different scales of time and space (Zenke and Gerstner 2017), neither the homeostatic inhibitory synaptic plasticity mechanism nor the homeostatic structural plasticity mechanism were found to be sufficient for repair in isolation.

An important observation in the simulations was the state of the network after repair. Although average activity is returned to the neurons of the LPZ, it is not in an AI state as before. Although the particular brain function chosen for the study, the recall of stored associative memory, was not affected by this change, synchronicity may affect other cortical functions. The model developed here is general enough for use in investigations of other network functions also. To ensure that it can be easily used by the research community, the source code for the model, the modified version of NEST, and the various tools and scripts used to analyse simulation data are all freely available under a Free Software license. The data generated by the multiple runs of the simulation is also publicly available and may be used to further study aspects of the repair process that could not be included here, such as the connectivity characteristics during repair. For example, Butz, Steenbuck and van Ooyen (2014b) found that the homeostatic structural plasticity process that preferred short term connections led to the formation of efficient small world networks common in the brain (Watts and Strogatz 1998; Sporns and Zwi 2004; Bullmore and Sporns 2009).

The final stage of the study used the developed model to study the recall performance of associative memory during repair after sensory deprivation. The results obtained here suggest that the recall performance deteriorates after deafferentation. Since the weights of synapses forming the associative memories are stronger than the rest of the excitatory connections in the network, the memory itself continues to exist the network. However, the changes in network connectivity by structural plasticity hamper its recall. A number of follow up questions arise from this result:

> Can the deterioration of recall performance be prevented?

Since the recall performance of memories was also found to be better without structural plasticity repair, this question includes exploration of how structural plasticity can be controlled, and perhaps disabled in certain scenarios. In the brain, recall of stored memories is thought to play an important role in their reconsolidation (Tronson and Taylor 2007). Thus, a question related to therapy would be:

> Does retraining of the memory by recall mechanisms during the repair process maintain its recall performance?

This would require certain modifications of the model since in its current state, efforts were made to keep the stored memory and the network unaffected by memory recall. Additionally, alterations to memory by activity would require the use of plastic synapses. This may have other effects on the balance of the network. Finally, if previous brain function cannot be protected:

> Does the new connectivity of the network lend itself to the storage of new associative memories and other network functions?

Although at this stage, there are few practical applications of this work, it is hoped that it provides a foundation for future multidisciplinary research that will add to our understanding of structural plasticity in the brain and perhaps aid in the development of treatments related to peripheral lesioning of the brain.

Abraham, Wickliffe C. and Anthony Robins (2005). 'Memory retention–the synaptic stability versus plasticity dilemma'. In: *Trends in neurosciences* 28.2, pp. 73–78. DOI: `10.1016/j.tins.2004.12.003` (cit. on p. 32).

Allard, T. et al. (1991). 'Reorganization of somatosensory area 3b representations in adult owl monkeys after digital syndactyly'. In: *Journal of neurophysiology* 66.3, pp. 1048–1058. DOI: `10.1152/jn.1991.66.3.1048` (cit. on p. 15).

Amit, D. J. and A. Treves (Oct. 1989). 'Associative memory neural network with low temporal spiking rates.' In: *Proceedings of the National Academy of Sciences* 86.20, pp. 7871–7875. DOI: `10.1073/pnas.86.20.7871` (cit. on p. 34).

Anishchenko, Anastasia and Alessandro Treves (2006). 'Autoassociative memory retrieval and spontaneous activity bumps in small-world networks of integrate-and-fire neurons'. In: *Journal of Physiology-Paris* 100.4, pp. 225–236 (cit. on p. 35).

Artola, Alain and Wolf Singer (1987). 'Long-term potentiation and NMDA receptors in rat visual cortex'. In: *Nature* 330.6149, pp. 649–652 (cit. on p. 32).

Basu, Sreetama and Raphael Lamprecht (2018). 'The role of actin cytoskeleton in dendritic spines in the maintenance of long-term memory'. In: *Frontiers in Molecular Neuroscience* 11, p. 143. DOI: `10.3389/fnmol.2018.00143` (cit. on p. 20).

Bi, Guo-qiang and Mu-ming Poo (1998). 'Synaptic modifications in cultured hippocampal neurons: dependence on spike timing, synaptic strength, and postsynaptic cell type'. In: *The journal of neuroscience* 18.24, pp. 10464–10472. DOI: `10.1523/jneurosci.18-24-10464.1998` (cit. on p. 36).

Blanquie, Oriane and Frank Bradke (2018). 'Cytoskeleton dynamics in axon regeneration'. In: *Current opinion in neurobiology* 51, pp. 60–69. DOI: `10.1016/j.conb.2018.02.024` (cit. on p. 20).

Bliss, Tim V. P. and Terje Lømo (1973). 'Long-lasting potentiation of synaptic transmission in the dentate area of the anaesthetized rabbit following stimulation of the perforant path'. In: *The Journal of physiology* 232.2, pp. 331–356. DOI: `10.1113/jphysiol.1973.sp010273` (cit. on pp. 32, 125).

Bohland, Jason W. and Ali A. Minai (2001). 'Efficient associative memory using small-world architecture'. In: *Neurocomputing* 38, pp. 489–496. DOI: `10.1016/S0925-2312(01)00378-2` (cit. on p. 34).

Börgers, Christoph and Nancy Kopell (Mar. 2003). 'Synchronization in Networks of Excitatory and Inhibitory Neurons with Sparse, Random Connectivity'. In: *Neural Computation* 15.3, pp. 509–538. DOI: 10.1162/089976603321192059 (cit. on p. 86).

Brette, Romain and Wulfram Gerstner (2005). 'Adaptive exponential integrate-and-fire model as an effective description of neuronal activity'. In: *Journal of neurophysiology* 94.5, pp. 3637–3642. DOI: 10.1152/jn.00686.2005 (cit. on p. 104).

Brunel, Nicolas (2000). 'Dynamics of sparsely connected networks of excitatory and inhibitory spiking neurons'. In: *Journal of computational neuroscience* 8.3, pp. 183–208. ISSN: 1573-6873. DOI: 10.1023/A:1008925309027 (cit. on pp. 35, 86).

Brünig, Ina et al. (2004). 'Influx of extracellular calcium regulates actin-dependent morphological plasticity in dendritic spines'. In: *Neuropharmacology* 47.5, pp. 669–676 (cit. on pp. 20, 26).

Buckingham, Jay and David Willshaw (1992). 'Performance characteristics of the associative net'. In: *Network: Computation in Neural Systems* 3.4, pp. 407–414. DOI: 10.1088/0954-898x/3/4/005 (cit. on p. 34).

Bullmore, Ed and Olaf Sporns (2009). 'Complex brain networks: graph theoretical analysis of structural and functional systems'. In: *Nature Reviews Neuroscience* 10.3, pp. 186–198. DOI: 10.1038/nrn2575. URL: https://doi.org/10.1016/j.tics.2004.07.008 (cit. on p. 107).

Butz, M., Konrad Lehmann et al. (2006). 'A theoretical network model to analyse neurogenesis and synaptogenesis in the dentate gyrus'. In: *Neural Networks* 19.10, pp. 1490–1505. DOI: 10.1016/j.neunet.2006.07.007 (cit. on p. 24).

Butz, M., Ines D. Steenbuck and A. van Ooyen (2014a). 'Homeostatic structural plasticity can account for topology changes following deafferentation and focal stroke'. In: *Frontiers in Neuroanatomy* 8, p. 115. DOI: 10.3389/fnana.2014.00115 (cit. on pp. 16, 31).

Butz, M., Ines D. Steenbuck and A. van Ooyen (2014b). 'Homeostatic structural plasticity increases the efficiency of small-world networks'. In: *Frontiers in synaptic neuroscience* 6. DOI: 10.3389/fnsyn.2014.00007 (cit. on pp. 16, 31, 107).

Butz, M. and G. Teuchert-Noodt (2006). 'A simulation model for compensatory plasticity in the prefrontal cortex inducing a cortico-cortical dysconnection in early brain development'. In: *Journal of neural transmission* 113.5, pp. 695–710. DOI: 10.1007/s00702-005-0403-4 (cit. on p. 24).

Butz, M., Gertraud Teuchert-Noodt et al. (2008). 'Inverse relationship between adult hippocampal cell proliferation and synaptic rewiring in the dentate gyrus'. In: *Hippocampus* 18.9, pp. 879–898. DOI: 10.1002/hipo.20445 (cit. on p. 25).

Butz, M. and A. van Ooyen (2013). 'A Simple Rule for Dendritic Spine and Axonal Bouton Formation Can Account for Cortical Reorganization after Focal Retinal Lesions'. In: *PLoS Comput Biol* 9.10, e1003259. DOI: 10.1371/journal.pcbi.1003259 (cit. on pp. 16, 24, 27–31, 87, 101, 102).

Butz, M. and A. van Ooyen (2014). 'Homeostatic structural plasticity–a key to neuronal network formation and repair'. In: *BMC Neuroscience* 15.Suppl 1, P17. DOI: 10.1186/1471-2202-15-s1-p17 (cit. on pp. 16, 31).

Butz, M., Arjen Van Ooyen and Florentin Wörgötter (2009). 'A model for cortical rewiring following deafferentation and focal stroke'. In: *Frontiers in Computational Neuroscience* 3. DOI: 10.3389/neuro.10.010.2009 (cit. on pp. 16, 25, 101).

Calford, Michael B. and Rowan Tweedale (1988). 'Immediate and chronic changes in responses of somatosensory cortex in adult flying-fox after digit amputation'. In: *Nature* 332.6163, pp. 446–448 (cit. on pp. 22, 25).

Chen, Jerry L., Walter C. Lin et al. (2011). 'Structural basis for the role of inhibition in facilitating adult brain plasticity'. In: *Nature neuroscience* 14.5, pp. 587–594 (cit. on pp. 15, 16, 20, 23, 25, 86).

Chen, Jerry L., Katherine L. Villa et al. (2012). 'Clustered dynamics of inhibitory synapses and dendritic spines in the adult neocortex'. In: *Neuron* 74.2, pp. 361–373. DOI: 10.1016/j.neuron.2012.02.030 (cit. on pp. 15, 16, 20, 24, 69, 86).

Chen, Shih-Yu et al. (2018). 'Regulation of axon repulsion by MAX-1 SUMOylation and AP-3'. In: *Proceedings of the National Academy of Sciences* 115.35, E8236–E8245. ISSN: 0027-8424. DOI: 10.1073/pnas.1804373115. eprint: http://www.pnas.org/content/115/35/E8236.full.pdf. URL: http://www.pnas.org/content/115/35/E8236 (cit. on p. 20).

Chen, Weiliang et al. (2011). 'Clustering predicts memory performance in networks of spiking and non-spiking neurons'. In: *Frontiers in Computational Neuroscience* 5.14. ISSN: 1662-5188. DOI: 10.3389/fncom.2011.00014 (cit. on p. 35).

Cohen, Neal J. et al. (1999). 'Hippocampal system and declarative (relational) memory: Summarizing the data from functional neuroimaging studies'. In: *Hippocampus* 9.1, pp. 83–98. DOI: 10.1002/(sici)1098-1063(1999)9:1<83::aid-hipo9>3.0.co;2-7 (cit. on p. 32).

Conti, Anna M., Stephanie J. Fischer and Anthony J. Windebank (2004). 'Inhibition of axonal growth from sensory neurons by excess nerve growth factor'. In: *Annals of Neurology* 42.6, pp. 838–846. DOI: 10.1002/ana.410420604. eprint: https://onlinelibrary.wiley.com/doi/pdf/10.1002/ana.410420604 (cit. on p. 20).

Crook, Sharon M., Andrew P. Davison and Hans E. Plesser (2013). 'Learning from the past: approaches for reproducibility in compu-

tational neuroscience'. In: *20 Years of Computational Neuroscience*. Springer, pp. 73–102. DOI: 10.1007/978-1-4614-1424-7_4 (cit. on p. 7).

Dammasch, I. E., G. P. Wagner and J. R. Wolff (1986). 'Self-stabilization of neuronal networks'. In: *Biological Cybernetics* 54.4-5, pp. 211–222. DOI: 10.1007/bf00318417 (cit. on p. 24).

Dammasch, I. E., G. P. Wagner and J. R. Wolff (1988). 'Self-stabilization of neuronal networks'. In: *Biological Cybernetics* 58.3, pp. 149–158. DOI: 10.1007/bf00364134 (cit. on p. 24).

Darian-Smith, Corinna and Charles D. Gilbert (1994). 'Axonal sprouting accompanies functional reorganization in adult cat striate cortex'. In: *Nature* 368.6473, pp. 737–740. DOI: 10.1038/368737a0 (cit. on pp. 15, 22, 25, 74).

Darian-Smith, Corinna and Charles D. Gilbert (1995). 'Topographic reorganization in the striate cortex of the adult cat and monkey is cortically mediated'. In: *The journal of neuroscience* 15.3, pp. 1631–1647. DOI: 10.1523/jneurosci.15-03-01631.1995 (cit. on pp. 15, 22, 25).

Davey, N. and R. Adams (Mar. 2004). 'High capacity associative memories and connection constraints'. In: *Connection Science* 16.1, pp. 47–65. DOI: 10.1080/09540090310001659981 (cit. on p. 34).

Davey, N., Lee Calcraft and R. Adams (2006). 'High capacity, small world associative memory models'. In: *Connection Science* 18.3, pp. 247–264 (cit. on p. 34).

Davey, N., S. P. Hunt and R. Adams (Dec. 2004). 'High capacity recurrent associative memories'. In: *Neurocomputing* 62, pp. 459–491. DOI: 10.1016/j.neucom.2004.02.007 (cit. on p. 34).

Dayan, Peter and David Willshaw (1991). 'Optimising synaptic learning rules in linear associative memories'. In: *Biological Cybernetics* 65.4, pp. 253–265 (cit. on pp. 34, 39).

De Paola, Vincenzo et al. (2006). 'Cell Type-Specific Structural Plasticity of Axonal Branches and Boutons in the Adult Neocortex'. In: *Neuron* 49.6, pp. 861–875. ISSN: 0896-6273. DOI: 10.1016/j.neuron.2006.02.017. URL: http://www.sciencedirect.com/science/article/pii/S0896627306001346 (cit. on pp. 15, 20, 24).

De Ridder, Dirk et al. (2007). 'Auditory cortex stimulation for tinnitus'. In: *Operative Neuromodulation*. Springer, pp. 451–462 (cit. on p. 107).

Deger, Moritz et al. (2012). 'Spike-timing dependence of structural plasticity explains cooperative synapse formation in the neocortex'. In: *PLoS computational biology* 8.9, e1002689. DOI: 10.1371/journal.pcbi.1002689 (cit. on p. 16).

Diaz-Pier, Sandra et al. (2016). 'Automatic generation of connectivity for large-scale neuronal network models through structural plasticity'. In: *Frontiers in neuroanatomy* 10. DOI: 10.3389/fnana.2016.00057 (cit. on pp. 16, 31, 53, 64).

Dickson, Barry J. (2002). 'Molecular mechanisms of axon guidance'. In: *Science* 298.5600, pp. 1959–1964. DOI: `10.1126/science.1072165` (cit. on p. 20).

Diesmann, Markus and Marc-Oliver Gewaltig (2001). 'NEST: An environment for neural systems simulations'. In: *Forschung und wissenschaftliches Rechnen, Beiträge zum Heinz-Billing-Preis* 58, pp. 43–70 (cit. on pp. 31, 101).

Djurfeldt, Mikael (2012). 'The connection-set algebra—a novel formalism for the representation of connectivity structure in neuronal network models'. In: *Neuroinformatics* 10.3, pp. 287–304. DOI: `10.1007/s12021-012-9146-1` (cit. on p. 64).

Eichenbaum, H. (2008). 'Memory'. In: *Scholarpedia* 3.3. revision #137659, p. 1747. DOI: `10.4249/scholarpedia.1747`. URL: `http://www.scholarpedia.org/article/Memory` (cit. on pp. 32, 33).

Fagiolini, Michela and Takao K. Hensch (2000). 'Inhibitory threshold for critical-period activation in primary visual cortex'. In: *Nature* 404.6774, pp. 183–186. DOI: `10.1038/35004582` (cit. on pp. 87, 107).

Fischer, Maria, Stefanie Kaech, Darko Knutti et al. (1998). 'Rapid actin-based plasticity in dendritic spines'. In: *Neuron* 20.5, pp. 847–854. DOI: `10.1016/s0896-6273(00)80467-5` (cit. on p. 20).

Fischer, Maria, Stefanie Kaech, Uta Wagner et al. (2000). 'Glutamate receptors regulate actin-based plasticity in dendritic spines'. In: *Nature neuroscience* 3.9, p. 887. DOI: `10.1038/78791` (cit. on p. 20).

Florence, Sherre L., Hilary B. Taub and Jon H. Kaas (1998). 'Large-scale sprouting of cortical connections after peripheral injury in adult macaque monkeys'. In: *Science* 282.5391, pp. 1117–1121. DOI: `10.1126/science.282.5391.1117` (cit. on pp. 15, 22, 25).

Galassi, Mark et al. (2002). *GNU scientific library*. Network Theory Limited (cit. on p. 56).

Gallinaro, Júlia V. and Stefan Rotter (2018). 'Associative properties of structural plasticity based on firing rate homeostasis in recurrent neuronal networks'. In: *Scientific reports* 8.1, p. 3754. DOI: `10.1038/s41598-018-22077-3` (cit. on p. 16).

Garraghty, P E, E A LaChica and J H Kaas (1991). 'Injury-induced reorganization of somatosensory cortex is accompanied by reductions in GABA staining.' In: *Somatosensory & motor research* 8 (4), pp. 347–354. ISSN: 0899-0220. DOI: `10.3109/08990229109144757` (cit. on pp. 87, 107).

Gasperini, Robert J. et al. (2017). 'How does calcium interact with the cytoskeleton to regulate growth cone motility during axon pathfinding?' In: *Molecular and Cellular Neuroscience*. DOI: `10.1016/j.mcn.2017.07.006` (cit. on pp. 20, 26).

Gewaltig, Marc-Oliver and Markus Diesmann (2007). 'NEST (NEural Simulation Tool)'. In: *Scholarpedia* 2.4, p. 1430 (cit. on p. 39).

Gilbert, Charles D. and Torsten N. Wiesel (1992). 'Receptive field dynamics in adult primary visual cortex'. In: *Nature* 356.6365, pp. 150–152. DOI: 10.1038/356150a0 (cit. on pp. 22, 25).

Gleeson, Padraig et al. (2017). 'A Commitment to Open Source in Neuroscience'. In: *Neuron* 96.5, pp. 964–965. DOI: 10.1016/j.neuron.2017.10.013 (cit. on p. 7).

Gogolla, Nadine, Ivan Galimberti and Pico Caroni (2007). 'Structural plasticity of axon terminals in the adult'. In: *Current opinion in neurobiology* 17.5, pp. 516–524. DOI: 10.1016/j.conb.2007.09.002 (cit. on pp. 15, 20).

Golomb, D. and D. Hansel (May 2000). 'The Number of Synaptic Inputs and the Synchrony of Large, Sparse Neuronal Networks'. In: *Neural Computation* 12.5, pp. 1095–1139. DOI: 10.1162/089976600300015529 (cit. on p. 86).

Gomez, Timothy M. and Paul C. Letourneau (2014). 'Actin dynamics in growth cone motility and navigation'. In: *Journal of neurochemistry* 129.2, pp. 221–234. DOI: 10.1111/jnc.12506 (cit. on p. 20).

Goodhill, G. J. (2013). 'Axonal growth and guidance'. In: *Scholarpedia* 8.10. revision #143360, p. 1663. DOI: 10.4249/scholarpedia.1663 (cit. on p. 86).

Graham, Bruce and David Willshaw (Mar. 1995). 'Improving recall from an associative memory'. In: *Biological Cybernetics* 72.4, pp. 337–346. DOI: 10.1007/bf00202789 (cit. on p. 34).

Graham, Bruce and David Willshaw (1997). 'Capacity and information efficiency of the associative net'. In: *Network: Computation in Neural Systems* 8.1, pp. 35–54. DOI: 10.1088/0954-898x/8/1/005 (cit. on pp. 34, 39).

Graham, Bruce and David Willshaw (Jan. 1999). 'Probabilistic Synaptic Transmission in the Associative Net'. In: *Neural Computation* 11.1, pp. 117–137. DOI: 10.1162/089976699300016845 (cit. on p. 34).

Grutzendler, Jaime, Narayanan Kasthuri and Wen-Biao Gan (2002). 'Long-term dendritic spine stability in the adult cortex'. In: *Nature* 420.6917, pp. 812–816. DOI: 10.1038/nature01276 (cit. on p. 24).

Haider, Bilal, Michael Häusser and Matteo Carandini (2013). 'Inhibition dominates sensory responses in the awake cortex'. In: *Nature* 493.7430, p. 97 (cit. on p. 60).

Halpain, Shelley (2000). 'Actin and the agile spine: how and why do dendritic spines dance?' In: *Trends in neurosciences* 23.4, pp. 141–146. DOI: 10.1016/s0166-2236(00)01576-9 (cit. on p. 20).

Hamming, Richard W. and J. F. Kaiser (1986). 'You and your research'. In: (cit. on p. 4).

Hebb, D. O. (1949). *The organization of behavior: A neuropsychological theory* (cit. on p. 32).

Heinen, S. J. and A. A. Skavenski (1991). 'Recovery of visual responses in foveal V1 neurons following bilateral foveal lesions in adult

monkey'. In: *Experimental Brain Research* 83.3, pp. 670–674. DOI: 10.1007/bf00229845 (cit. on pp. 15, 22, 25).

Hensch, Takao K. (2005). 'Critical period plasticity in local cortical circuits'. In: *Nature Reviews Neuroscience* 6.11, p. 877. DOI: 10.1038/nrn1787 (cit. on pp. 87, 107).

Hickmott, Peter W. and Patricia A. Steen (2005). 'Large-scale changes in dendritic structure during reorganization of adult somatosensory cortex'. In: *Nature neuroscience* 8.2, pp. 140–142. DOI: 10.1038/nn1384 (cit. on pp. 16, 86).

Hiratani, Naoki, Jun-Nosuke Teramae and Tomoki Fukai (2013). 'Associative memory model with long-tail-distributed Hebbian synaptic connections'. In: *Frontiers in Computational Neuroscience* 6. DOI: 10.3389/fncom.2012.00102 (cit. on p. 35).

Holtmaat, Anthony J. G. D. et al. (2005). 'Transient and Persistent Dendritic Spines in the Neocortex In Vivo'. In: *Neuron* 45.2, pp. 279–291. ISSN: 0896-6273. DOI: 10.1016/j.neuron.2005.01.003. URL: http://www.sciencedirect.com/science/article/pii/S0896627305000048 (cit. on pp. 15, 20, 24).

Hopfield, John J. (1982). 'Neural networks and physical systems with emergent collective computational abilities'. In: *Proceedings of the National Academy of Sciences* 79.8, pp. 2554–2558. DOI: 10.1142/9789812799371_0043. URL: http://www.scholarpedia.org/article/Hopfield_network (cit. on p. 34).

Hopfield, John J. (2007). 'Hopfield network'. In: *Scholarpedia* 2.5, p. 1977. DOI: 10.4249/scholarpedia.1977 (cit. on p. 34).

Isaacson, Jeffry S. and Massimo Scanziani (2011). 'How inhibition shapes cortical activity'. In: *Neuron* 72.2, pp. 231–243. DOI: 10.1016/j.neuron.2011.09.027 (cit. on pp. 39, 71).

Izhikevich, Eugene M. (2004). 'Which model to use for cortical spiking neurons?' In: *IEEE transactions on neural networks* 15.5, pp. 1063–1070 (cit. on p. 63).

Izhikevich, Eugene M. and Niraj S. Desai (2003). 'Relating stdp to bcm'. In: *Neural computation* 15.7, pp. 1511–1523 (cit. on p. 104).

Jordan, Jakob, Tammo Ippen et al. (2018). 'Extremely scalable spiking neuronal network simulation code: from laptops to exascale computers'. In: *Frontiers in neuroinformatics* 12, p. 2. DOI: 10.3389/fninf.2018.00002 (cit. on p. 64).

Jordan, Jakob, Håkon Mørk et al. (2019). *NEST 2.18.0.* DOI: 10.5281/zenodo.2605422. URL: https://doi.org/10.5281/zenodo.2605422 (cit. on pp. 56, 64, 101).

Kang, Kukjin, Michael Shelley and Haim Sompolinsky (2003). 'Mexican hats and pinwheels in visual cortex.' In: *Proceedings of the National Academy of Sciences of the United States of America* 100 (5), pp. 2848–2853. ISSN: 0027-8424. DOI: 10.1073/pnas.0138051100 (cit. on p. 60).

Kater, Stanley B. et al. (1988). 'Calcium regulation of the neuronal growth cone'. In: *Trends in neurosciences* 11.7, pp. 315–321. DOI: 10.1016/0166-2236(88)90094-x (cit. on p. 26).

Keck, Tara, Georg B. Keller et al. (2013). 'Synaptic scaling and homeostatic plasticity in the mouse visual cortex in vivo'. In: *Neuron* 80.2, pp. 327–334. DOI: 10.1016/j.neuron.2013.08.018 (cit. on p. 87).

Keck, Tara, Thomas D. Mrsic-Flogel et al. (2008). 'Massive restructuring of neuronal circuits during functional reorganization of adult visual cortex'. In: *Nature neuroscience* 11.10, pp. 1162–1167. DOI: 10.1038/nn.2181 (cit. on pp. 16, 22, 23, 25, 69, 74, 86).

Keck, Tara, Volker Scheuss et al. (2011). 'Loss of sensory input causes rapid structural changes of inhibitory neurons in adult mouse visual cortex'. In: *Neuron* 71.5, pp. 869–882. ISSN: 0896-6273. DOI: 10.1016/j.neuron.2011.06.034. URL: http://www.sciencedirect.com/science/article/pii/S0896627311005642 (cit. on pp. 16, 23, 25, 86).

King, Michael A. et al. (1989). 'Biocytin: a versatile anterograde neuroanatomical tract-tracing alternative'. In: *Brain Research* 497.2, pp. 361–367. DOI: 10.1016/0006-8993(89)90281-3 (cit. on p. 22).

Knott, Graham W., Anthony Holtmaat et al. (2006). 'Spine growth precedes synapse formation in the adult neocortex in vivo'. In: *Nature neuroscience* 9.9, pp. 1117–1124. DOI: 10.1038/nn1747 (cit. on pp. 62, 106).

Knott, Graham W., Charles Quairiaux et al. (2002). 'Formation of dendritic spines with GABAergic synapses induced by whisker stimulation in adult mice'. In: *Neuron* 34.2, pp. 265–273. DOI: 10.1016/s0896-6273(02)00663-3 (cit. on pp. 15, 20, 86, 106).

Krucker, Thomas, George R. Siggins and Shelley Halpain (2000). 'Dynamic actin filaments are required for stable long-term potentiation (LTP) in area CA1 of the hippocampus'. In: *Proceedings of the National Academy of Sciences* 97.12, pp. 6856–6861. DOI: 10.1073/pnas.100139797 (cit. on p. 20).

Kunkel, Susanne, Abigail Morrison et al. (2017). *NEST 2.12.0*. DOI: 10.5281/zenodo.259534 (cit. on pp. 53, 101).

Kunkel, Susanne, Tobias C. Potjans et al. (2011). 'Meeting the memory challenges of brain-scale network simulation'. In: *Frontiers in neuroinformatics* 5. DOI: 10.3389/fninf.2011.00035 (cit. on p. 53).

Kunkel, Susanne, Maximilian Schmidt et al. (2014). 'Spiking network simulation code for petascale computers'. In: *Frontiers in neuroinformatics* 8. DOI: 10.3389/fninf.2014.00078 (cit. on p. 53).

Lansner, Anders (Mar. 2009). 'Associative memory models: from the cell-assembly theory to biophysically detailed cortex simulations'. In: *Trends in Neurosciences* 32.3, pp. 178–186. DOI: 10.1016/j.tins.2008.12.002 (cit. on p. 35).

Lee, Wei-Chung Allen et al. (2005). 'Dynamic remodeling of dendritic arbors in GABAergic interneurons of adult visual cortex'. In: *PLoS*

biology 4.2, e29. DOI: 10.1371/journal.pbio.0040029 (cit. on pp. 15, 20).

Linssen, Charl et al. (2018). *NEST 2.16.0*. DOI: 10.5281/zenodo.1400175 (cit. on p. 101).

Liu, Bao-hua et al. (2011). 'Broad inhibition sharpens orientation selectivity by expanding input dynamic range in mouse simple cells'. In: *Neuron* 71.3, pp. 542–554. DOI: 10.1016/j.neuron.2011.06.017 (cit. on p. 60).

Liu, Ying et al. (2018). 'Structural Basis for Draxin-Modulated Axon Guidance and Fasciculation by Netrin-1 through DCC'. In: *Neuron*. ISSN: 0896-6273. DOI: 10.1016/j.neuron.2018.02.010 (cit. on p. 20).

Llinás, Rodolfo et al. (June 2005). 'Rhythmic and dysrhythmic thalamocortical dynamics: GABA systems and the edge effect'. In: *Trends in Neurosciences* 28.6, pp. 325–333. DOI: 10.1016/j.tins.2005.04.006 (cit. on p. 107).

Lohmann, Christian, Alexei Finski and Tobias Bonhoeffer (2005). 'Local calcium transients regulate the spontaneous motility of dendritic filopodia'. In: *nature neuroscience* 8.3, pp. 305–312. DOI: 10.1038/nn1406 (cit. on p. 26).

Lohmann, Christian and Rachel O. L. Wong (2005). 'Regulation of dendritic growth and plasticity by local and global calcium dynamics'. In: *Cell calcium* 37.5, pp. 403–409. DOI: 10.1016/j.ceca.2005.01.008 (cit. on p. 26).

Lowery, Laura Anne and David Van Vactor (2009). 'The trip of the tip: understanding the growth cone machinery'. In: *Nature reviews Molecular cell biology* 10.5, p. 332. DOI: 10.1038/nrm2679 (cit. on p. 86).

Lu, Han, Júlia V. Gallinaro and Stefan Rotter (2018). 'Network remodeling induced by transcranial brain stimulation: A computational model of tDCS-triggered cell assembly formation'. In: *Network Neuroscience*, pp. 1–21. DOI: 10.1101/466136 (cit. on p. 16).

Majewska, Ania K., Jessica R. Newton and Mriganka Sur (2006). 'Remodeling of synaptic structure in sensory cortical areas in vivo'. In: *Journal of Neuroscience* 26.11, pp. 3021–3029. DOI: 10.1523/jneurosci.4454-05.2006 (cit. on pp. 15, 20).

Marik, Sally A., Homare Yamahachi, Stephan Meyer zum Alten Borgloh et al. (2014). 'Large-scale axonal reorganization of inhibitory neurons following retinal lesions'. In: *Journal of Neuroscience* 34.5, pp. 1625–1632. DOI: 10.1523/jneurosci.4345-13.2014 (cit. on pp. 15, 20, 24, 25, 74, 86).

Marik, Sally A., Homare Yamahachi, Justin N. J. McManus et al. (2010). 'Axonal dynamics of excitatory and inhibitory neurons in somatosensory cortex'. In: *PLoS Biology* 8.6, e1000395. DOI: 10.1371/journal.pbio.1000395 (cit. on pp. 15, 16, 20, 24, 25, 74, 86).

Massie, Ann et al. (2003). 'Extracellular GABA concentrations in area 17 of cat visual cortex during topographic map reorganization following binocular central retinal lesioning.' In: *Brain research* 976 (1), pp. 100–108. ISSN: 0006-8993 (cit. on pp. 87, 107).

Matus, Andrew (2000). 'Actin-based plasticity in dendritic spines'. In: *Science* 290.5492, pp. 754–758. DOI: 10.1126/science.290.5492.754 (cit. on p. 20).

Matus, Andrew, Heike Brinkhaus and Uta Wagner (2000). 'Actin dynamics in dendritic spines: a form of regulated plasticity at excitatory synapses'. In: *Hippocampus* 10.5, pp. 555–560. DOI: 10.1002/1098-1063(2000)10:5<555::aid-hipo5>3.3.co;2-q (cit. on p. 20).

May, Arne (2011). 'Experience-dependent structural plasticity in the adult human brain'. In: *Trends in cognitive sciences* 15.10, pp. 475–482. DOI: 10.1016/j.tics.2011.08.002 (cit. on pp. 15, 20).

Meffin, Hamish, Anthony N. Burkitt and David B. Grayden (2004). 'An analytical model for the 'large, fluctuating synaptic conductance state' typical of neocortical neurons in vivo'. In: *Journal of computational neuroscience* 16.2, pp. 159–175. URL: https://link.springer.com/article/10.1023/B:JCNS.0000014108.03012.81 (cit. on pp. 54, 63).

Merzenich, Michael M. et al. (1984). 'Somatosensory cortical map changes following digit amputation in adult monkeys'. In: *Journal of Comparative Neurology* 224.4, pp. 591–605. DOI: 10.1002/cne.902240408 (cit. on pp. 22, 25).

Mikhaylova, Marina et al. (2018). 'Caldendrin Directly Couples Postsynaptic Calcium Signals to Actin Remodeling in Dendritic Spines'. In: *Neuron* 97.5, 1110–1125.e14. ISSN: 0896-6273. DOI: 10.1016/j.neuron.2018.01.046 (cit. on p. 26).

Al-Mohanna, Futwan A., Jane Cave and Stephen R. Bolsover (1992). 'A narrow window of intracellular calcium concentration is optimal for neurite outgrowth in rat sensory neurones'. In: *Developmental Brain Research* 70.2, pp. 287–290. DOI: 10.1016/0165-3806(92)90209-f (cit. on p. 26).

Nowke, Christian et al. (2018). 'Toward Rigorous Parameterization of Underconstrained Neural Network Models Through Interactive Visualization and Steering of Connectivity Generation'. In: *Frontiers in Neuroinformatics* 12, p. 32. ISSN: 1662-5196. DOI: 10.3389/fninf.2018.00032. URL: https://www.frontiersin.org/article/10.3389/fninf.2018.00032 (cit. on p. 64).

Nowotny, T. and R. Huerta (Oct. 2003). 'Explaining synchrony in feedforward networks:' in: *Biological Cybernetics* 89.4, pp. 237–241. DOI: 10.1007/s00422-003-0431-9 (cit. on p. 86).

Oertner, Thomas G. and Andrew Matus (2005). 'Calcium regulation of actin dynamics in dendritic spines'. In: *Cell calcium* 37.5, pp. 477–482. DOI: 10.1016/j.ceca.2005.01.016 (cit. on p. 26).

Okun, M. and I. Lampl (2009). 'Balance of excitation and inhibition'. In: *Scholarpedia* 4.8. revision #149451, p. 7467. DOI: `10.4249/scholarpedia.7467` (cit. on pp. 30, 71).

Okun, Michael and Ilan Lampl (2008). 'Instantaneous correlation of excitation and inhibition during ongoing and sensory-evoked activities'. In: *Nature neuroscience* 11.5, p. 535. DOI: `10.1038/nn.2105` (cit. on pp. 30, 71).

Palm, G. (1980). 'On associative memory'. In: *Biological Cybernetics* 36.1, pp. 19–31. DOI: `10.1007/bf00337019` (cit. on p. 34).

Papadopoulou, M. et al. (May 2011). 'Normalization for Sparse Encoding of Odors by a Wide-Field Interneuron'. In: *Science* 332.6030, pp. 721–725. DOI: `10.1126/science.1201835` (cit. on p. 86).

Perez, Yaël et al. (1996). 'Axonal Sprouting of CA1 Pyramidal Cells in Hyperexcitable Hippocampal Slices of Kainate-treated Rats'. In: *European Journal of Neuroscience* 8.4, pp. 736–748. DOI: `10.1111/j.1460-9568.1996.tb01259.x` (cit. on pp. 86, 106).

Peyser, Alexander et al. (2017). *NEST 2.14.0*. DOI: `10.5281/zenodo.882971` (cit. on p. 101).

Pons, Tim P. et al. (1991). 'Massive cortical reorganization after sensory deafferentation in adult macaques'. In: *Science* 252.5014, pp. 1857–1860. DOI: `10.1126/science.1843843` (cit. on pp. 15, 22, 25).

Qu, Jingyi et al. (Sept. 2013). 'Oscillations and synchrony in a cortical neural network'. In: *Cognitive Neurodynamics* 8.2, pp. 157–166. DOI: `10.1007/s11571-013-9268-7` (cit. on p. 86).

Rajan, R. et al. (1993). 'Effect of unilateral partial cochlear lesions in adult cats on the representation of lesioned and unlesioned cochleas in primary auditory cortex'. In: *Journal of Comparative Neurology* 338.1, pp. 17–49. DOI: `10.1002/cne.903380104` (cit. on pp. 15, 22, 25).

Rao, Anuradha and Ann Marie Craig (2000). 'Signaling between the actin cytoskeleton and the postsynaptic density of dendritic spines'. In: *Hippocampus* 10.5, pp. 527–541. DOI: `10.1002/1098-1063(2000)10:5<527::aid-hipo3>3.0.co;2-b` (cit. on p. 20).

Rasmusson, Douglas D. (1982). 'Reorganization of raccoon somatosensory cortex following removal of the fifth digit'. In: *Journal of Comparative Neurology* 205.4, pp. 313–326. DOI: `10.1002/cne.902050402` (cit. on pp. 15, 21, 25).

RedHat (2008). *Fedora Project* (cit. on pp. 4, 103).

Rich, Shannon K. and Jonathan R. Terman (2018). 'Axon formation, extension, and navigation: only a neuroscience phenomenon?' In: *Current Opinion in Neurobiology* 53. Developmental Neuroscience, pp. 174–182. ISSN: 0959-4388. DOI: `10.1016/j.conb.2018.08.004`. URL: `http://www.sciencedirect.com/science/article/pii/S0959438818301363` (cit. on p. 20).

Richards, David A. et al. (2005). 'Glutamate induces the rapid formation of spine head protrusions in hippocampal slice cultures'. In:

Proceedings of the National Academy of Sciences 102.17, pp. 6166–6171. DOI: 10.1073/pnas.0501881102 (cit. on pp. 86, 106).

Rosier, Anne-Marie et al. (1995). 'Effect of sensory deafferentation on immunoreactivity of GABAergic cells and on GABA receptors in the adult cat visual cortex'. In: *Journal of Comparative Neurology* 359.3, pp. 476–489. DOI: 10.1002/cne.903590309 (cit. on pp. 15, 87, 107).

Rudiger, Philipp et al. (2013). 'Developing orientation maps using realistic patterns of lateral connectivity'. In: *BMC Neuroscience* 14.1, P21. ISSN: 1471-2202. DOI: 10.1186/1471-2202-14-S1-P21. URL: https://doi.org/10.1186/1471-2202-14-S1-P21 (cit. on p. 60).

Salin, Paul et al. (1995). 'Axonal sprouting in layer V pyramidal neurons of chronically injured cerebral cortex'. In: *Journal of Neuroscience* 15.12, pp. 8234–8245. URL: http://www.jneurosci.org/content/15/12/8234/tab-article-info (cit. on p. 15).

Sammons, Rosanna P. and Tara Keck (2015). 'Adult plasticity and cortical reorganization after peripheral lesions'. In: *Current Opinion in Neurobiology* 35. Circuit plasticity and memory, pp. 136–141. ISSN: 0959-4388. DOI: 10.1016/j.conb.2015.08.004. URL: http://www.sciencedirect.com/science/article/pii/S0959438815001312 (cit. on p. 15).

Schuemann, Anne et al. (2013). 'Structural plasticity of GABAergic axons is regulated by network activity and GABAA receptor activation'. In: *Frontiers in neural circuits* 7, p. 113. DOI: 10.3389/fncir.2013.00113 (cit. on pp. 86, 106).

Sinha, Ankur, Luis Bazan et al. (2019). 'NeuroFedora: a ready to use Free/Open Source platform for Neuroscientists'. In: *BMC Neuroscience* 20. ISSN: 1471-2202. URL: https://neuro.fedoraproject.org (cit. on p. 103).

Sinha, Ankur, Neil Davey et al. (2015). 'Structural plasticity and associative memory in balanced neural networks with spike-time dependent inhibitory plasticity'. In: *BMC Neuroscience* 16.1, p. 1. URL: http://www.biomedcentral.com/1471-2202/16/S1/P235 (cit. on pp. 43, 102).

Sinha, Ankur, C. Metzner et al. (2017). 'The effect of homeostatic structural plasticity on associative memory in a network with spike-time dependent inhibitory synaptic plasticity.' In: *BMC Neuroscience, 18(Suppl.1)*. DOI: 10.1186/s12868-017-0370-3 (cit. on p. 102).

Sinha, Ankur, Christoph Metzner, Roderick Adams et al. (2018). 'The combined effect of homeostatic structural and inhibitory synaptic plasticity during the repair of balanced networks following deafferentation'. In: *BMC Neuroscience* 19.2, pp. 129–130. ISSN: 1471-2202. DOI: 10.1186/s12868-018-0451-y (cit. on p. 103).

Sinha, Ankur, Christoph Metzner, Neil Davey et al. (2019a). 'Growth rules for repair of asynchronous irregular network models follow-

ing peripheral lesions'. In: *BMC Neuroscience* 20. ISSN: 1471-2202 (cit. on pp. 53, 67, 103).

Sinha, Ankur, Christoph Metzner, Neil Davey et al. (2019b). 'Growth Rules for the Repair of Asynchronous Irregular Neuronal Networks after Peripheral Lesions'. In: *bioRxiv*. DOI: 10.1101/810846. eprint: https://www.biorxiv.org/content/early/2019/10/21/810846.full.pdf. URL: https://www.biorxiv.org/content/early/2019/10/21/810846 (cit. on pp. 53, 67, 103).

Sjöström, J. and Wulfram Gerstner (2010). 'Spike-timing dependent plasticity'. In: *Scholarpedia* 5.2, p. 1362. DOI: 10.4249/scholarpedia.1362 (cit. on p. 36).

Sporns, Olaf and Jonathan D. Zwi (2004). 'The small world of the cerebral cortex'. In: *Neuroinformatics* 2.2, pp. 145–162. DOI: 10.1385/ni:2:2:145 (cit. on p. 107).

Sprekeler, Henning (2017). 'Functional consequences of inhibitory plasticity: homeostasis, the excitation-inhibition balance and beyond'. In: *Current Opinion in Neurobiology* 43, pp. 198–203. DOI: 10.1016/j.conb.2017.03.014 (cit. on pp. 39, 105).

Stallman, Richard (2002). *Free software, free society: Selected essays of Richard M. Stallman*. Lulu. com (cit. on pp. 4, 7).

Star, Erin N., David J. Kwiatkowski and Venkatesh N. Murthy (2002). 'Rapid turnover of actin in dendritic spines and its regulation by activity'. In: *Nature neuroscience* 5.3, p. 239. DOI: 10.1038/nn811 (cit. on p. 20).

Stepanyants, Armen et al. (2009). 'The fractions of short-and long-range connections in the visual cortex'. In: *Proceedings of the National Academy of Sciences* 106.9, pp. 3555–3560 (cit. on p. 60).

Stettler, Dan D. et al. (2006). 'Axons and Synaptic Boutons Are Highly Dynamic in Adult Visual Cortex'. In: *Neuron* 49.6, pp. 877–887. ISSN: 0896-6273. DOI: 10.1016/j.neuron.2006.02.018. URL: http://www.sciencedirect.com/science/article/pii/S0896627306001358 (cit. on pp. 15, 20, 24).

Stöckel, Andreas et al. (Aug. 2017). 'Binary Associative Memories as a Benchmark for Spiking Neuromorphic Hardware'. In: *Frontiers in Computational Neuroscience* 11. DOI: 10.3389/fncom.2017.00071 (cit. on p. 35).

Suzuki, Wendy A. and Mark G. Baxter (Mar. 2009). 'Memory, Perception, and the Medial Temporal Lobe: A Synthesis of Opinions'. In: *Neuron* 61.5, pp. 678–679. DOI: 10.1016/j.neuron.2009.02.009 (cit. on p. 32).

Suzuki, Wendy A. and H. Eichenbaum (Jan. 2006). 'The Neurophysiology of Memory'. In: *Annals of the New York Academy of Sciences* 911.1, pp. 175–191. DOI: 10.1111/j.1749-6632.2000.tb06726.x (cit. on p. 32).

Tessier-Lavigne, Marc and Corey S. Goodman (1996). 'The molecular biology of axon guidance'. In: *Science* 274.5290, pp. 1123–1133. DOI: 10.1126/science.274.5290.1123 (cit. on p. 20).

Trachtenberg, Joshua T. et al. (2002). 'Long-term in vivo imaging of experience-dependent synaptic plasticity in adult cortex'. In: *Nature* 420.6917, pp. 788–794. DOI: 10.1038/nature01273 (cit. on pp. 15, 16, 20, 24, 62, 86, 106).

Tronson, Natalie C. and Jane R. Taylor (2007). 'Molecular mechanisms of memory reconsolidation'. In: *Nature Reviews Neuroscience* 8.4, pp. 262–275. DOI: 10.1038/nrn2090 (cit. on p. 108).

Turrigiano, Gina G. (1999). 'Homeostatic plasticity in neuronal networks: the more things change, the more they stay the same'. In: *Trends in neurosciences* 22.5, pp. 221–227. DOI: 10.1016/s0166-2236(98)01341-1 (cit. on p. 34).

Turrigiano, Gina G. (2008). 'The self-tuning neuron: synaptic scaling of excitatory synapses'. In: *Cell* 135.3, pp. 422–435. DOI: 10.1016/j.cell.2008.10.008 (cit. on p. 87).

van Ooyen, A. (2011). 'Using theoretical models to analyse neural development'. In: *Nature Reviews Neuroscience* 12.6, pp. 311–326. DOI: 10.1038/nrn3031 (cit. on p. 24).

van Ooyen, A. and M. Butz (2017). *The rewiring brain*. Academic Press. ISBN: 9780128038727. URL: https://www.elsevier.com/books/the-rewiring-brain/van-ooyen/978-0-12-803784-3 (cit. on pp. 16, 34).

Versendaal, Daniëlle van et al. (2012). 'Elimination of inhibitory synapses is a major component of adult ocular dominance plasticity'. In: *Neuron* 74.2, pp. 374–383. DOI: 10.1016/j.neuron.2012.03.015 (cit. on pp. 87, 107).

Vetencourt, José Fernando Maya et al. (2008). 'The antidepressant fluoxetine restores plasticity in the adult visual cortex'. In: *Science* 320.5874, pp. 385–388. DOI: 10.1126/science.1150516 (cit. on pp. 24, 87, 107).

Villa, Katherine L. et al. (2016). 'Inhibitory Synapses Are Repeatedly Assembled and Removed at Persistent Sites In Vivo.' In: *Neuron* 89 (4), pp. 756–769. ISSN: 1097-4199. DOI: 10.1016/j.neuron.2016.01.010 (cit. on pp. 15, 20, 24).

Vogels, T. P. et al. (2011). 'Inhibitory plasticity balances excitation and inhibition in sensory pathways and memory networks'. In: *Science* 334.6062, pp. 1569–1573. DOI: 10.1126/science.1211095. URL: http://www.sciencemag.org/content/334/6062/1569.short (cit. on pp. 17, 35–39, 41, 43, 45, 62, 75, 93, 101, 104, 105).

Vogels, T. P. et al. (2012). 'Corrections and Clarifications'. In: *Science* 336.6083, pp. 802–802. ISSN: 0036-8075. DOI: 10.1126/science.336.6083.802-c. eprint: https://science.sciencemag.org/content/336/6083/802.3.full.pdf. URL: https://science.sciencemag.org/content/336/6083/802.3 (cit. on pp. 38, 105).

Wall, J. T. and C. G. Cusick (1984). 'Cutaneous responsiveness in primary somatosensory (SI) hindpaw cortex before and after partial hindpaw deafferentation in adult rats'. In: *The journal of neuroscience* 4.6, pp. 1499–1515. DOI: 10.1523/jneurosci.04-06-01499.1984 (cit. on pp. 15, 22).

Watts, Duncan J. and Steven H. Strogatz (1998). 'Collective dynamics of 'small-world'networks'. In: *Nature* 393.6684, pp. 440–442. DOI: 10.1515/9781400841356.301 (cit. on p. 107).

Willshaw, David (1971). 'Models of distributed associative memory'. PhD thesis. University of Edinburgh (cit. on p. 34).

Willshaw, David, O. Peter Buneman and Hugh Christopher Longuet-Higgins (1969). 'Non-holographic associative memory.' In: *Nature* (cit. on p. 34).

Wolff, J. R. and M. Missler (1992). 'Synaptic reorganization in developing and adult nervous systems'. In: *Annals of Anatomy-Anatomischer Anzeiger* 174.5, pp. 393–403. DOI: 10.1016/s0940-9602(11)80257-8 (cit. on p. 20).

Wolff, J. R. and G. P. Wagner (1983). 'Self-organization in synaptogenesis: interaction between the formation of excitatory and inhibitory synapses'. In: *Synergetics of the Brain*. Springer, pp. 50–59 (cit. on p. 25).

Wong, Rachel O. L. and Anirvan Ghosh (2002). 'Activity-dependent regulation of dendritic growth and patterning'. In: *Nature reviews neuroscience* 3.10, pp. 803–812. DOI: 10.1038/nrn941 (cit. on p. 26).

Woodin, Melanie A., Karunesh Ganguly and Mu-ming Poo (2003). 'Coincident pre-and postsynaptic activity modifies GABAergic synapses by postsynaptic changes in Cl- transporter activity'. In: *Neuron* 39.5, pp. 807–820. DOI: 10.1016/s0896-6273(03)00507-5 (cit. on pp. 36, 38, 39, 105).

Yamahachi, Homare et al. (2009). 'Rapid axonal sprouting and pruning accompany functional reorganization in primary visual cortex'. In: *Neuron* 64.5, pp. 719–729. DOI: 10.1016/j.neuron.2009.11.026 (cit. on pp. 15, 23, 25, 74, 86).

Yuste, Rafael, Ania Majewska and Knut Holthoff (2000). 'From form to function: calcium compartmentalization in dendritic spines'. In: *Nature neuroscience* 3.7, p. 653. DOI: 10.1038/76609 (cit. on p. 63).

Zenke, Friedemann, Everton J. Agnes and Wulfram Gerstner (2015). 'Diverse synaptic plasticity mechanisms orchestrated to form and retrieve memories in spiking neural networks'. In: *Nature communications* 6, p. 6922. DOI: 10.1038/ncomms7922 (cit. on p. 105).

Zenke, Friedemann and Wulfram Gerstner (2014). 'Limits to high-speed simulations of spiking neural networks using general-purpose computers'. In: *Frontiers in neuroinformatics* 8. DOI: 10.3389/fninf.2014.00076 (cit. on pp. 39, 43, 53, 56, 101).

Zenke, Friedemann and Wulfram Gerstner (2017). 'Hebbian plasticity requires compensatory processes on multiple timescales'.

In: *Philosophical Transactions of the Royal Society of London B: Biological Sciences* 372.1715. ISSN: 0962-8436. DOI: 10.1098/rstb.2016.0259. eprint: http://rstb.royalsocietypublishing.org/content/372/1715/20160259.full.pdf. URL: http://rstb.royalsocietypublishing.org/content/372/1715/20160259 (cit. on p. 107).

LIST OF TERMS

AdEx neuron model   A general point neuron model using an exponential function that can be used to model various spiking characteristics by modifying its free parameters. 104

AI   Asynchronous Irregular. 9, 35, 37, 38, 41, 43–45, 50, 53, 60, 61, 63, 67, 75, 78–80, 85, 88, 90, 91, 93, 101, 107

E-I balance   balance between excitation and inhibition. 30, 70, 71, 81, 87, 102

LGN   lateral geniculate nucleus. 22

LPZ   Region of network that has lost projections on account of deafferentation. 9, 12, 13, 16, 22–25, 27–30, 61, 68–70, 74, 75, 78–87, 90–99, 102, 107

LTP   A temporally asymmetric form of Hebbian learning in which near co-incident spiking of the post-synaptic neuron after the pre-synaptic neuron results in strengthening of the synapse between them (Bliss and Lømo 1973) 32

memory   Record of experience represented in the brain. 32

MPI   a message-passing library interface specification. 106

MSP   Model of Structural Plasticity. 12, 16, 24–27, 31, 53, 56, 57, 63, 64, 101, 102, 104–106

SNR   Signal to Noise Ratio. 17, 35, 39–41, 43–47, 50, 52, 92–95

STDP   Spike Timing Dependent Plasticity. 12, 35–39, 41, 45, 50, 75, 83, 85, 86, 101, 105

structural plasticity   The formation and deletion of axonal boutons and dendritic spines in neurons that may lead to formation of new synapses or removal of existing ones 20

synaptogenesis   formation of synapses between neurons in the nervous system. 20